NASA TECHNICAL TRANSLATION

NASA TT F-538

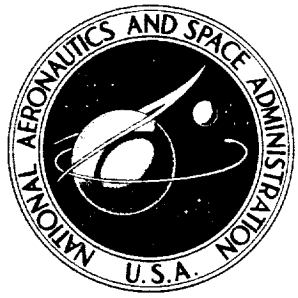

NASA TT F-538

PHYSICS OF AERODYNAMIC NOISE

A. V. Rimskiy-Korsakov, Editor

"Nauka" Press
Moscow, 1967

NATIONAL AERONAUTICS AND SPACE ADMINISTRATION • WASHINGTON, D. C. • NOVEMBER 1969

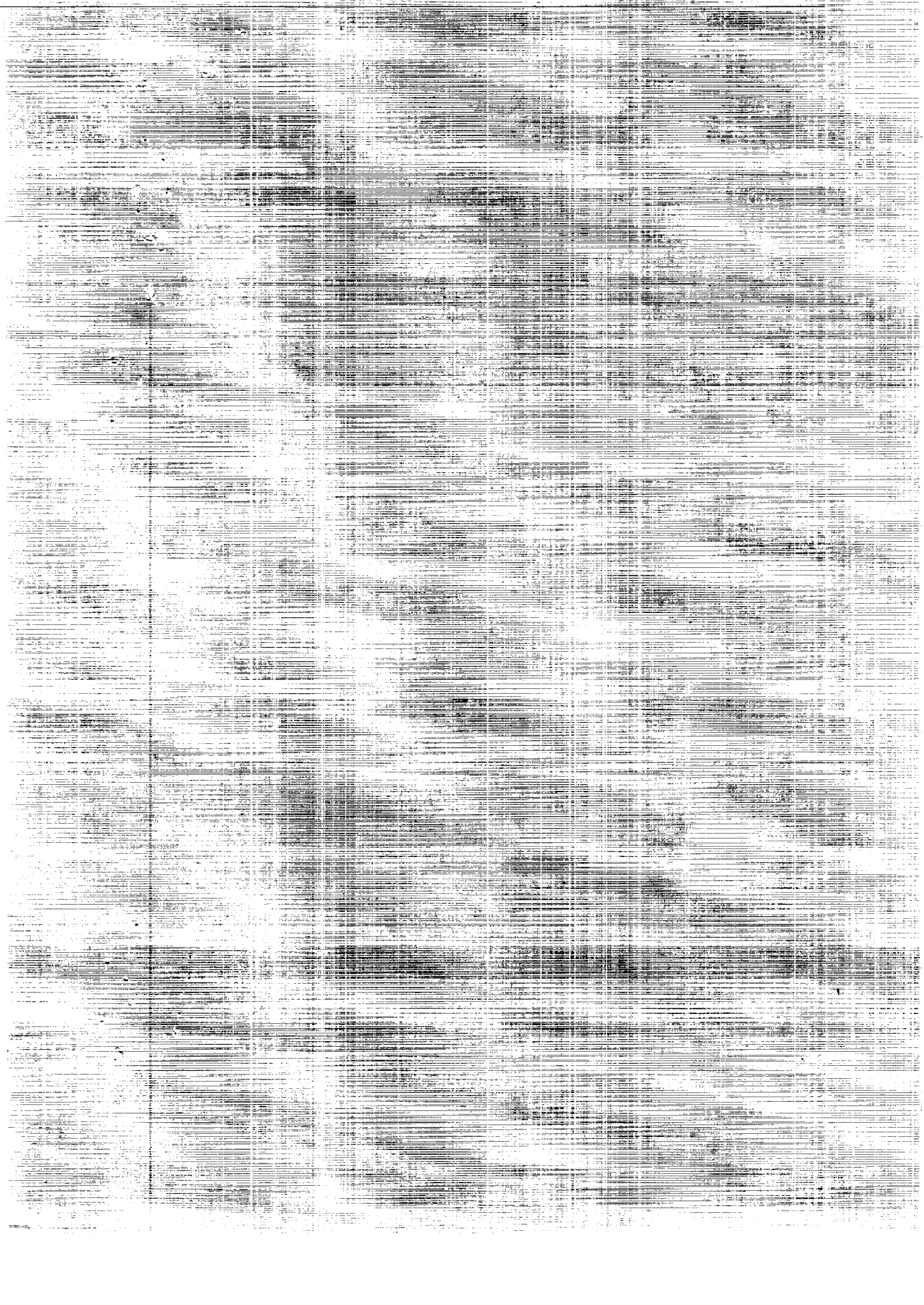

NASA TT F-538

PHYSICS OF AERODYNAMIC NOISE

A. V. Rimskiy-Korsakov, Editor

Moscow Society for Natural Research
Physics Section
Institute of Acoustics of the USSR Academy of Sciences

Translation of "Fizika Aerodinamicheskikh Shumov."
"Nauka" Press, Moscow, 1967

NATIONAL AERONAUTICS AND SPACE ADMINISTRATION

For sale by the Clearinghouse for Federal Scientific and Technical Information
Springfield, Virginia 22151 – CFSTI price $3.00

TABLE OF CONTENTS

A STUDY OF DISCRETE COMPONENTS OF THE NOISE SPECTRUM OF AN AXIAL COMPRESSOR

D. V. Bazhenov, L. A. Bazhenova and A. V. Rimskiy-Korsakov 1

EFFECT OF THE DESIGN OF WALLS OF THE AIR INTAKE DUCT OF AN AXIAL COMPRESSOR ON THE PROPAGATION OF SOUND

D. V. Bazhenov, L. A. Bazhenova, Yu. V. Kravchenko and A. V. Rimskiy-Korsakov 12

EXPERIMENTAL STUDY OF THE EFFECT OF ROUGHNESS OF A SURFACE OF A BAR ON THE INTENSITY AND FREQUENCY OF VORTEX SOUND

D. V. Bazhenov, L. A. Bazhenova and A. V. Rimskiy-Korsakov 26

PROPAGATION OF SOUND IN A CYLINDRICAL PIPE WITH STREAMLINED IMPEDANCE WALLS

A. V. Rimskiy-Korsakov and P. G. Kolev 35

EFFECT OF THE REACTION OF THE MEDIUM ON THE OPERATION OF A RADIATOR IN A WAVEGUIDE

A. D. Lapin and Yu. P. Lysanov 40

RADIATION OF AN ELASTIC DISCONTINUOUS WALL IN A MOVING MEDIUM

A. D. Lapin 47

PULSATIONS OF COLLIDING AXISYMMETRICAL JETS OF GASEOUS OXIDIZER AND PROPELLANT

V. I. Kondrat'yev 56

FREQUENCY CHARACTERISTICS OF BAR-TYPE GAS-JET ACOUSTIC GENERATORS

Yu. Ya. Borisov and N. M. Gykina 58

THE SUPERSONIC AIR JET AS A SOURCE OF SOUND

V. M. Mamin and A. V. Rimskiy-Korsakov 66

THE FREQUENCY SPECTRUM OF THE NOISE OF A SUPERSONIC JET

T. Kh. Sedel'nikov 71

THE DISCRETE COMPONENT OF THE FREQUENCY SPECTRUM OF THE NOISE OF A FREE SUPERSONIC JET

T. Kh. Sedel'nikov 76

THE DISPERSION EQUATION OF A PLANE EJECTOR

L. I. Nazarova and T. Kh. Sedel'nikov 90

THE DISPERSION EQUATIONS FOR MULTILAYER JETS AND FOR SEVERAL JETS

T. Kh. Sedel'nikov 97

The articles in the present collection deal with the generation of noise by bodies moving in a flow of gas (homogeneous and inhomogeneous) and on discharge of gas jets (axial compressor, propeller, bar source, supersonic nozzle).

In addition, the collection contains articles dealing with the propagation of sound in a flow channel with flexible walls, as well as with sound generation by fuel jets colliding with the oxidizing agent.

This collection is intended for researchers in acoustics, as well as for engineers who encounter problems of machine noise in their work.

Chief Editor: Doctor of
Physical and Mathematical Sciences,
Professor A. V. Rimskiy-Korsakov

FOREWORD

The present collection is concerned with acoustic-aerodynamic and acoustic-gasdynamic phenomena accompanying the basic processes in several engineering devices. Noise of air-blower units, reaction jets, and pulsed combustion, although taking up only a small part of the power of aircraft engines, combustion chambers, etc., do nevertheless, due to the high power of these machines, have a harmful effect on their operation and on hearing.

While in the past the problems of jet stability and of interaction of flames and thermal fluxes with sonic waves were of so-called "purely scientific" importance (such as, for example, studies of the vibrations of Rayleigh's jets, of the stability of flow boundaries and vibrations in the Rieke tube), today they have also acquired practical significance. Of course, we are talking primarily about phenomena which occur in high-speed gas flows (supersonic jets) or high-flow rate phenomena (turbocompressors), rather than about topics treated in the above classical works.

This collection contains experimental and theoretical papers of the staffs of the Institute of Acoustics of the USSR Academy of Sciences, and of the Department of Acoustics and Ultrasonic Engineering of the Moscow Mining Institute. These papers can be divided into the following groups: those devoted to the stability and vibrations of supersonic jets and to the sound generation by these jets (articles by Yu. Ya. Borisov, N. M. Gynkina; V. M. Mamin; L. I. Nazarova, T. Kh. Sedel'nikov), those devoted to the generation of sound by multibladed compressor impellers (the article by D. V. Bazhenov and L. A. Bazhenova), those dealing with the problem of sound generation by plates and waveguide-type propagation of sound in channels, in particular, in the presence of air flow (articles by D. V. Bazhenov, L. A. Bazhenova, Yu. B. Kravchenko; P. G. Kolev; A. D. Lapin; Yu. P. Lysanov), and those devoted to the problem of vibrations attendant to combustion (the article by V. I. Kondrat'yev).

These articles can, in our opinion, be of interest to researchers in acoustics, as well as to engineers who encounter problems of machine noise in their work.

A. V. Rimskiy-Korsakov

CUT ALONG THIS LINE

FOLD LINE

NATIONAL AERONAUTICS AND SPACE ADMINISTRATION
WASHINGTON, D.C. 20546

OFFICIAL BUSINESS

POSTAGE AND FEES PAID
NATIONAL AERONAUTICS & SPACE ADMINISTRATION

NATIONAL AERONAUTICS AND SPACE ADMINISTRATION
CODE USS-T
WASHINGTON, D.C. 20546

NASA TTF No.
538

FOLD LINE

CUT ALONG THIS LINE

NATIONAL AERONAUTICS AND SPACE ADMINISTRATION
TECHNICAL TRANSLATION EVALUATION

Budget Bureau No. 104-R037
Approval Expires: Sept. 30, 1969

TO: THE USERS OF THIS TRANSLATION →

NASA TTF NO. 538

MAINTAINING THE QUALITY OF NASA TRANSLATIONS REQUIRES A CONTINUOUS EVALUATION PROGRAM. PLEASE COMPLETE AND MAIL THIS FORM TO AID IN THE EVALUATION OF THE USEFULNESS AND QUALITY OF THE TRANSLATING SERVICE.

THIS PUBLICATION *(Check one or more)*

- [ ] FURNISHED VALUABLE NEW DATA OR A NEW APPROACH TO RESEARCH.
- [ ] VERIFIED INFORMATION AVAILABLE FROM OTHER SOURCES.
- [ ] FURNISHED INTERESTING BACKGROUND INFORMATION.
- [ ] OTHER *(Explain)*: _____

FOLD LINE FOLD LINE

TRANSLATION TEXT *(Check one)*

- [ ] IS TECHNICALLY ACCURATE.
- [ ] IS SUFFICIENTLY ACCURATE FOR OUR PURPOSE.
- [ ] IS SATISFACTORY, BUT CONTAINS MINOR ERRORS.
- [ ] IS UNSATISFACTORY BECAUSE OF *(Check one or more)*:
  - [ ] POOR TERMINOLOGY.
  - [ ] NUMERICAL INACCURACIES.
  - [ ] INCOMPLETE TRANSLATION.
  - [ ] ILLEGIBLE SYMBOLS, TABULATIONS, OR CURVES.
  - [ ] OTHER *(Explain)*: _____

FOLD LINE FOLD LINE

REMARKS

FROM

DATE

NOTE: REMOVE THIS SHEET FROM THE PUBLICATION, FOLD AS INDICATED, STAPLE OR TAPE, AND MAIL. NO POSTAGE NECESSARY.

NASA Form 1332 AUG 66

GPO 915-777

CUT ALONG THIS LINE

CUT ALONG THIS LINE

A STUDY OF DISCRETE COMPONENTS OF THE NOISE SPECTRUM OF AN AXIAL COMPRESSOR

D. V. Bazhenov, L. A. Bazhenova and A. V. Rimskiy-Korsakov

ABSTRACT. The article deals with the mechanism of formation of the discrete components of the noise spectrum at the intake of an axial compressor. It shows that the intensity of this noise is highly dependent on the blade ratio of the stationary and rotating blading. It shows that this noise can be reduced by changing the distance between the two types of blading as well as the blade angle.

Aerodynamic noise produced by fans and axial compressors is made up of /5* individual components formed via different mechanisms. The basic noise is that produced by vortices formed when the air sucked in by the compressor flows around intake duct parts, noise due to the motion of impeller blades which produce periodic disturbances of the medium in the plane of the impeller (the so-called sound of rotation), and finally, the noise due to discontinuities in the flow past the blades. The sound of rotation is produced in a completely uniform flow, impinging on the plane of the impeller. It is due to blade reaction to this flow, whereby this reaction is constant in the coordinate system rotating together with the blades. Noise due to flow discontinuity is produced by additional reaction forces on the blades; these forces are generated because the local velocities of the impinging flow are discontinuous over the plane of the impeller. These velocity differences may be brought about by flow turbulence (due to streamlining of the the air intake duct obstructions), as well as by rigidly specifiable distortion of the velocity field produced by the flow pattern past the guide vanes and the prerotation vanes of the stator.

Noise due to vortex formation usually has a wide frequency spectrum, while the sound of rotation and the noise due to flow discontinuity (sometimes called the "siren effect") have a clearly pronounced discrete character. The intensity of discrete components of compressor noise produced by regular flow /6 discontinuity can be quite high, and development of methods for preventing this kind of sound generation is of great practical interest.

The formation of discrete components due to flow discontinuity was considered by Ye. Ya. Yudin in his study of noise generated in ventilation units [1]. The literature on these problems is sufficiently extensive. We note here work by A. F. Deming [2], H. H. Hubbard [3], as well as later work by E. I. Richards, I. J. Sharland [4] and J. Nemec [5]. Finally, just as the present

---

*Numbers in the margin indicate pagination in the foreign text.

study was drawing to a close, there appeared a thorough study by I. Sharland [6], many of whose conclusions are similar to those obtained by us.

Theoretical Discussion

Let us examine the passage of rotor blades past a single flow discontinuity (inhomogeneity) formed by one guide vane. A pressure pulse is produced (and propagated) each time the rotor blade passes this inhomogeneity. The repetition frequency of these pulses is Nz_1, where N is the rotor rps and z_1 is the number of rotor blades. The periodic pressure fluctuations which are experienced at any arbitrary observation point can be represented in the form of a Fourier series:

$$P = \sum_{-\infty}^{+\infty} C'_m \exp(-j\omega_m t), \tag{1}$$

where $\omega_m = 2\,Nz$ and C'_m are factors of the expansion ($m = 1, 2, 3, \ldots$). Factor C'_m are functions of the frequency, the pattern of the flow inhomogeneity and of the blades. They can also depend on the angular coordinates of the line to the observation point relative to the axis of rotation of the rotor (the pulse propagation from a blade intersecting a flow inhomogeneity is bipolar). The specific form of factors C'_m thus depends on the geometry of flow and impellers in the given compressor. If the stator has z_0 vanes, which produce components P_ν similar to (1), then these components should be expressed in a way which takes account of the difference in the time of arrival of the waves produced by them to the observation point. These time differences are due, first, to the fact that these inhomogeneities are situated at different distances from the observation point (A), and second, to the fact that the time instants when the rotor blades enter these inhomogeneities are shifted by the time during which the rotor rotates through an angle (α) between the first and the νth inhomogeneity (Fig. 1). The overall sonic pressure produced by all discontinuities can be written as /7

$$P_0 = \sum_{\nu=0}^{z_0-1} C_m \exp\{j[k_m R_\nu - \omega_m(t-\tau_\nu)]\}. \tag{2}$$

where $k_m R_\nu = \frac{\omega_m}{c} R_\nu$ is the phase lag of the sound, corresponding to the distance R_ν from the νth stator vane to the observation point; t_ν is the time needed for passage of the rotor blade from the νth to the first stator vane; and c is the speed of sound. On the assumption that the observation point is far away (the existence of a Fraunhofer region), the distance R_ν is expressed by radius vector r_0, which is directed from the center of the rotor disk to the observation point (its polar coordinates are θ, φ) and the radius d of the circle along which the inhomogeneities are located

$$R_\nu = r_0 - d\cos\theta\cos(\varphi - \varphi_\nu), \tag{3}$$

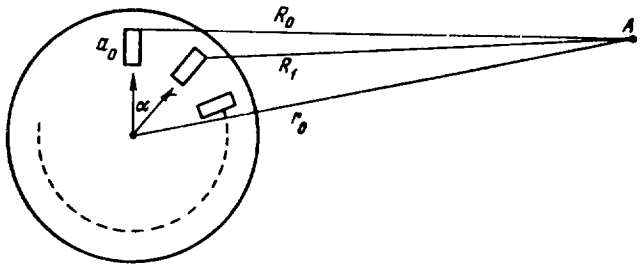

Figure 1. Calculation of Acoustic Radiation Created by Impeller Blades. r_0 - Radius Vector Directed from the Center of the Rotor Disk to the Observation Point; R_0 - Distance from the Zero Stator Vane to the Observation Point; R_1 - Distance from the First Stator Vane to the Observation Point; α - Angle of Rotation of the Rotor Between the First and the νth Inhomogeneities.

where $\varphi_\nu = \frac{2\pi}{z_0}\nu$ is the angle between the first and νth stator vanes. Using the Bessel function relationship

$$\exp(jx\cos\psi) = J_0(x) + 2\sum_{p=1}^{\infty} j^p J_p(x)\cos(p\psi),$$

we can transform Eq. (2) to

$$P = \sum_{m=-\infty}^{m=+\infty} C_m \exp[j(k_m r_0 - \omega_m t)]\left\{\sum_{\nu=0}^{z_0-1}\exp\left(j2\pi m\frac{z_1}{z_0}\nu\right)\times J_0\left(-k_m d\cos\theta\right) + \right.$$

$$\left. + 2\sum_{\nu=0}^{z_0-1}\exp\left(j2\pi m\frac{z_1}{z_0}\nu\right)\sum_{p=1}^{\infty} j^p J_p(-k_m d\cos\theta)\times\cos p\left(\varphi - \frac{2\pi\nu}{z_0}\right)\right\}. \qquad (4)$$

The first term in braces in the above expression corresponds to the expression obtained by J. Nemec [5] for the discrete components neglecting the differences /8 in the phase lags $k_m d$, i.e., on the assumption that

$$\frac{\omega_m d}{c} \ll 1, \quad J_0(-k_m d\cos\theta)\approx 1 \text{ и } J_p(-k_m d\cos\theta)\approx 0$$

when $p \neq 0$. In this assumption

$$P = \sum_{m=-\infty}^{m=+\infty} C_m \exp[j(k_m r_0 - \omega_m t)]\sum_{\nu=1}^{z_0-1}\exp\left(j2\pi m\frac{z_1}{z_0}\nu\right) = 0$$

for a nonintegral z_1/z_0 since the sum

$$\sum_{\nu=1}^{z_0-1}\exp\left(j2\pi m\frac{z_1}{z_0}\nu\right) = \frac{\sin\pi z_1 m}{\sin\frac{\pi z_1 m}{z_0}}\begin{cases} = 0, & \text{if} \quad z_1 \neq kz_0, \\ = z_0, & \text{if} \quad z_1 = kz_0. \end{cases}$$

Thus, if z_1 and z_0 are relatively prime numbers (as is the case in practice), then according to [5] only discrete sound components propagate from the discontinuities. The frequencies of these components are multiples of the product $z_1 z_0$ (number of rotor blades by the number of stator vanes, which produce the

discontinuities). On the other hand, it has been established experimentally that frequencies which are multiples of the number of rotor blades are always propagated, despite the fact that due to strength considerations, z_1 and z_0 are always made to be mutually prime.

The first term in braces of Eq. (4), which specifies the maximum sound propagation in the direction of the compressor axis, is of importance only for discrete components of quite high frequencies $\omega_m = 2\pi k z_1 z_0$, which as a rule lie outside the range of sonic frequencies.

Changing the order of summation in the second term in braces of Eq. (4), we can reduce it to

$$\sum_{p=1}^{\infty} \frac{\sin \pi (z_1 m - p)}{\sin \frac{\pi}{z_0} (z_1 m - p)} j^p J_p (- k_m d \cos\theta) \exp (jp\varphi) + \\ + \sum_{p=1}^{\infty} \frac{\sin \pi (z_1 m + p)}{\sin \frac{\pi}{z_0} (z_1 m + p)} j^p J_p (- k_m d \cos\theta) \exp (- jp\varphi). \quad (5)$$

These two terms are nonzero when

$$\frac{\sin \pi (z_1 m - p)}{\sin \frac{\pi}{z_0} (z_1 m - p)} \neq 0, \quad \frac{\sin \pi (z_1 m + p)}{\sin \frac{\pi}{z_0} (z_1 m + p)} \neq 0. \quad (6)$$

Since z_1, z_0 and p are positive integers and m are any integers, then, in order to satisfy inequalities (6) it is required that

$$z_1 m - p = \pm q z_0 \quad (z_1 m + p) = \pm q z_0, \quad (7)$$

where q can be any integers. If we assume, for simplicity, that z_0 is an odd number, then the fractions in the left-hand sides of Eq. (6) will, assuming condition (7) holds, become z_0, and then we will have for Eq. (5) /9

$$z_0 \Bigg(\sum_{p = mz_1 - qz_0}^{\infty} j^p J_p (- d k_m \cos\theta) \exp (jp\varphi) + \sum_{p = -(mz_1 - qz_0)}^{\infty} j^p \times \\ \times J_p (- k_m d \cos\theta) \exp (- jp\varphi). \quad (8)$$

According to Eq. (7) it is always possible to find q such that when m = 1, 2, 3, ..., the sums of Eq. (8) will contain at least some terms satisfying the condition p > 0 and, consequently, the amplitudes of harmonics of the number of passes by the rotor blades will be nonzero even if z_1 and z_0 are mutually prime.

The problem of the effect of the relationship between z_1 and z_0 on the intensity of discrete components is of great interest. Since

$$J_p (x) \leqslant 0{,}07 \text{ when } p + 2 \geqslant x,$$

then the main terms in summations of Eq. (8) will be terms with the lowest p. Examining Eq. (8) we see that for values of z_1 and z_0 used in practice the main contribution is made by the term with $p = |z_1 - z_0|$. The p-order Bessel function reaches its first maximum at an argument whose value is close to p; the larger p, the lower the value of this maximum. It is thus desirable that $|z_1 - z_0|$ be as large as possible and that $|z_1 - z_0| + 2 > \frac{2\pi z_1 Nd}{c}$. Since we virtually always have $|z_1 - z_0| \ll z_1$ then, simplifying, we get

$$3 > \frac{2\pi Nd}{c} = \frac{2\pi d}{\lambda_0}; \quad \frac{d}{\lambda_0} < 0.5,$$

where λ_0 is the wavelength corresponding to the given rotor rps. Since in the region of small arguments J_p increases with the argument to the power (p + 2), then a reduction in d/λ_0 and increase in ($|z_1 - z_0|$) have a very strong effect. In practice, a reduction in d involves an increase in N for a given compressor delivery; this means that the most sensible approach is to attempt to increase the difference ($|z_1 - z_0|$).

The direction of maximum sound propagation is determined from $k_m d \cos \theta_{max} = x_{max}$, where x_{max} corresponds to the maximum of $J_p(x)$. If $k_m d < x_{max}$, then the propagation maximum lies in the plane of the impeller. If C_m are functions of θ, producing bipolar pressure propagation, or radiation of 0 + 1 order, then, according to a well known principle, the directivity of the entire group can be found from the product $C_m(\theta) J_p(-k_m d \cos \theta)$.

The above calculations of the directivity and intensity of sound propagation /10
do not take into account the effect of the air intake duct, which could appreciably change the conditions of sound propagation, if the intake duct axis is not coaxial with the direction of θ_{max}. Thus it is recommended that the air intake duct have a shape in which the θ_{max} direction is screened by sound-absorbing duct walls.

Experimental

The measurements were made on a turbocompressor which was disconnected from the turbine and coupled to an electric motor (Fig. 2a). Since it was established by measurements with the fully-assembled turbocompressor unit that turbocompressor stages far removed from the intake part do not appreciably contribute to the energy of the noise emanating from it, only the first compressor stage with guide and prerotation vanes was tested. This made it possible to remove the blades from all the rotor stages with the exception of the first and thus to reduce the power needed for driving the compressor. The

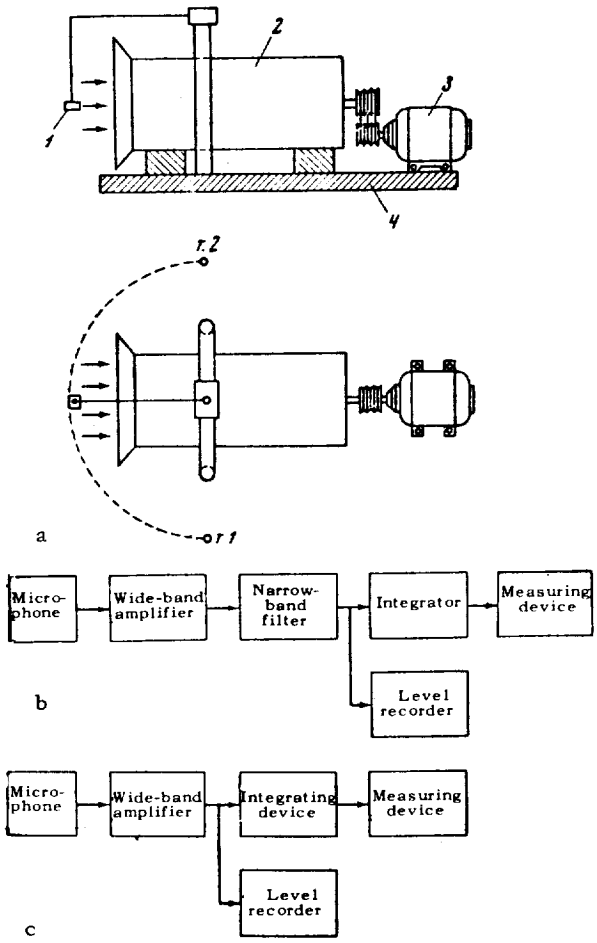

Figure 2. Schematic of Experimental Setup. a) Overall view of setup (side and top views); 1) microphone; 2) compressor; 3) electric motor; 4) foundation; b) and c) block diagrams of the setup.

axis of the rotor, which was installed in the open air, was 1 m from the ground One end of a horizontal bar, which was free to rotate parallel to the plane of the ground and was driven by means of an electric motor, was fastened to a pole above the compressor. The measuring microphone was fastened to the other end of the 5 m long bar. By smoothly moving the bar the microphone could be moved over a full circle about the compressor. In the majority of cases, the noise radiation directivity diagrams were taken in the half-space in front of the compressor intake. The standard inlet guide vane apparatus was replaced by an experimental unit with simplified elliptical vane cross sections. This apparatus made it possible to study the effect (on the noise) of the number of vanes, their mutual arrangement, angle of inclination of the guide vanes relative to the rotor blades and the distance between the rotor blades and the guide vanes. The compressor rpm was varied in steps by means of interchangeable sheaves. The block diagrams of the setup are shown in Figs. 2b and c. The signal from the microphone was fed to a wide-band amplifier. In the studies of the behavior of some discrete component of the noise frequency spectrum, the amplified signal

was also fed to a filter with a 4 cps passband, which was tuned to the frequency of this component. From the filter, the signal went to an automatic level recorder with a recording range of 50 db. With the recording tape moving continuously, the microphone was moved along the circle having the compressor as its center, so that a diagram of the directivity of the discrete component of the noise was recorded. At the same time the signal from the output of the filter was fed to an integrator. The detector of the integrator was linear, so /11
that its output current was proportional to the amplitude of the sonic pressure. The time needed by the microphone to travel over the semicircle is much smaller than the time constant RC of the integrator circuit, so that the integrator,output voltage at the end of the measurement is proportional to the average amplitude of the sound pressure over the entire semicircle about the compressor. To achieve this, the microphone rotation rate was the same during all measure- /12
ments. The average pressure describes the sound radiation emanating from the compressor much better than measurements taken at one specific point.

During the runs, we monitored the compressor output by means of an anemometer, which measured the flow velocity in three points at the outlet; these three measurements were then averaged. In addition, the power consumption per volume of air delivered, as well as the rpm were recordered. All the accoustical measurements were relative, although calibration data could have been used to calculate the absolute sound pressure. The principal measuring error is due to differences in compressor operation, and possibly also to variations in atmospheric conditions. Narrow band measurements made in succession were reproducible to within 5%. Measurements made during different days and during different times of the day gave a greater scatter, so that the error of an individual measurement in the 4 cps band was as high as 1 db. The measurement error in a wider band was always less and never exceeded 5%.

Contribution to Noise by the Guide Vane Array

It can be seen from comparing Figs. 3a and 3b that when the guide vanes are removed (Fig. 3a), the discrete components of the noise disappear practically completely. With a guide vane array made up of 16 vanes (Fig. 3b), the intensity of the discrete components is approximately 26 db higher, and the overall noise level is by about 4 db higher than without the guide vanes. The entire noise increase in the wide band was produced by the discrete components. As can be seen from the directivity diagram for wide band noise (Fig. 4a) and for the discrete component (Fig. 4b) whose frequency is that of the first harmonic of the rotor $\omega = 2\pi Nz_1$, all the maxima of these diagrams fully coincide. The mutual correlation coefficient of diagrams of Figs. 4a and 4b is 0.87, which indicates an appreciable effect of the discrete component on the overall noise level.

Effect of the Vane Angle

The angle between the guide vanes and the radius of the disk of this apparatus was varied by using different vanes. It was possible to place three vanes in five specific positions (0, 12.5, 25, 37.5 and 50°) relative to the leading edge of the rotor blade. Since the number of blades was low, the sound field

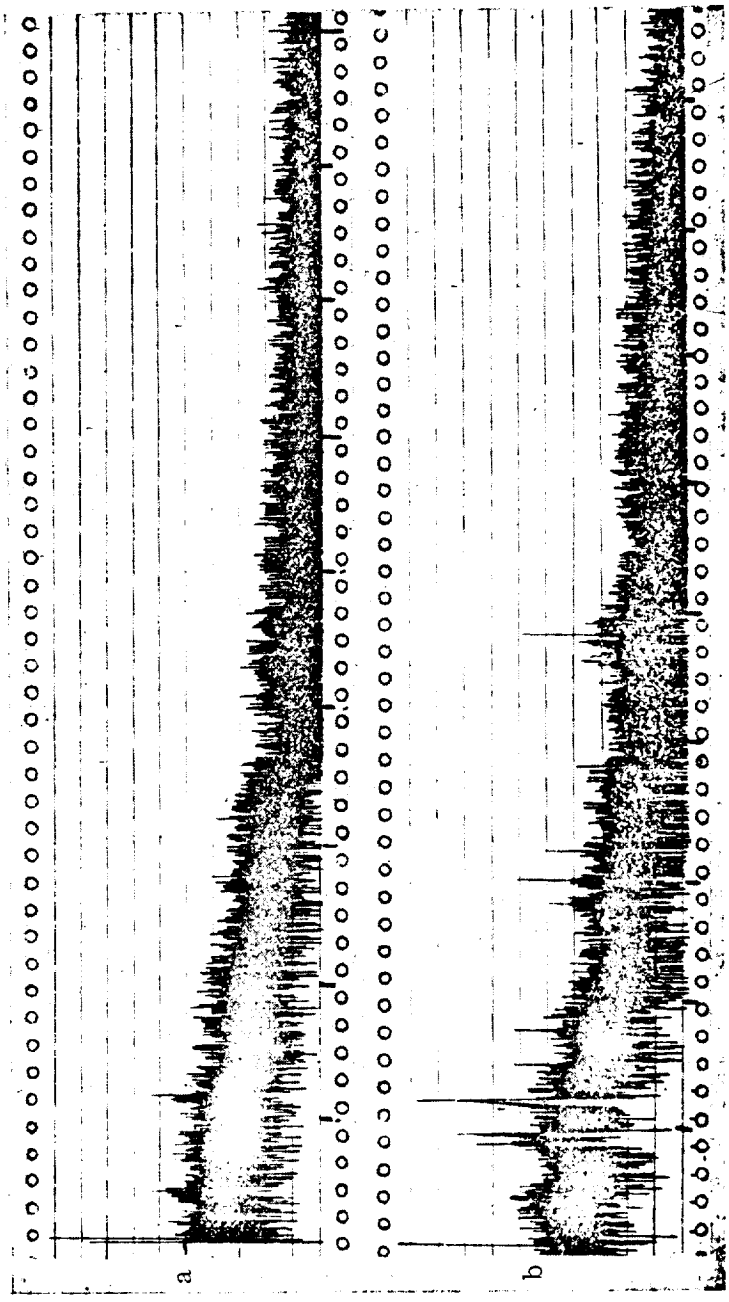

Figure 3. A Noise Spectrum. a) Without Guide Vanes; b) with Guide Vanes.

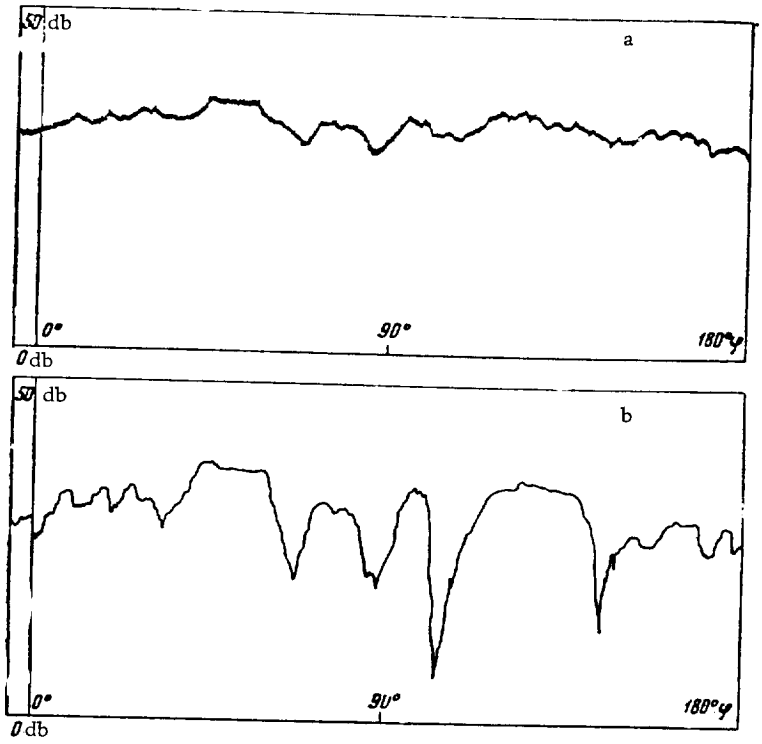

Figure 4. The Directivity of the Emitted Noise. a) In a Wide Frequency Band (20-20,000 cps); b) at the Frequency of a Discrete Component (4 cps Band, First Harmonic).

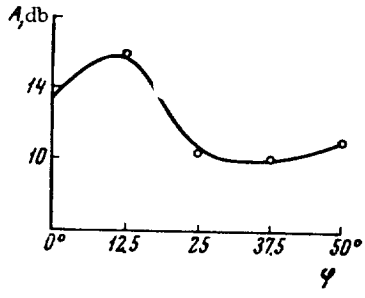

Figure 5. Discrete Component Intensity as a Function of the Guide-Vane Angle.

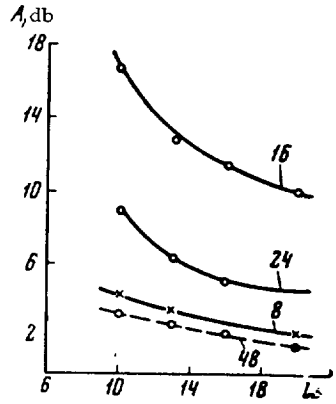

Figure 6. Discrete Component Intensity as a Function of Distance Between the Rotor and Stator at Various Numbers of Stator Vanes.

obviously could not have circular symmetry and the measurements were made by averaging at four positions of the guide vane apparatus, obtained by rotating /14
it by 0, 90, 180 and 270° about the compressor's axis. The sound pressure was measured in a narrow band at the frequency of the first harmonic of the rotor. As can be seen from the graph (Fig. 5), maximum radiation is observed at an angle of 12.5°, which differs somewhat from results obtained by Sharland [2]. This may be attributed to the fact that the rotor blades in our compressor were twisted, as a result of which their velocity field was displaced relative to the radius. In addition, according to our data, displacing the vane angle by 12.5° from the maximum radiation angle reduces this noise by 4 db, while according to Sharland this angle should be 20°. This is possibly due to the fact that Sharland has measured only one point in the field, for which this effect may be different from that averaged over a semicircle.

Effect of the Distance Between the Stator Disk and the Guide Vane Apparatus /15

The experimental guide vane apparatus used permitted to set up distances l between the rotor and stator of 10, 13, 16 and 20 mm and to vary the number of vanes (to insert 8, 16, 24 and 48 vanes). The results are presented in graphs (Fig. 6). It can be seen from these graphs that in all the cases, putting the disk from 10 to 20 mm away reduces the discrete wise component by 5-6 db.

Effect of the Number of Guide Vanes

It was shown in the theoretical part of this article that it is desirable to increase the difference between the number of rotor blades and stator vanes in order to reduce the discrete noise components. Here, however, no consideration was given to the effect of the air intake duct and the directivity of the radiation. Therefore it is desirable to experimentally check the effect of the ratios between the number of rotor blades and stators. The experimental guide vane devices used could be equipped with 2, 4, 6, 8, 12, 16, 24 and 48 vanes with the impeller blading held constant at 25 blades. It can be seen from Fig. 7 that the dependence of noise on the number of vanes is very appreciable. At 4000 rpm the maximum first-harmonic radiation took place when the stator had 16 vanes. As the distance between the rotor and stator is made larger, the radiation decreases. By

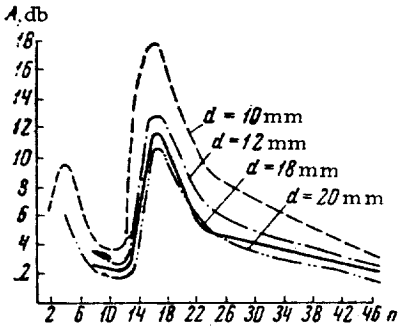

Figure 7. Discrete Component Intensity as a Function of the Number of Stator Vanes n for Various Distances d Between the Propellers.

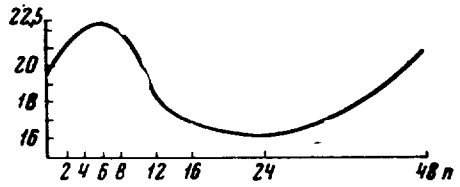

Figure 8. The Efficiency of a Stage as a Function of the Number of Stator Vanes.

increasing this distance and varying the number of guide vanes it becomes possible to reduce the radiation of the discrete component by more than 20 db, /16
i.e., to approach the sound radiation which is observed in a compressor with the guide vane apparatus removed.

Measurement of aerodynamic parameters shows that obtaining the same air flow rate with different numbers of guide vanes requires different power inputs. The efficiency of a compressor as a function of the number of stator vanes is shown in Fig. 8. It can be seen that the efficiency varies by as much as 20% as a function of this number. Comparing the graphs of Figs. 7 and 8 it is possible to obtain a compromise solution between noise and efficiency. However, in a real compressor the redesign of the guide vane apparatus of only the first stage will change the compressor efficiency very little, while the noise will be reduced appreciably (since the stages not immediately adjoining the compressor inlet make no appreciable contribution to the discrete components).

REFERENCES

1. Yudin, Ye. Ya. Issledovaniye shuma ventilyatornykh ustanovok i metodov bor'by s nim [Study of the Noise of Ventilation Units and Methods of Its Attenuation]. Trudy TsAGI, Issue 713, 1958.
2. Deming, E.A. J.A.S.A., July, 1940.
3. Hubbard, H.H. NACA, 1953. Technical Report 2968.
4. Richards, E.I. and I.J. Sharland. Sources of Noise in Axial Flow Fans. Fourth International Congress on Acoustics. Copenhagen, August 21-28, 1962.
5. Nemec, Dr. Jaroslaw. Eng. The Blading of Fans and Its Influence on Noise. Fourth International Congress on Acoustics. Copenhagen, August 21-28, 1962.
6. Sharland, J. J. Sound Vib. Vol. 1, No. 3, 302-322, 1964.

EFFECT OF THE DESIGN OF WALLS OF THE AIR INTAKE DUCT OF AN AXIAL COMPRESSOR ON THE PROPAGATION OF SOUND

D. V. Bazhenov, L. A. Bazhenova, Yu. V. Kravchenko and A. V. Rimskiy-Korsakov

ABSTRACT: The present article examines a method for simulating, under laboratory conditions, sound sources which have parameters close to those existing in axial turbocompressors with guide vanes. Thereupon the propagation of such sound over a coaxial waveguide with parameters close to those of a turbocompressor air intake duct is considered. The effect of resonators and active absorptive linings on the attenuation of sound propagating in the waveguide is also examined.

Abatement of noise from multi-stage axial compressors is of great practical importance. This can be done in two ways: 1) prevention of noise at the source; 2) prevention of its propagation. The first problem was discussed in [1], while the second is examined in the present paper. /17*

One of the methods of preventing noise from propagating from its source is its attenuation in the air ducts. This problem was examined extensively by a number of Soviet and Western authors. The pioneering work in this field was done by A. I. Belov [2, 3] who has formulated the problem of acoustic design of ventilation units and proposed basic methods for solving it. Among earlier efforts we should also note work by Yu. I. Shneyder [4] and S. P. Alekseyev [5] who have experimented with special cases of noise attenuation in ducts. Among later efforts we should note the work by Ye. Ya. Yudin [6, 7], which is both theoretical and experimental, as well as experimental work by R. D. Filippova [8, 9], which was performed under laboratory, as well as under actual operating conditions.

The basic types of sound attenuating air ducts are active (lined with porous, sound-absorbing material), and reactive. The simplest active sound attenuator is a duct with its inside surface lined with a sound absorbing material.

The attentuation of noise by the sound-absorbing lining of the duct can be calculated from A. I. Belov's formula /18

$$\delta = 1{,}1\,\frac{\varphi(\alpha)\cdot \Pi}{S}\,l\ [\text{db}],$$

*Numbers in the margin indicate pagination in the foreign text.

where l is the length of the lined part of the duct, in m; α is the material's absorption coefficient; π is the perimeter of the duct's cross section, in m; if (α) is an experimentally tabulated function; and S is the cross sectional area of the duct, in m^2. This formula was derived by Belov on the assumption that the acoustic energy is distributed over the air duct cross section just in the case of diffuse sound, i.e., with a uniform density. The wave pattern of sound propagation was not taken into account in deriving this expression. It was shown experimentally that the formula is in satisfactory agreement with experimental results for duct cross sections which are smaller than the wavelength of the sound and for sound-absorbing linings with low sound-absorption coefficients.

G. D. Malyuzhinets [10] has derived a more rigorous formula for calculating the attentuation of low-frequency sound waves in straight, lined ducts, with the wave nature of sound propagation taken into account

$$\Delta L = -8.6 \frac{\pi f}{c} \frac{d}{b^{1/3}},$$

where ΔL is the attenuation of sound per unit length; f is the frequency of the sound; and c is the speed of sound

$$d = \frac{R}{\frac{2\pi f}{c} a (R^2 + Y^2)}; \quad b = \left[1 - \frac{R}{\frac{2\pi f}{c} a (R^2 + R^2)}\right]$$

where a is the distance between walls, while R and Y are the real and imaginary parts of the normal impendance of the absorber.

This formula was checked experimentally by R. D. Filippova who has shown that it is applicable on the condition that $|G|ka \ll 3$, where $G = \rho c/Z$ is the reduced normal admittance of the system.

Investigating noise attenuation in air ducts by means of sound-absorbing liners over a wide frequency range under laboratory conditions (where the sound was produced by a loudspeaker), Ye. Ya. Yudin [17] has concluded that the attenuation per unit length of the lining is constant for most frequencies and over the major part of the sound-absorbing material. Yudin has suggested that engineering calculations be made on the basis of a table which gives the average attenuation per one unit line thickness when the duct is lined with absorbing material such as felt or VT-4 fiber:

TABLE /19

Thickness of sound absorbing material, mm	15	40	100	250
Attentuation, db/unit thickness	0.6	1.4	2.0	3.0

The author [Yudin] emphasizes that he has studied the noise from fans, whose noise spectrum is made up primarily of low-frequency components.

Units with large-size air ducts frequently use several parallel dampers of the lining type, i.e., a honeycomb silencer. To determine the attentuation

of such a silencer, composed of many identical cells, it is sufficient to calculate this quantity for one cell.

In addition to honeycomb dampers, use is also made of baffle-type dampers which consists of a number of sound-absorbing baffles placed in the duct parallel to the direction of flow. The sound attenuation in a baffle-type damper can be calculated from Belov's formula

$$\delta_{baf} = 2.2\alpha' \frac{l}{a} [\text{db}],$$

where α' is the sound-absorption coefficient of the lining, and a is the distance between baffles.

The use of honeycomb or baffle-type dampers makes it possible to increase the damping per unit length of sound-absorbing lining by reducing the distance between baffles, but this increases the hydraulic resistance of the damper, and consequently the compressors experience a head loss. With large air flow velocities in air shafts, these losses may be quite appreciable. The hydraulic resistance H can be calculated from

$$H = \zeta \frac{\rho v^2}{2g},$$

where ξ is the hydraulic resistance factor, ρ is the air density, v is the air velocity, and g is the acceleration of gravity.

The hydraulic resistance factor for a baffle-type damper has the form

$$\zeta = 2\left(\frac{\delta}{a+\delta}\right)^2 + \frac{\delta}{a+\delta} + \frac{0.015}{a} l,$$

where δ is the baffle thickness, and a is the distance between baffles (see [11]). To illustrate the above, Fig. 1 shows a curve obtained by simple engineering calculations using Belov's formulas.

The hydraulic resistance of the baffle-type damper (in mm H_2O), which /20
increases with the number of baffles (and, consequently, also with a reduction of their spacing) is laid off on the abscissa. The attenuation per unit length of damping lining for a lining absorption coefficient of 1 is laid off on the ordinate. The baffle thickness is taken as 50 mm, the air flow velocity as v = 60 m/sec. It can be seen from the graph that even at these low wind velocities, the head losses with baffle-type dampers can be quite appreciable.

In addition to active dampers, aerodynamic noise is frequently silenced by reactive dampers, which use the reflection of the sound to the source in branch resonators. Dampers of this type are superior to others in that they have low hydraulic resistance and do not require a porous, sound-absorbing material, the volume and weight of which must be quite high if it is to dampen low frequencies. The resonators can be either cavities whose dimensions are appreciably smaller than the sonic wavelengths, i.e., Helmholtz resonators, or branches the length of which is approximately 1/4 of the wavelength.

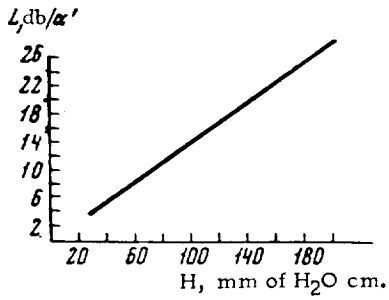

Figure 1. The Attenuation per Unit Length of Baffle-Type Damper as a Function of Its Hydrodynamic Resistance

If we disregard the active resistance of radiation and the attenuation by friction on the resonator walls, then the impedance of the resonator entrance at resonance frequency should be zero, so that the space velocity at the resonator entrance should be very high. Hence the amplitude of sonic vibrations which propagate through the duct should be attenuated. If the sonic frequency is such that only the zero normal wave of this frequency can propagate in the waveguide, then a single resonator would be able to fully reflect the sound wave toward the source. The more rigorous two-dimensional theory [12], which takes into account the fact that the sound needs some finite time to reach the resonator when starting from any point of the duct cross section not directly adjoining the entrance, shows that even for zero impendence the damping is finite and is equal to approximately 14 db per unit graduation.

The pioneer in the field of theory and technology of resonance sound absorptions is by all counts S. N. Rzhevkin. His resonators make use of the fact that, on resonance, the rate of vibration of air at the resonator entrance exceeds the vibratory velocity in the free space by many times. Hence, if a layer of sound absorbing material is placed in the resonator entrance, i.e., at /21
the point where the rate of vibration air molecules is at maximum, then the absorption properties of the system will be very much enhanced.

The maximum absorption for a single resonator with resonance frequency f_0 is

$$A_{\max} = \frac{1}{2\pi}\left(\frac{c}{f_0}\right)^2,$$

where

$$f_0 = \frac{c}{2\pi}\sqrt{\frac{S}{l_k V}}.$$

Here c is the speed of sound, S is the cross-sectional area of the resonator entrance, V is the resonator volume l_k is the equivalent entrance length (for a circular neck with radius r $l_k = l = 1.57r$). Single resonators are capable of appreciable sound absorption only in a narrow frequency band near resonance. A much wider frequency range can be obtained by single- or multi-layer resonant dampers, which were designed by Rzhevkin and V. S. Nesterov [13]. The damper provides for satisfactory damping ($\alpha > 0.5$) in the frequency range of 400-4000 cps.

Of particular interest in damping of aerodynamic noise are simple resonant dampers in the form of pipe branches closed at the other side, which can be used for damping low-frequency noise with discrete components. An

experimental study of such dampers was performed by Yudin together with A. G. Munin [15] and Filippova [9] at frequencies at which the wavelength was greater than or equal to the duct width. The sound source was a dynamic microphone, to which a signal was supplied from a tape recorder or signal generator. The studies showed that all the damping curves of the duct with branches have a clearly expressed resonance character with odd harmonics; here the maximum damping at the fundamental resonance frequency is from 6 to 12 db per unit.

It should be noted that complete reflection of sound to the source with branch resonators is possible only when the sound in the duct slides along the resonator opening. No sound absorption takes place at normal incidence in a resonator without damping. Thus, the reflection will be complete if the sound frequency is such that only a zero normal wave of this frequency can propagate in the waveguide. On the other hand, if higher order modes can /22
also propagate in the waveguide, then the quarter-wave branch will not be an ideal reflector, but should be treated as some sort of discontinuity in the waveguide wall.

As was shown by A. D. Lapin, the presence of a discontinuity (in our case of a branch resonator) results in redistribution of the sound wave energy in the waveguide space beyond the resonator. This redistribution proceeds in a direction such that the higher natural modes of the waveguides become more intense. Thus a branch resonator serves as some kind of converter, which transforms the excitation of low natural modes of the waveguide into high modes. This phenomenon may be useful for sound attenuation, since the high modes, which are multiply reflected from the waveguide walls on their propagation, can be successfully absorbed by the sound-absorbing lining of the duct.

The study of feasibility of maximum sound damping in short waveguides, i. e., in guides whose length is commensurable with their diameter, acquires high importance in reducing the noise of axial compressors. Presently available turbo compressors use an intake duct for sucking in the air. The overall dimensions of these ducts are such that they should be regarded as short waveguides. Roughly speaking, such an intake duct consists of two concentric pipes between which the sound propagates. The diameter of the outer pipe varies from 40 cm to 1 m, while the length is usually 50-60 cm. The annular space between the inner and outer pipe is usually 15-25 cm. It is desirable to use the sound propagation in this space to reduce the sound radiation by the compressor.

Assuming that the pipes are lined with material with absorption coefficient $\alpha = 0.8$ and an applying Belov's formula, we will get that the expected sound attenuation for an annular space of 15 cm will be about 10 db over the entire air intake duct. However, if Yudin's formula is used, then the sound attenuation (with the same data) is only 4 db. Hence it seemed expedient to make an experimental study of the propagation and damping of sound in intake ducts such as compressor air intakes, taking into account the specifics of sound generation (guide vane apparatus and impeller), as well as the frequency region of the highest sound intensity in real compressors. For this purpose we

designed an experimental setup in which it was possible to simulate the mechanism of sound excitation in a turbocompressor with guide vanes, and to study propagation and damping in a coaxial space which simulates the intake duct of a turbocompressor.

The Experimental Setup and Measuring Techniques /23

The propagation of sound in short air intake ducts with impedance walls was studied in a setup which made it possible to approximately simulate the operation of a compressor air intake duct.

The test space in such a duct was formed by an outer and inner pipe. If necessary, the inner pipe could be easily removed. The pipe bodies were made from wood slats held together by circular metal hoops. The inside surface of the outer pipe was lined by 2 mm thick textolite sheet. The inner tube was also lined with sheet textolite along its outer diameters. The spaces between slats of the outer pipe were carefully stuffed with cotton; in addition, the entire pipe was sheated from the outside by a 20 mm thick Prolon sheet. This prevented sound from penetrating outside the test space. The inner pipe was rigidly connected to the outer one by means of pins which were seated in the metal hoops. Rows of 48 mm deep holes were drilled in the slats of the outer and inner pipes. The hole diameters in the outer pipe were 15 mm, while in the inner they were 10 mm. These rows of holes form a system of branching resonators, whose effectiveness we wanted to determine. The branches were of adjustable height. Some resonator rows could be closed partially or completely by means of 20 mm thick Prolon sheets. Guides for the coordinate bar were placed between two slats of the outer pipe. The measuring microphone was fastened to this bar, which made it possible to move the microphone smoothly along the pipe axis. The bar had markings for positioning the microphone. The microphone could be placed in different points of the test space by means of interchangeable adapters of different length. Sound was produced in the test space by means of loudspeakers placed in a rigid foam plastic box with dimensions of 800 x 800 x 800 mm^3. The loudspeakers which were mounted on a reflecting board, radiated virtually exclusively into the test space, since the box itself was sound-absorbing. The air duct model was rigidly connected to the loudspeaker box through a Prolon adapter-gasket. To perform the experiment it was necessary to smoothly rotate the measuring microphone along a circle at the air intake inlet. For this purpose a sleeve was pressed into the metal hoop of the inner pipe. A balanced beam, on which the microphone was tightly fitted, was placed on the axis of this sleeve. The system was connected to the shaft of an electric motor by a flexible coupling.

The design of the inner pipe and the geometric dimensions of the air duct model were close to those encountered in real compressors. The general view of the air intake duct model is shown in Fig. 2 .

A major part of the work was simulating the sound-generation mechanism /24
of a stage of a compressor with a guide vane apparatus. A 24-channel electronic commutator was used as the model.

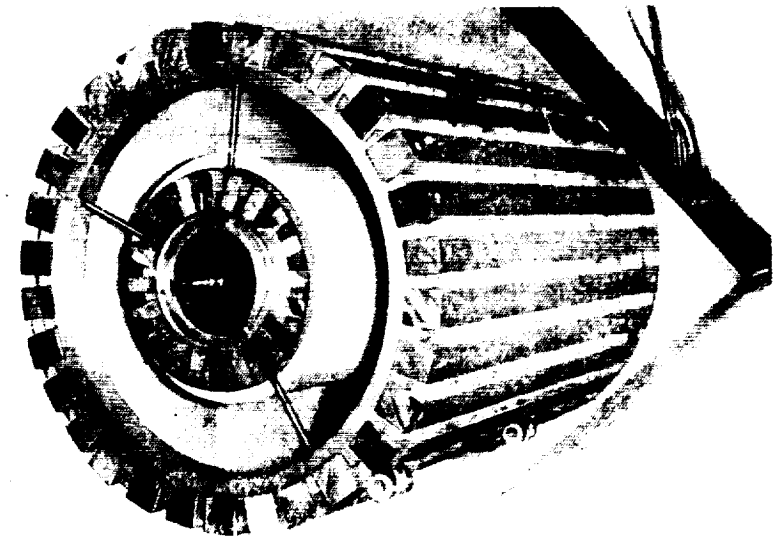

Figure 2. Model of Air Intake Duct.

In an operating compressor a sound pulse is produced whenever the rotor blade intersects a guide vane wake. The problem thus reduced to obtaining sound pulses formed on intersection of the wake of a stationary vane by a moving blade. The structure of the model was as follows. A frame with 24 lamps located along a circle was fastened on the end of the housing of a DC motor. Each lamp simulated a guide vane. Then a disk with 25 slits was fastened on the motor shaft. The slits simulated the rotor blades of a real compressor. It should be noted that the number of light sources and slits on the disk is close to the number of guide vanes and blades of the first-stage rotor of an ordinary turbocompressor. Another frame with 24 devices for converting the light signals into electrical signals was situated directly in the back of the rotating disk. These were photodiodes with a very high sensitivity and response. When the motor rotated the solid parts ("teeth") of the rotating disk intermittently shields or uncovers the light source for a given photodiode, thus producing voltage /25
pulses. The pulse frequency could be varied over a wide range by changing the motor rpm. The pulse generated in each photodiode was fed to the grid of an appropriate tube, which served as a power amplifier. The power amplifier loads were small electrodynamic loudspeakers. All the 24 loudspeakers, which were located on a circle and were phased by this electronic commutator, supplied sound to the test space of the air duct model. The radiation intensity was continuously adjustable from 0 to 150 milliwatts. Each commutator channel thus consisted of a light source, a photodiode, a power amplifier and a loudspeaker. A schematic of one such channel is shown in Fig. 3. Since the loudspeakers may have different acoustic outputs, each channel was calibrated. For this the measuring microphone was placed opposite each loudspeaker at a specified distance from it and the acoustic output was equalized by adjusting the electrical sensitivity of the channels. The loudspeakers were mounted on a plywood reflecting board 12 mm thick along a circle 460 mm in diameter. The reflecting board served as the front wall of the infinite baffle enclosure.

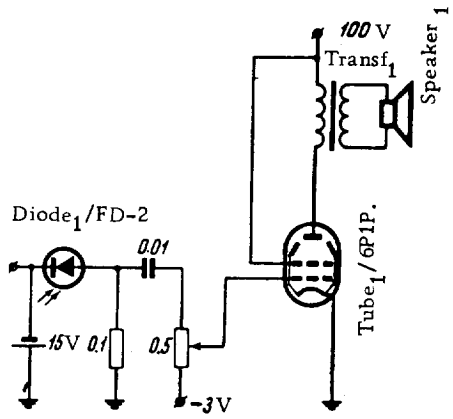

Figure 3. Schematic of One Channel of the Electronic Commutator.

The Experimental Procedures

1. Plotting the sound pressure distribution along the axis of the air intake duct model.

The block diagram for read-off of the sound pressure distribution along the axis of the model is shown in Fig. 4. The microphone was placed by means of one of the adapters on the coordinate bar, which is used for moving it smoothly along the axis of the test space when taking the readings. The position of the microphone in this space is determined from markings on the bar and is recorded by a pen on the level-recording tape. As a result, a curve of the sound pressure distribution as a function of the distance along the axis of the model is obtained on the recording tape. To eliminate /26 the effect of waves reflected from walls of the room, provisions were made for closing the intake section of the air intake duct by a sound-absorbing pad and for reading the pressure distribution pattern by the above method.

2. Obtaining averaged characteristics of the energy radiated by the duct's inlet section.

The block diagram for obtaining the frequency characteristics of the energy radiated by the pipe inlet section, averaged over the cross section, is shown in Fig. 5. The measuring circuit includes an integrator with a dynamic range of 50 db whose integration time can be varied from 1 to 100 seconds.

As was pointed out above, the model was designed so as to make it possible for the measuring microphone to rotate at a constant speed in the plane of the pipe's intake section. The level recorder's motor was used as a drive for obtaining this motion. The signal from the microphone in the frequency band of 1000-5000 cps was averaged by the integrator per one full revolution of the microphone. The time needed for a revolution was 15 seconds. Since the time constant of the charging circuit of the integrator is much greater than the integration time, the averaging accuracy was at least 3%.

The integrator start was synchronized with the start of the microphone travel, and the reading was taken on a dial instrument after the end of the cycle. Simultaneously with this, the level recorder was drawing diagrams of the sound pressure distribution in the plane of the pipe inlet section. The measurements were taken on the test space of the model in the following arrangements: a) space fully closed off by sound-absorbing material; b) space 2/3 closed off by sound-absorbing material; c) all the rows of branch resonators in the test space open; d) some branch resonators in the test space open.

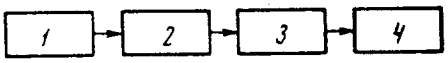

Figure 4. Block Diagram of Pressure Measurements Along the Model's Axis. 1) Microphone; 2) Amplifier; 3) Analyzer; 4) Level Recorder.

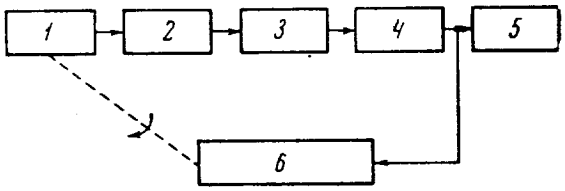

Figure 5. Block Diagram for Averaging the Readings over the Model's Cross Section. 1) Microphone; 2) Amplifier; 3) Analyzer; 4) Integrator; 5) Indicator; 6) Level Recorder.

The sensitivity of the measuring channel was calibrated in the process of measurements by supplying a constant-amplitude 1000 cps signal. The error of the measuring channel used was not more than 3 db.

Experimental Results /27

The experiment was set up to determine means for appreciably reducing the sound while it was passing through the model of a turbocompressor intake duct. As was pointed out in the introduction, the difference between the present experiment and those performed by other authors consisted in the fact that the excitation produced by the sound source was not arbitrary, but fully defined and close in its properties to that actually prevailing in turbocompressors with vane guides. The importance of this kind of excitation is highly obvious, since the damping along a pipe with active impedance walls will depend appreciably on the predominant modes excited by the sound source.

The basis of the experiment was measurement of the average sound pressure over the entire open inlet section of the air intake duct at different motor rpm. Since changing the motor rpm also changes the frequency of radiation of the rotor, first harmonic, which was the principal variable measured in the experiment, the curve of the average sound pressure over the inlet section as a function of the motor rpm can be easily represented as a frequency curve.

The experiments were performed by comparing the frequency curve obtained at the inlet section of an air duct with rigid walls, with that obtained at this section in an inlet duct whose walls were lined with an active sound-absorbing material (20 mm Prolon sheet). The absorption coefficient of this material for diffuse sound incidence in the frequency range under study was 0.8-0.9.

The experimental results are shown in Fig. 6 with the excitation frequency on the abscissa and the logarithm of a quantity proportional to the sound pressure averaged over the entire intake section of the duct on the ordinate. The graph shows three curves. Curve 1 is for a duct with rigid walls, curve 3 is /29 for a duct fully lined with Prolon, while curve 2 is for a duct lined only over two thirds of its length, i.e., for approximately 60 cm. The remaining part of the duct was not lined, and thus had rigid walls.

As can be seen from the graphs, when the sound-absorbing material was placed over the entire length (1 m), the sound pressure was attenuated by an

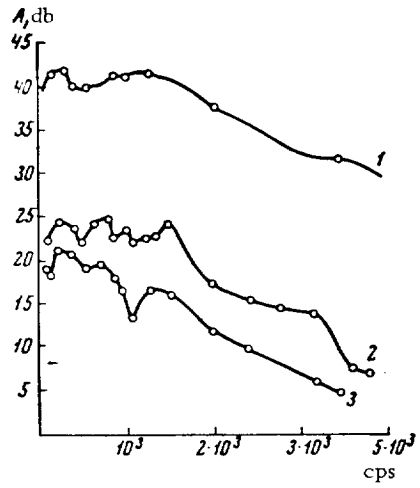

Figure 6. Effect of Sound Absorption by the Walls of the Model.

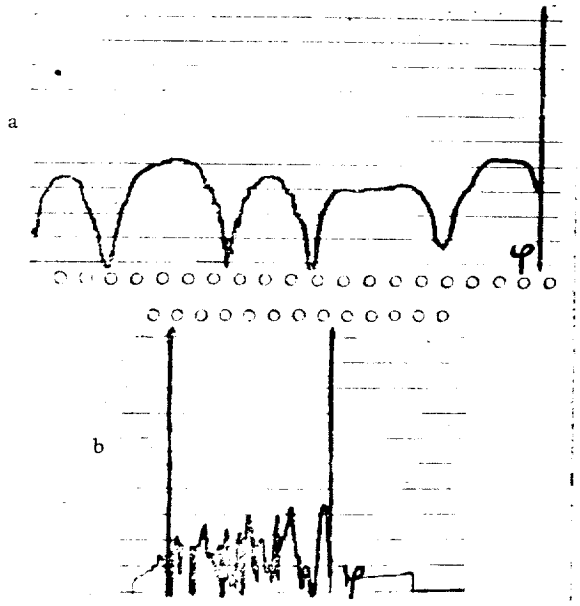

Figure 7. The Sound Pressure as a Function of the Polar Angle at the Model Outlet.

average of 25 db over the range. On the other hand, when only a part of the duct was lined, the attenuation was naturally less and equal to only 19 db over the range in question.

Comparison of experimental data with those computed from Belov's or Yudin's formulas shows a high degree of disagreement. The appreciably higher sound absorption than predicted theoretically is attributable to two causes. The first are the specifics of the excitation used in the experiment, while the second is attributable to the fact that we have studied a comparatively high frequency range in which even the relatively thin Prolon layer was a satisfactory damper.

The complexity of the excitation uses is reflected directly in the pattern of the sound field existing in the air ducts. To illustrate this, Fig. 7 shows the sound pressure at the inlet section of the duct as a function of the polar angle φ over a circle with a constant radius. The logarithm of the sound pressure is laid off on the ordinate axis, while polar angle φ is laid off on the abscissa.

Figure 7a shows the sound pressure as a function of angle φ for an excitation frequency of 1000 cps, while Fig. 7b shows the same relationship for 4000 cps. The presence of the many minima and maxima points to the fact that a large number of higher resonance modes of the duct are excited. This is also shown by the complex distribution of minima and maxima when measuring the pressure along the pipe axis.

Figure 8 shows the sound pressure distribution along the duct with rigid walls for an excitation frequency of 2400 cps (Fig. 8a) and 1850 cps (Fig. 8b). Despite the complexity of the pattern it is still possible to state that there is practically no attenuation on propagation along the pipe. The marks on the graph correspond to moving the microphone along the pipe in steps of 10 cm. The position of the sound source is also marked directly on the graphs.

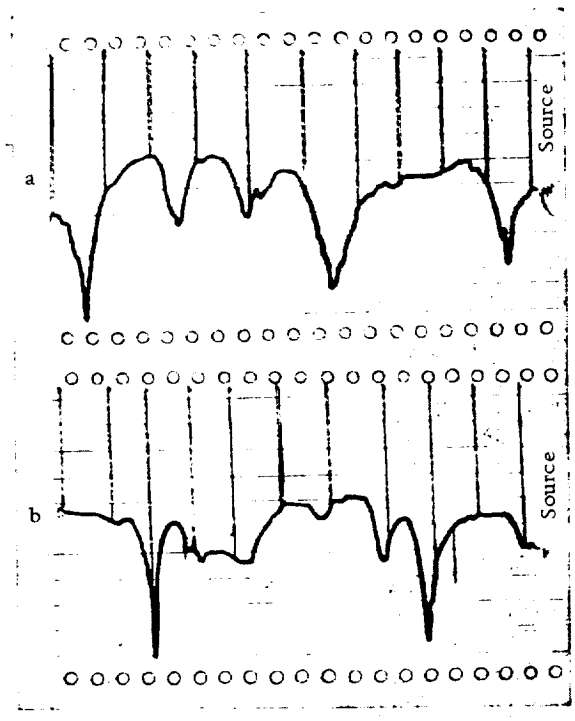

Figure 8. Distribution of Sound Pressure Along a Model with Rigid Walls. a) 2400 cps; b) 1850 cps.

Figure 9 shows the sound pressure distribution along a duct with lined walls. As can be seen from comparison of Figs. 8 and 9, the presence of the Prolon liner has no appreciable effect on the sound field in the immediate vicinity of the source (the absolute level is the same), but appreciably increases sound attenuation along the lined duct. Consequently the pressure drop at the /30
pipe inlet section of a Prolon-lined air intake, which is shown in Fig. 6, is the result of sound absorption in impedance walls, rather than that of reduction in the sound output of sources.

As was pointed out above, the resonators should transform the low modes excited in the waveguide into higher modes after the sound wave passes the resonator. In turn, the higher modes should be more effectively absorbed by active dampers as the sound propagates further down the waveguide.

The effectiveness of the resonators was checked by comparing the sound attenuation in a coaxial waveguide equipped with several rows of resonators located along the circumferences of the outer and inner pipes with the attenuation of sound in a similar waveguide, but without resonators. In both cases the entire surface of the waveguide walls free of resonators was lined with a sound- /31
absorbing material. The measuring procedure consisted in measuring the average pressure over the entire waveguide section (at the outside section of the waveguide) as a function of the excitation frequency.

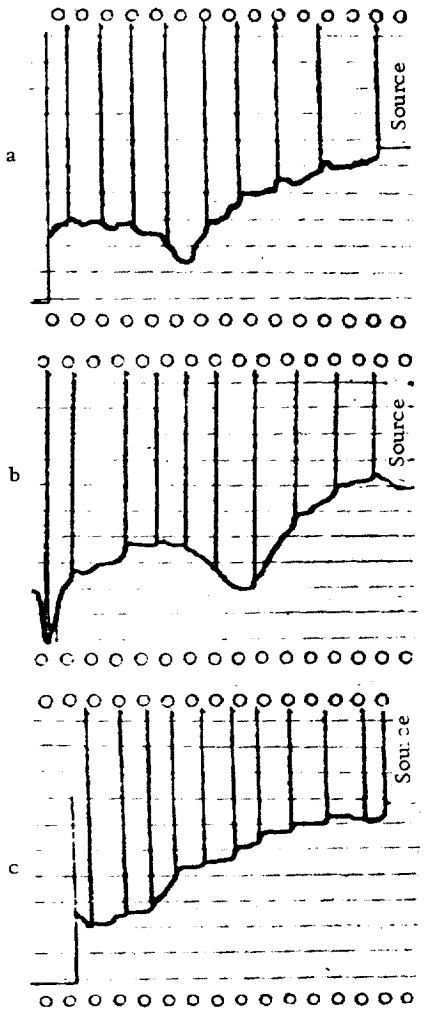

Figure 9. Distribution of Sound Pressure Along a Model with Absorbing Walls.

Figure 10. Sound Pressure Averaged over the Outlet Cross Section of the Waveguide as a Function of the Frequency. 1) Without Resonators; 2) with Resonators.

The experimental results are depicted in Fig. 10. The logarithm of a quanitity proportional to the average sound pressure was laid off on the ordinate, while the excitation frequency was plotted on the abscissa. Curve 1 pertains to the case of a waveguide without resonators, while curve 2 is for a waveguide with resonators. The resonators were tuned to 1400 cps and had a Q-factor of 6-8. Here we should note that the frequencies to which the resonator was tuned, as well as the Q-factors, were measured on a separate resonator situated in free space. It is therefore possible that due to the changed conditions under which radiation emanates from the open end of the resonator when the latter is placed in the duct, both its Q-factor and the tuning frequency change, but apparently this change is insignificant with one waveguide demension. /32

It can be seen from examination of Fig. 10 that in the case of a waveguide with resonators (of which there were 140) and f = 1500 cps, an insignificant increase in attenuation is observed as compared with damping in the absence of resonators. This increase, which amounted to 2.5 db, lies on the borderline of experimental accuracy and hence more refined experiments are needed to clarify the qualitative effect.

From our point of view the smallness of the effect noted may be due to the fact that the excitation source had a complex phasing and apparently excited primarily higher modes, which were absorbed successfully even without the resonators.

The following conclusions can be drawn from our experiment:

1. The use of Prolon coatings on walls of compressor air ducts shows great promise with respect to sound attenuation and can result in a noise reduction by 15-20 db.

2. The use of branch resonators for increasing the damping of sound at discrete frequencies cannot be regarded as a good method due to the small effect obtained and the difficulties in producing branches with proper frequency tuning.

REFERENCES

1. Bazhenov, D. V., et al. A Study of Discrete Components of the Noise Spectrum of an Axial Compressor. First article in present collection.
2. Belov, A. I. Ob akusticheskom raschete ventilyatsionnykh ustroystv [On Acoustical Design of Ventilation Units]. Zh. Tech. Fiz., Vol. 8, No. 7, 1938.
3. Belov, A. I. and N. D. Faynshteyn. Eksperimental'noy issledovaniye zaglusheniya zvuka v ventilyatsionnykh kanalakh [Experimental Study of Sound Attenuation in Ventilation Ducts]. Zh. Tech. Fiz., Vol. 8, No. 16, 1938.
4. Shneyder, Yu. I. Bor'ba s shumom v ventilyatsionnykh kanalakh promyshlennykh i obshchestvennykh sooruzheniy [Reduction of Noise in Ventilation Ducts of Industrial and Public Buildings]. Zh. Tech. Fiz., Vol. 8 No. 18, 1938.
5. Alekseyev, S. P. Shum ventilyatsionnykh shakht metro i bor'ba s nim [Noise of Ventilation Shafts of Subways and Its Reduction]. Zh. Tech. Fiz., Vol. 7, No. 3, 1937.
6. Yudin, Ye. Ya. Glushiteli ventilatornogo shuma v vozdukhovodakh [Dampers of Fan Noise in Air Ducts]. In the collection Promyshlennaya aerodinamika [Industrial Aerodynamics]. B. N. I. TsAGI, No. 3, 1947.
7. Yudin, Ye. Ya. Issledovaniye shuma ventilyatsionnykh ustanovok i metodov bor'by s nim [Study of Noise of Ventilation Facilities and of Methods for Reducing It]. Trudy TsAGI, Issue 713, 1958.
8. Filippova, R. D. Eksperimental'noye issledovaniye modeley glushiteley s nasypnym poglotitelem [Experimental Study of Silencer Models Using Bulk Damping Materials]. In the collection Promyshlennaya aerodinamika [see item 6], No. 18, 1960.
9. Filippova, R. D. and Ye. Ya. Yudin. Eksperimental'noye issledovaniye glushiteley v vide trub s otrostkami [Experimental Study of Silencers in the Form of Pipes with Branch Resonators]. In the collection Promyshlennaya aerodinamika [see item 6], No. 18, 1960.
10. Malyuzhinets, G. D. and R. D. Filippova. Rasprostraneniye zatukhaniya zvukovykh voln nizkikh chastot v pryamykh oblitsovannykh kanalakh [Propagation of the Attenuation of Low-Frequency Sound Waves in Straight Line Ducts]. In the collection Promyshlennaya aerodinamika [see item 6], No. 18, 1960.
11. Idel'chik, Ye. I. Gidravlicheskiye soprotivleniya [Hydraulic Resistances]. Gosenergoizdat. Moscow-Leningrad. 1964.
12. Cremer, L. Theorie der Luftschall-Dämpfung im Rechteckanal mit schluckender Wand und das sich dabei ergebende höchste Dämpfungs.

[Theory of Sound Damping in a Rectangular Channel by Absorbing Walls and the Highest Damping Achievable Therein]. Acustica, 3, 1953. Akustische Beihefte, H. 2, 264-270.

13. Rzhevkin, S. N. and V. S. Nesterov. Rezonansnye zvukopoglotiteli dlya stroitel'noy praktiki [Resonance Sound Absorbers for the Building Trades]. Trudy sektsii elektroakustiki i zvukozapisi NTO im. A. S. Popova [Transactions of the Electroacoustics and Sound Recording Section of the A. S. Popov Scientific and Technical Society]. 1947.
14. Yudin, Ye. Ya. and A. G. Munin. Eksperimental'noye issledovaniye rezonatornykh glushiteley [Experimental Study of Resonance Dampers]. In the collection Promyshlennaya aerodinamika [see item 6], No. 10, 1958.

EXPERIMENTAL STUDY OF THE EFFECT OF ROUGHNESS OF A SURFACE OF A BAR ON THE INTENSITY AND FREQUENCY OF VORTEX SOUND

D. V. Bazhenov, L. A. Bazhenova and A. V. Rimskiy-Korsakov

ABSTRACT: The present article deals with the effect of different rough surfaces of a bar on the intensity and frequency of the vortex sound generated by it as it moves through air, and on its aerohydrodynamic head drag. Described are tests of smooth cylindrical bars, bars covered by brass mesh or a perforated brass tube, as well as grooved bars (bars were rotated in the "windmill" or "squirrel-cage" fashion).

It is known that vortex sound is produced whenever a body moves through a liquid or gas. The study of this sound is of theoretical interest for clarifying some problems of fluid flow, and is of practical importance for control of noise. Vortex sound usually predominates in the noise of fans, pumps and other fast-moving machinery parts. /34*

As far as its spectrum is concerned, vortex sound is a relatively wide-band noise with a maximum at the frequency

$$f = \varkappa \frac{v}{r},$$

where v is the flow velocity, d is the characteristic dimension of the body (for a sphere or cylinder d is the radius, for a plate with width l and thickness b and situated at an angle φ to the flow, d = l sinφ + b cosφ), x is the Strouhal number, which is a function of the shape of the body and of the Reynolds number.

On the other hand, since the maximum frequency of vortex sound is equal to the frequency with which the eddies separate from the body, f can be represented in the form

$$f = \frac{v - u}{l},$$

where u is the velocity of the eddies relative to the body, and l is the distance between the eddies. /35

*Numbers in the margin indicate pagination in the foreign text.

Karman and Rubach [1] related the drag of a body to the same quantities (i.e., to l and u). According to their formula, the head drag coefficient is

$$\psi = \left\{0.799\frac{u}{v} - 0.323\left(\frac{u}{v}\right)^2\right\}\frac{l}{d}$$

It can thus be expected that given the same characteristic dimensions of the body and the same body velocity but different drags, the vortex frequency maximum should change.

As to the expression of the vortex sound intensity, it can be written in the form

$$I \sim \frac{ldv^n}{r^2},$$

where r is the distance from the radiator to the measurement point; n according to various authors lies between 6 and 8 (the formula is qualitative).

As to the intensity of vortex sound accompanied by head drag, it would at first sight appear that the intensity should be proportional to the drag. However, this is not always so. For example, it was shown by measuring the intensity of vortex sound generated by a diagonally placed bar of rectangular cross section that in the velocity range from 20 to 45 m/sec it is lower than the intensity of a circular cylinder of the same diameter. At the same time, the head drag of a rectangular cross sectional bar is appreciably higher. On the other hand experiments with bars with rough surfaces, produced by milling grooves in the bars, show that this kind of surface reduces the intensity of vortex sound while at the same time reducing the head drag. The feasibility of reducing the noise of fans by use of corrugated blades (which reduce the dimensions of eddies separating from the blades), was pointed out by Berthold [2] as early as in 1931. However, this suggestion was not followed up.

In view of the above it is of interest to determine the possibility of sound attenuation by means of rough coatings of different kinds and to clarify the effect of these coatings on the head drag.

The Experimental Setup and Principal Results of Measurements

The intensity and frequency spectrum were measured on rotating cylindrical bars. The first measurements were made for bars rotating in "windmill" fashion. The measuring setup is shown in Fig. 1. The bars (2) were rotated by a /36
DC motor (1) through a shaft with a flexible clutch. The rpm could be adjusted from 1000 to 3000 and was measured by a tachometer. The sound pressure was detected by a MK-5A condenser microphone (3) and was fed through wide-band amplifier (4) to a N-110 level recorder equipped with a 50 db potentiometer. When recording the frequency curve of the vortex sound, the signal from the amplifier was fed to an analyzer produced by Marconi Instrument Co. (5) and only then to the level recorder (6). The response of the equipment did not change in comparative measurements. The microphone was placed on an extension of the axis of revolution of the bar under study, i.e., in the direction

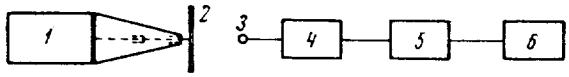

Figure 1. Schematic of a Setup for Measuring the Noise of a "Windmill."

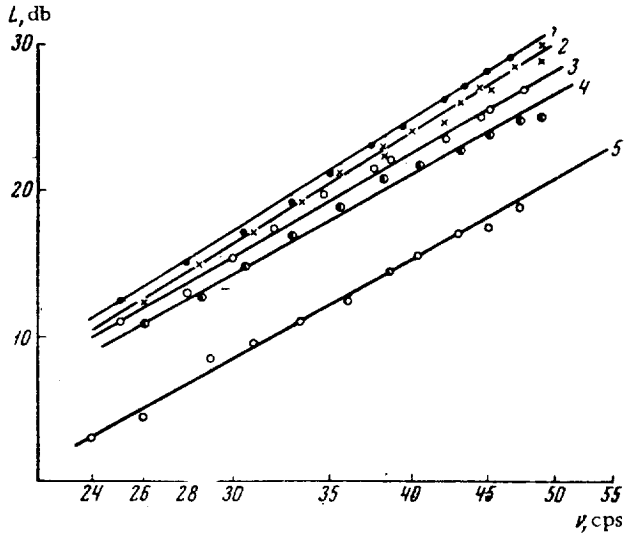

Figure 2. Noise of a Bar. 1) Smooth Bar, 1.8 cm in Diameter; 2) Smooth Bar, 1.2 cm in Diameter; 3) Smooth Bar, 0.95 cm in Diameter; 4) Grooved Bar, 1.2 cm in Diameter; 5) Mesh-Covered Smooth Bar, 1.2 cm in Diameter.

of maximum radiation of vortex sound and of absence of rotation sound. We have measured the level of the vortex sound produced by bars with length $\underline{1}$ = 37 cm and diameter of 1.2 cm. The bars either had smooth surfaces or were covered with metal mesh with 3 x 3 mm holes.

The metah mesh adhered tightly to the bar and was fastened on it by means of wood screws at the bar ends. The curve of the sound intensity as a function of the frequency is shown in Fig. 2. The graph was constructed on the basis of averaged data. The standard deviation of a single measurement was 0.9 db. The relative location of the microphone was the same for both bars.

It can be seen from Fig. 2 that the mesh placed on the bar surface quite appreciably reduces the intensity of the vortex sound produced by the rotating bar. Thus, when the bar is covered with a mesh with 3 x 3 mm holes the noise reduction was 7-8.5 db in the range of rotation rates under study. The cause of this should apparently be sought in the reduction of dimensions of eddies because of the presence of rough spots on the bar surface.

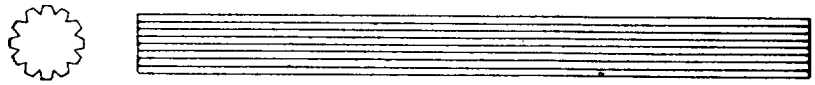

Figure 3. A Grooved Bar.

In another series of experiments, the bar surface was made rough by milling transverse and longitudinal grooves on it. The bars were 37 cm long and 1.2 cm in diameter, with grooves 1 mm wide and 1 mm deep; the distance between the transverse or longitudinal grooves was 3 mm (Fig. 3). The graph (Fig. 2) presents the results of sound intensity measurements for a grooved bar (curve 4). It can be seen from the graph that grooving of the bar reduces the vortex sound level by 3 db.

We have measured the intensity of the vortex sound as a function of revolution of bars with grooves of different depth (0.25, 0.5 and 1 mm). The measurements showed that the deeper the grooves, the greater the reduction in the vortex sound pressure; however, this reduction is only moderate in absolute terms. /37

In order to make sure that the noise reduction due to grooves was not merely due to effective reduction of the bar cross section, we have measured the dependence of the vortex sound intensity on the frequency for bars of the same length (l = 37 cm) and different diameters (d = 9.5 mm, 12 mm and 18 mm—Fig. 2, curves 3, 2, and 1, respectively).

The graphs demonstrate that the reduction of the noise level due to surface roughness is appreciably greater than that due to reducing the diameter by almost a factor of two).

In order to determine the aerodynamic drag of bars with rough surfaces we have measured the power consumed by the motor in rotating the bars. For this purpose we have first measured the motor efficiency as a function of load torque at 25, 30, 35, 40 and 45 rps, and then we measured the load torque produced by each of the bars being tested at the same rps. The graph thus obtained is shown in Fig. 4. /38

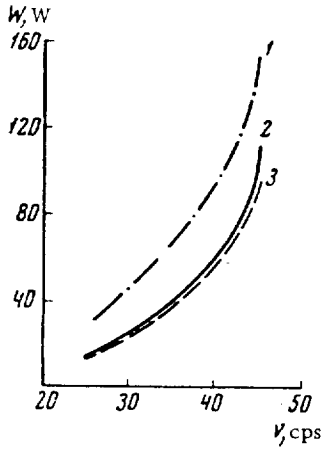

Figure 4. Power Consumed for Rotating the Bar. 1) Bar Covered with Mesh; 2) Grooved Bar; 3) Smooth Bar.

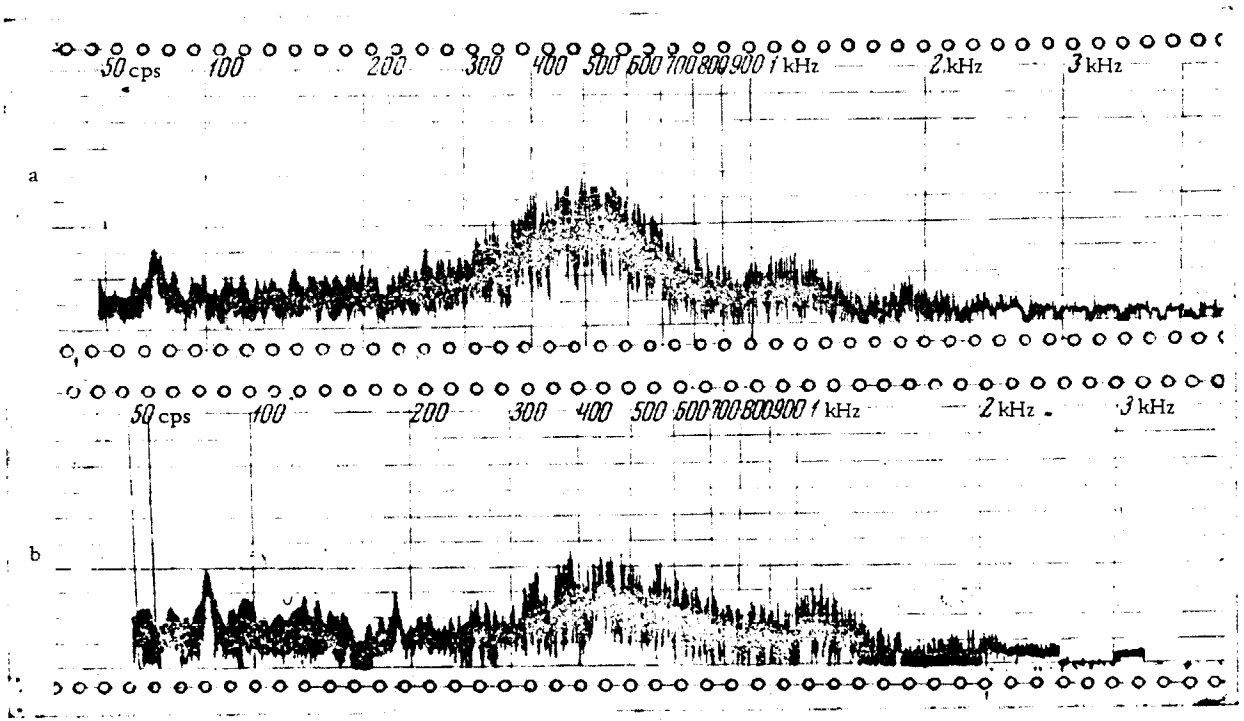

Figure 5. Noise spectrograms. a) For a Smooth Bar; b) for a Bar Covered with a Mesh with 3×3 mm^2 Holes.

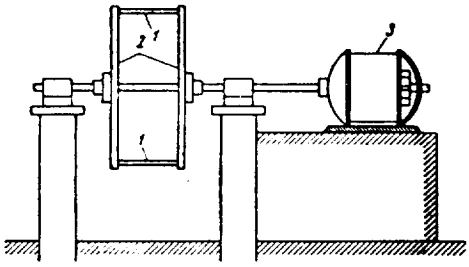

Figure 6. Device with Two Rotating Bars. 1) Bar; 2) Disks; 3) Electric Motor.

It can be seen that the power used by the motor when rotating a smooth bar (curve 3) and a grooved bar (curve 2) is virtually the same; however, in the case of the mesh-covered bar (curve 1) the power consumption, which means also the resistance to the air flow, increases.

With all the above bars, we also measured the frequency spectra of vortex sound at different rotational speeds. The spectrogram shown in Fig. 5 for a smooth bar (5a) and a bar covered with a mesh with 3 x 3 mm^2 holes (Fig. 5b) are typical. The spectrograms show graphically the effectiveness of using such a coating for reducing the vortex sound level.

By virtue of the fact that the noise reduction on grooved bars is not accompanied by an increase in the aerodynamic drag, the subsequent experiments were performed only with such bars or with indented bars (with round depressions). The depressions in the bars were obtained by tightly fitting a thin brass tube over the smooth bar, with round holes predrilled in the tube.

The "windmill" experiments are convenient in that by placing the microphone along the direction of the windmill's axis of rotation, the vortex sound is recorded in a practically pure form, without being accompanied by the sound of

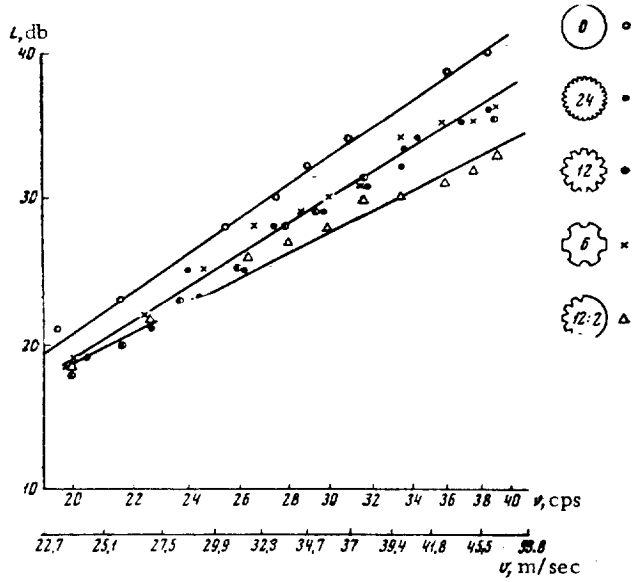

Figure 7. The Noise of Grooved Bars as a Function of the Velocity.

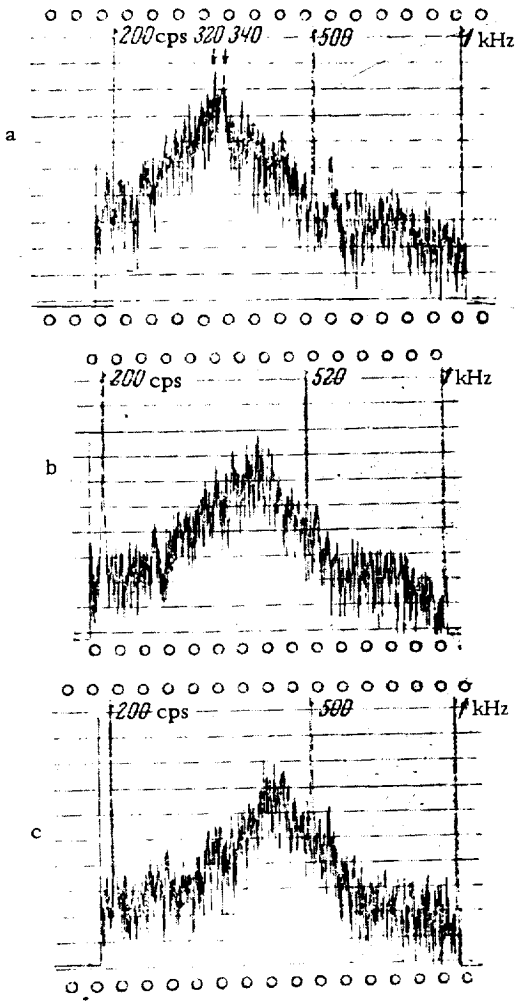

Figure 8. Noise Spectrum. a) Of a Smooth Bar; b) of a Grooved Bar; c) of a Bar Grooved Only In its Forward Part.

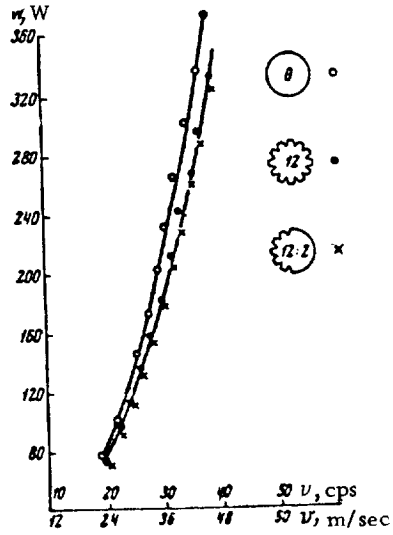

Figure 9. Resistance of a Bar with Grooves on the Forward Part and Over the Entire Perimenter.

rotation. However, due to the fact that the linear velocity on the windmill increases along the bar, it is inconvenient to measure the vortex sound as a function of this velocity. Hence we have performed a series of experiments with two bars, which were placed along generatrixes of a cylinder ("squirrel cage"), between two coaxial solid disks, so that the system would be dynamically balanced.

The presence of the circular disks /40 between which the bars were fastened does not introduce any errors; as was shown by preliminary tests, the noise level produced by the disks proper (without the bars) lies appreciably below the level of the vortex sound of the bars. The bars tested were 18 cm long and 1.4 cm in diameter. It follows from the results shown in Fig. 7 that the presence of longitudinal grooves on the entire bar surface gives a reduction in the intensity of vortex noise (which increases with the velocity of the bar). The number of grooves has no appreciable effect on this reduction (no perceptible noise reduction is produced by transverse grooves). On the other hand, the presence of grooves only on the forward part of the bar increases the effect at highest velocities by a factor of two. The vor- /42 tex sound maximum for a grooved bar (Fig. 8b) is displaced in the direction of higher frequencies as compared with a smooth bar (Fig. 8a); in addition, when only the forward part of the bar is grooved (Fig. 8c), this displacement is greater. The frequency characteristics were read with the bars rotating at 26

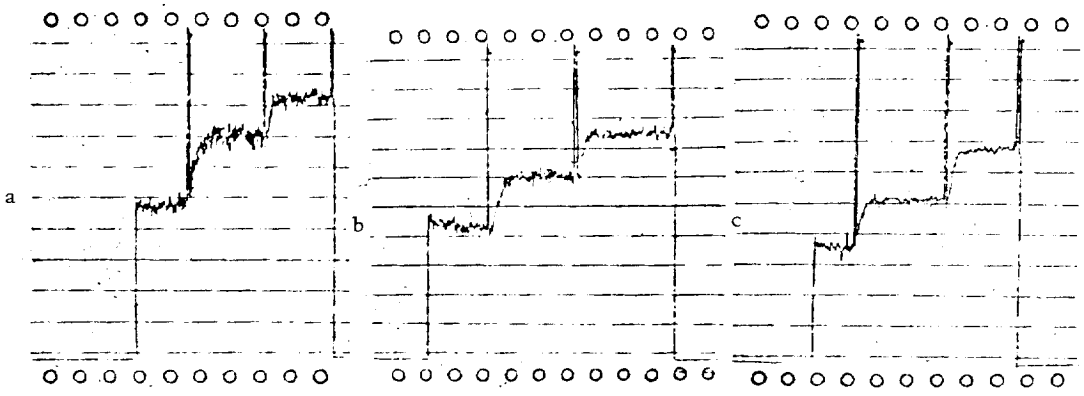

Figure 10. Noise of Indented Bars. a) Smooth Bar; b) Indentations (4 mm in Diameter); c) Indentations (8 mm in Diameter). The Rotational Frequencies were 19.7, 29.4 and 38.4 cps.

cps. The head drag, determined by measuring the motor power consumption, is lower for the grooved bar and is the same for a completely grooved bar and for a bar with only the forward part grooved (see Fig. 9). A grooved bar thus has a lower drag than a smooth one, i.e., it behaves as if it were more streamlined. This is substantiated by measuring the velocity of the wind produced by the bars. This was measured by an anemometer, placed in the immediate vicinity of the moving bars. The results are tabulated below.

TABLE

Description of Bar	Frequency, cps	Wind Velocity, m/sec
Smooth	34.7	7.1
	43.5	8.8
Grooved	34.7	5.9
	43.5	7.6

It can be seen from the table that the velocity of the wind produced by the smooth bar is higher than that due to the smooth bar. The grooved bar thus entrains less air, and consequently the absolute velocity with which it impinges onto the medium is greater than in the case of the smooth bar. The sound radiation is also lower than that of a smooth bar. It may be assumed that at equal speeds of impinging onto the medium, the noise reduction gain produced by the grooves would be even more appreciable.

The total noise level for the three indented bars rotated at 19.7, 29.4 and 38.4 cps is shown in Fig. 10. The greatest effect is obtained with a bar with 8 mm indentations. At a frequency of 29.4 cps the noise level produced by this bar is 10 db lower.

A quite substantial contribution to the total level measured on the "squirrel cage" is made by the sound of rotation, which becomes particularly perceptible

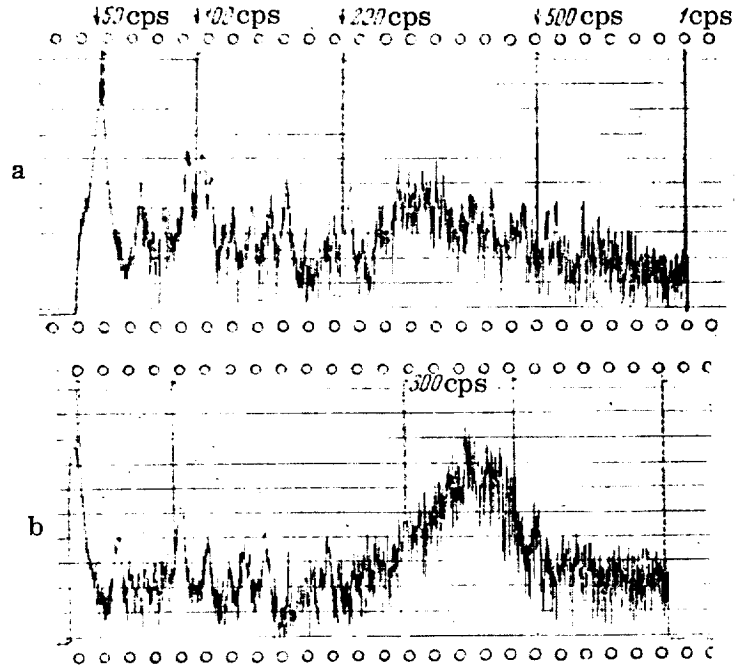

Figure 11. Noise Spectra of Bars. a) Indented Bar (8mm Diameter Indentations); b) Smooth Bar.

when vortex noise level is reduced. The frequency characteristics determined for the bar with 8 mm indentations (Fig. 11a) and for the smooth bar (Fig. 11b) clearly exhibit the presence of discrete components at frequencies of 52, 104, 156 and 208 cps, which correspond to the frequency of the sound of rotation and its harmonics. The actual effectiveness of the indentations and grooves is thus even greater than that resulting from comparison of the total levels. /44

It can be seen from the frequency characteristics presented here that the use of these surfaces not only reduces the peak of the vortex sound, but also shifts it in the direction of lower frequencies.

The head drag for the perforated and smooth bars remains the same.

REFERENCES

1. Karman, T. and H. Rubach. Über den Mechanismus des Flüssigkeits-und Luftwiderstandes. [The Mechanism of Liquid and Air Resistance] Phys. Zs., Vol. 13, 49, 1921.
2. Berthold, R.G. Geräuschverhutung an Luftbewegenden Maschinen [Noise Abatement in Air-Displacing Machines] Siemens. -Z., Vol. 11, 1931.

PROPAGATION OF SOUND IN A CYLINDRICAL PIPE WITH STREAMLINED IMPEDANCE WALLS

A. V. Rimskiy-Korsakov and P. G. Kolev

ABSTRACT: The article proposes extending the problem of sound propagation in a pipeline with impedance walls to the case of a moving medium with mth symmetry of the wave being excited.

This problem, was considered by B. P. Konstantinov [1] but without taking /45* into account the motion of the medium. Konstantinov has also taken into account the effect of the thermal conductivity of the walls on the manner in which the sound propagates in cylindrical pipes. The motion of the medium should introduce corrections to the problem. Hence we shall solve the problem of sound with the mth symmetry in a pipe with an impedance wall taking into account the motion of the medium but not considering its viscosity and thermal conductivity.

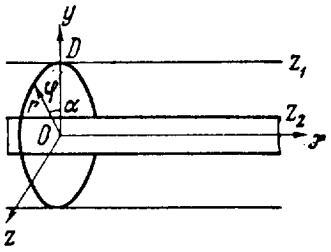

Orientation of Coordinate Axes.

The wave equation for a moving medium in a stationary coordinate system (see the figure) has the form (see, for example, [2])

$$\Delta P - \frac{1}{c^2}\left(\frac{\partial}{\partial t} + V\frac{\partial}{\partial x}\right)^2 P = 0, \tag{1}$$

where V is the speed of the medium and c is the speed of sound. We seek the solution of Eq. (1) in the form

$$P = \exp\left[-i\omega t + ik_x x + im\varphi\right] R(r), \tag{2}$$

where $r = \sqrt{y^2 + z^2}$; $k = \frac{\omega}{c}$. Let V/c = β, then Eq. (1) in cylindrical coordinates

*Numbers in the margin indicate pagination in the foreign text.

will have the form

$$P_{xx}+\frac{1}{r}\frac{\partial}{\partial r}(rP_r)+\frac{1}{r^2}P_{\varphi\varphi}-\beta^2P_{xx}-\frac{2\beta}{c}P_{xt}-\frac{1}{c^2}P_{tt}=0. \tag{1'}$$

Substituting Eq. (2) into the above expression and dividing through by exp [$-i\omega t + ik_x x + im\varphi$] we have /46

$$\frac{1}{r}\frac{\partial}{\partial r}[rR_r(r)]+\left[k^2-(1-\beta^2)k_x^2-2\beta kk_x-\frac{m^2}{r^2}\right]R(r)=0. \tag{3}$$

The general solution of Eq. (3) for integral m has the form

$$R(r)=a_1J_m(\gamma r)+a_2N_m(\gamma r),$$

where

$$\gamma=\sqrt{k^2-k_x[k_x(1-\beta^2)+2\beta k]}. \tag{4}$$

We now introduce the boundary conditions. The pressures and displacements in both media must be equal at the boundary. In the moving medium, we have

$$\frac{\partial v}{\partial t}+V\frac{\partial v}{\partial x}=-\frac{\nabla P}{\rho}, \tag{5}$$

$$\frac{\partial\xi}{\partial t}=v_r-V\frac{\partial\xi}{\partial x}, \tag{6}$$

where v_r is the rth component of the vibratory rate, and ξ is the displacement of the boundary.

From Eq. (5) we have

$$v_r=\frac{\frac{1}{\rho}\frac{\partial P}{\partial r}}{i\omega-ik_xV} \tag{5'}$$

while displacement ξ is sought in the form proportional to the same factor exp [$-i\omega t + ik_x x + im\varphi$]. From Eq. (6) we get

$$v_r=-\xi(i\omega-ik_xV). \tag{6'}$$

We assign the subscript 1 to the moving medium and subscript 2 to the stationary medium, and then from Eqs. (5') and (6')

$$-\xi_1=\frac{1}{\rho_1}\frac{\partial P_1}{\partial r}\frac{1}{(i\omega-ik_xV)^2}. \tag{7}$$

Similarly, for the stationary medium, V = 0

$$-\xi_2 = \frac{1}{\rho_2}\frac{\partial P_2}{\partial r}\frac{1}{(i\omega)^2} \tag{8}$$

The boundary conditions give

$$-\xi = \frac{1}{\rho_1}\frac{\partial P_1}{\partial r}\frac{1}{(i\omega - ik_x V)^2} = \frac{1}{\rho_2}\frac{\partial P_2}{\partial r}\frac{1}{(i\omega)^2}. \tag{9}$$

Let the wave impedance of the stationary medium be Z; then

$$Z = \frac{P_2}{v_2} = \frac{P_1}{\frac{1}{\rho_1}\frac{\partial P_1}{\partial r}\frac{i\omega}{(i\omega - ik_x V)^2}}. \tag{10}$$

Making use of Eqs. (2) and (4) we will get for the two boundaries in the cylindrical pipe /47

$$Z_1 = \frac{-i\rho c\,(k_x\beta - k)^2\,[a_1 J_m(\gamma D) + a_2 N_m(\gamma D)]}{k\gamma\,[a_1 J'_m(\gamma D) + a_2 N'_m(\gamma D)]},$$
$$Z_2 = \frac{-i\rho c\,(k_x\beta - k)^2\,[a_1 J_m(\gamma d) + a_2 N_m(\gamma d)]}{k\gamma\,[a_1 J'_m(\gamma d) + a_2 N'_m(\gamma d)]}. \tag{11}$$

The above expressions form a homogeneous system of two equations with two unknowns a_1 and a_2; hence if a nontrivial solution is to exist, it is necessary and sufficient that the determinant of the system be equal to zero. This determinant has the form

$$\begin{vmatrix} a_{11} & a_{12} \\ a_{21} & a_{21} \end{vmatrix}, \tag{12}$$

where

$$a_{11} = i\rho c\,\frac{(k_x\beta - k)^2}{k} J_m(\gamma D) + Z_1\gamma J'_m(\gamma D); \quad a_{12} = i\rho c\,\frac{(k_x\beta - k)^2}{k} \times$$
$$\times N_m(\gamma D) + Z_1\gamma N'_m(\gamma D); \quad a_{21} = i\rho c\,\frac{(k_x\beta - k)^2}{k} J_m(\gamma d) + Z_2\gamma J'_m(\gamma d);$$
$$a_{22} = i\rho c\,\frac{(k_x\beta - k)^2}{k} N_m(\gamma d) + Z_2\gamma N'_m(\gamma d).$$

We now analyze the results obtained above. For simplicity we shall consider the case when there is no internal boundary, i.e., propagation of sound

in a hollow pipe. In this case the field has no singular points, i.e., in Eq. (4) $a_2 = 0$ and

$$P = [\exp(-i\omega t + ik_x x + im\varphi)]\, a_1 J_m(\gamma r).$$

The first of Eqs. (11) takes on the form

$$Z_1 = \frac{-i\rho c\,(k_x\beta - k)^2 J_m(\gamma D)}{\gamma k J'_m(\gamma D)}. \tag{11'}$$

For the case of a solid boundary $Z_2 = \infty$, i.e.,

$$J'_m(\gamma D) = 0. \tag{13}$$

The roots of the above equation are

$$\gamma_h D \neq 0.$$

Knowing the roots of Eq. (13), we can write an expression for k_x

$$\gamma_h^2 = \gamma^2 = k^2 - k_x^2(1-\beta^2) - 2\beta k k_x \tag{14}$$

or

$$k_x = \frac{-\beta k \pm \sqrt{k^2 - \gamma_h^2 + \beta^2\gamma_h^2}}{1-\beta^2}. \tag{14'}$$

If $Z_1 \neq \infty$, then it becomes possible to influence γ_h, which also means influencing k_x by proper selection of boundary impedance conditions.

The complete problem can be solved only by numerical methods [computer]. /48

An approximate solution is possible in the limiting case of $\gamma D \ll 1$. In this case and with $Z_1 = iZ_0$, Eq. (11') becomes

$$\frac{Z_0}{\rho c} = \frac{(k-\beta k_x)^2}{k}\frac{D}{m},$$

from where it is seen that k_x is real and the propagation of a wave with mth symmetry is possible

$$k_x = \left(k - \frac{Z_0}{\rho c}\frac{m}{D}\right)\frac{c}{v}.$$

If $\gamma D \ll 1$, but $Z_1 = Z_0$ is real, then

$$k_x = \left(k + \frac{iZ_0 m}{\rho c D}\right)\frac{c}{v}.$$

This shows that the wave being considered is damped due to absorption at the impedance boundary. However, the absorption obviously is reduced when the intake pipe diameter is sufficiently large. Rigorous analysis makes it necessary to numerically calculate roots of a transcendental equation. The relative part of the energy contained in the given normal wave is determined by the character of excitation along the pipe radius.

REFERENCES

1. Konstantinov, B. P. O gidrodinamicheskom zvukoobrazovanii i rasprostranenii zvuka v ogranichennoy srede [On Hydrodynamic Sound Formation and Propagation of Sound in a Bounded Medium]. Doctoral dissertation. Kazan', FIAN [Physics Institute of the USSR Academy of Sciences named after P. N. Lebedev]. 1942.
2. Blokhintsev, D. I. Akustika neodnorodnoy dvizhushcheysya sredy [Acoustics of an Inhomogeneous Moving Medium]. GITTL [State Publishing House of Scientific and Technical Literature]. Moscow-Leningrad. 1946.

EFFECT OF THE REACTION OF THE MEDIUM ON THE OPERATION OF A RADIATOR IN A WAVEGUIDE

A. D. Lapin and Yu. P. Lysanov

ABSTRACT: This article presents calculations of the radiation impedance and of the associated mass of a cylindrical radiator, situated in a waveguide with perfect reflecting boundaries.

It is known that the sound field in a waveguide with perfect plane reflecting walls can be represented as a sum of normal waves [1]. In the case of a "point" radiating source (the dimensions of the radiator are much smaller than the sonic wavelength) with a given space velocity, the lth normal wave is proportional to a first kind, zero-order Hankel function, i.e., /49*

$$\psi_l \sim H_0^{(1)}(\xi_l r), \tag{1}$$

where r is the horizontal distance from the observer to the radiator, and ξ_l is the horizontal component of the wave factor for the given normal wave. In this case $\xi_l = \sqrt{k^2 - \left(\frac{l\pi}{h}\right)^2}$, if both boundaries of the waveguide are perfectly stiff or perfectly compliant, and $\xi_l = \sqrt{k^2 - \left[\frac{\pi(l+1/2)}{h}\right]^2}$, if one boundary is perfectly stiff and the other perfectly compliant. Here h is the thickness of the waveguide and $l = 0, 1, 2, \ldots$ It follows from Eq. (1) that the sound pressure in an lth normal wave becomes infinite whenever $\xi_l = 0$. In this case the normal wave becomes a standing wave across the thickness of the layer. Obviously, this result has no physical meaning. The infinite increase of the sound pressure in an lth normal wave at its "critical" frequency, which is determined from the condition that $\xi_l = 0$, has been called transverse resonance. It is pointed out in [1] that "the radiation impedance of the source in this case goes to infinity." However, as far as known to the authors, the radiation impedance of any source located in a waveguide has not as yet been calculated. /50

It is of interest to examine the causes of transverse resonance and at the same time to calculate the radiation impedance of a source with finite dimensions located in a waveguide. We made the calculations for the following arrangement. Let the radiator be a cylinder with radius a and height 2b, and let it execute radial oscillations; the top and bottom surfaces of the cylinders are regarded as perfectly stiff. The top boundary of the waveguide (the plane z = h)

*Numbers in the margin indicate pagination in the foreign text.

is perfectly compliant, while the lower boundary (the plane z = 0) is perfectly stiff (see figure).

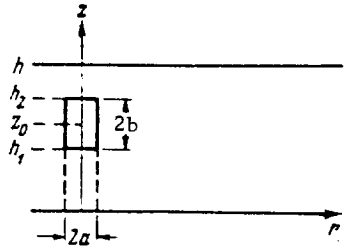

Schematic of a Waveguide with a Source.

We formulate the problem. It is required to find the solution of the equation

$$\frac{\partial^2\psi}{\partial r^2}+\frac{1}{r}\frac{\partial\psi}{\partial r}+\frac{\partial^2\psi}{\partial z^2}+k^2\psi=0, \tag{2}$$

which would satisfy: a) boundary conditions $\psi = 0$ at $z = h$, $\partial\psi/\partial z = 0$ at $z = 0$; $\partial\psi/\partial z = 0$ at $z = h_1$ and $z = h_2$ and for $r \leq a$; b) the condition at the radiator that $\partial\psi/\partial r = v_0$ at $r = a$ and $h_1 \leq z \leq h_2$, where v_0 is the radial velocity of the surface of the radiator, and c) the condition at infinity, that the field at $r \to \infty$ should consist of diverging waves.

Denoting the space velocity of the radiator by $V_0 = 4\pi abv_0$, we can represent the sound fields in different regions of the waveguides in the form

$$\psi(r, z) = V_0 \sum_{n=0}^{\infty} A_n H_0^{(1)}(\xi_n r)\cos(k_n z),\ (r \geqslant a,\ 0 \leqslant z \leqslant h), \tag{3}$$

$$\widetilde{\psi}(r, z) = V_0 \sum_{n=0}^{\infty} \widetilde{A}_n I_0(\widetilde{\xi}_n r)\cos(\widetilde{k}_n z),\ (r \leqslant a,\ 0 \leqslant z \leqslant h_1), \tag{4}$$

$$\widetilde{\widetilde{\psi}}(r, z) = V_0 \sum_{n=0}^{\infty} \widetilde{\widetilde{A}}_n I_0(\widetilde{\widetilde{\xi}}_n r)\cos[\widetilde{\widetilde{k}}_n (z - h_2)],\ (r \leqslant a,\ h_2 \leqslant z \leqslant h), \tag{5}$$

where we have used the notation /51

$$k_n = \frac{(1+2n)\pi}{2h};\quad \widetilde{k}_n = \frac{n\pi}{h_1};\quad \widetilde{\widetilde{k}}_n = \frac{(1+2n)\pi}{2(h-h_2)};$$
$$\xi_n = \sqrt{k^2 - k_n^2};\quad \widetilde{\xi}_n = \sqrt{k^2 - \widetilde{k}_n^2};\quad \widetilde{\widetilde{\xi}}_n = \sqrt{k^2 - \widetilde{\widetilde{k}}_n^2}; \tag{6}$$

and I_0 is a zero-order Bessel function.

It is easy to see that Eqs. (3)-(5) satisfy Eq. (2) and the boundary conditions at z = 0, h_1, h_2 and h.

The constants A_n, $\tilde{A}_n$ and $\tilde{\tilde{A}}_n$ can be determined uniquely at the junction (sewing together) of the fields at r = a. From the condition of continuity of sound pressure at r = a, $0 \leq z \leq h_1$, we get

$$\tilde{A}_m = \sum_{n=0}^{\infty} \frac{\tilde{\alpha}_{nm} H_0^{(1)}(\xi_n a)}{I_0(\tilde{\xi}_m a)} A_n, \tag{7}$$

where

$$\tilde{\alpha}_{nm} = \frac{2}{\theta_m h_1} \int_0^{h_1} \cos(k_n z) \cos(\tilde{k}_m z)\, dz =$$

$$= \begin{cases} 1 \text{ when } k_n = \tilde{k}_m, \\ (-1)^m \dfrac{2k_n \sin(k_n h_1)}{\theta_m h_1 (k_n^2 - \tilde{k}_m^2)}; \quad \text{when} \quad k_n \neq \tilde{k}_m. \end{cases} \tag{8}$$

Here $\theta_m = \begin{cases} 2 & \text{when} \quad m = 0, \\ 1 & \text{when} \quad m \neq 0. \end{cases}$

Similarly, from continuity of sound pressure at r = a, $h_2 \leq z \leq h$, we have

$$\tilde{\tilde{A}}_m = \sum_{n=0}^{\infty} \frac{\tilde{\tilde{\alpha}}_{nm} H_0^{(1)}(\xi_n a)}{I_0(\tilde{\tilde{\xi}}_m a)} A_n, \tag{9}$$

where

$$\tilde{\tilde{\alpha}}_{nm} = \frac{2}{(h - h_2)} \int_{h_2}^{h} \cos(k_n z) \cos[\tilde{\tilde{k}}_m (z - h_2)]\, dz =$$

$$= \begin{cases} (-1)^{n+m}, \text{ when } k_n = \tilde{\tilde{k}}_m; \\ -\dfrac{2k_n \sin(k_n h_2)}{(h - h_2)(k_n^2 - \tilde{\tilde{k}}_m^2)}, \text{ when } k_n \neq \tilde{\tilde{k}}_m. \end{cases} \tag{10}$$

Finally, from continuity of the radial velocity /52

$$\left(\frac{\partial \psi}{\partial r}\right)_{r=a} = \begin{cases} \left(\dfrac{\partial \tilde{\psi}}{\partial r}\right)_{r=a}, & (0 \leqslant z \leqslant h_1) \\ v_0, & (h_1 \leqslant z \leqslant h_2) \\ \left(\dfrac{\partial \tilde{\tilde{\psi}}}{\partial r}\right)_{r=a}, & (h_2 \leqslant z \leqslant h) \end{cases} \tag{11}$$

we get an infinite system of linear algebraic equations for determining the amplitudes A_m :

$$A_m = \frac{1}{\xi_m h H_1^{(1)}(\xi_m a)} \sum_{l=0}^{\infty} \left[D_l H_0^{(1)}(\xi_l a) A_l - \frac{\beta_m}{\pi a} \right], \tag{12}$$

where

$$\beta_m = \frac{\sin(k_m b)}{(k_m b)} \cos(k_m z_0), \tag{13}$$

$$D_l = \sum_{n=0}^{\infty} \left[\theta_n h_1 \tilde{\xi}_n \tilde{\alpha}_{mn} \tilde{\alpha}_{ln} \frac{I_1(\tilde{\xi}_n a)}{I_0(\tilde{\xi}_n a)} + (h - h_2) \tilde{\tilde{\xi}}_n \tilde{\tilde{\alpha}}_{mn} \tilde{\tilde{\alpha}}_{ln} \frac{I_1(\tilde{\tilde{\xi}}_n a)}{I_0(\tilde{\tilde{\xi}}_n a)} \right]. \tag{14}$$

Equations (12) through (14) give a rigorous solution of the problem. Analysis of the results can be appreciably simplified if we restrict ourselves to the case when ka $\rightarrow$ 0 (the cylinder radius is very small compared with the sonic wavelength). In this approximation, we get

$$D_l \rightarrow 0; \; A_m \rightarrow \frac{-i\beta_m}{2h}. \tag{15}$$

Then the expression

$$\psi(r, z) = -\frac{iV_0}{2h} \sum_{m=0}^{\infty} \beta_m H_0^{(1)}(\xi_m r) \cos(k_m z) \tag{16}$$

defines the sound field for a known radiator velocity V_0. It follows from Eq. (16) that when $\xi_l \rightarrow 0$, the sound pressure in an lth normal wave goes to infinity due to the fact that Hankel's function increases beyond bounds.

The preceding discussion was based on the assumption of a constant space velocity of the source in the waveguide. We shall now show that at frequencies close to the critical frequency of one of the normal wave, this assumption does not hold even approximately.

We now calculate the value of V_0 which is produced at the radiator by a force $F = F_0 e^{-i\omega t}$ when the reaction of the medium is taken into account. We denote the mass of the radiator by m_0, the frictional resistance by R_0, the

compliance by $\varkappa$ and the deflection of the cylinder's radius from its equilibrium position (which is a) by ζ (t). The equation of motion for the radiator can then be written as /53

$$m_0\ddot{\zeta} + R_0\dot{\zeta} + \frac{1}{\varkappa}\zeta = (F_0 - \Phi_0)\, e^{-i\omega t}, \tag{17}$$

where the dot denotes differentiation with respect to time. Φ_0, the reaction of the medium, is defined as

$$\Phi_0 = 2\pi a \int_{z_0-b}^{z_0+b} [P(r, z)]_{r=a}\, dz. \tag{18}$$

Substituting Eq. (3) into Eq. (18) and making use of the fact that $v_0\, e^{-i\omega t} = \dot{\zeta}$, it is possible to write Eq. (18) in the form

$$\Phi_0 = v_0 (R_{\text{rad}} - i\omega m) = (R_{\text{rad}}\dot{\zeta} + m\ddot{\zeta})\, e^{i\omega t},$$

where $R_{\text{rad}} = \text{Re}\left\{i\omega\rho S_0^2 \sum_{n=0}^{\infty} A_n\beta_n H_0^{(1)}(\xi_n a)\right\}$ is the radiation impedance, $m = -$

$= -\frac{1}{\omega}\text{Im}\left\{i\omega\rho S_0^2 \sum_{n=0}^{\infty} A_n\beta_n H_0^{(1)}(\xi_n a)\right\}$ is the associated mass, $S_0 = 4\pi ab$ is the area of the radiating surface, and ρ is the density of the medium.

The solution of Eq. (17) is

$$\zeta(t) = \frac{iV_0}{\omega Z_{\text{rad}}}\, e^{-i\omega t}, \tag{19}$$

where

$$Z_{\text{rad}} = \left[R + i\left(\frac{1}{\omega\varkappa} - \omega M\right)\right]. \tag{20}$$

$R \equiv R_0 + R_{\text{rad}}$, $M \equiv m_0 + m$ is the effective mass of the radiator.

Now we can get an expression for the space velocity of the radiator with the reaction of the medium taken into account

$$V_0 = \frac{F_0 S_0}{Z_{\text{rad}}}. \tag{21}$$

We analyze the solution thus obtained again for the case of $ka \ll 1$. Here the amplitudes of normal waves will be obtained from Eq. (15), while

$$R_{\text{rad}} \simeq \text{Re}\left\{\frac{i\omega\rho S_0^2}{\pi h}\sum_{n=0}^{\infty}\beta_n^2 \ln\left(\frac{\xi_n a}{2}\right)\right\} \tag{22}$$

and /54

$$m \simeq -\frac{1}{\omega}\,\text{Im}\left\{\frac{i\omega\rho S_0^2}{\pi h}\sum_{n=0}^{\infty}\beta_n^2 \ln\left(\frac{\xi_n a}{2}\right)\right\}. \tag{23}$$

It follows from Eqs. (22) and (23) that, as the frequency of sound approaches the critical frequency of the lth wave, $\xi_l \to 0$ and, consequently, the radiation impedance or the associated mass of the radiator go to infinity as $l\text{n}(\xi_l a/2)$, and the space velocity V_0, according to Eq. (21), goes to zero. Since V_0 goes to zero according to the same law which governs the increase of function $H^{(1)}_0(\xi_l r)$, the sound pressure in the given normal wave remains finite.

It is of interest to determine the character of the sound field in a waveguide at a frequency which coincides with the critical frequency of one of the normal waves. As is known, normal waves at frequencies above their critical frequencies are waves traveling along the waveguide, while at frequencies below their critical frequencies these are inhomogeneous waves which are damped exponentially as they move away from the source.

Let us assume that the sonic frequency approaches the critical frequency of the lth normal wave, i.e., $\xi_l \to 0$. We isolate in Eq. (16) the term corresponding to such a wave

$$\psi(r, z) = \frac{-iV_0}{2h}\sum_{n\neq l}^{\infty}\beta_n H_0^{(1)}(\xi_n r)\cos(k_n z) - \frac{iV_0}{2h}\beta_l H_0^{(1)}(\xi_l r)\cos(k_l z). \tag{24}$$

Knowing that $\xi_l \to 0$, it is possible to retain in Eqs. (22) and (23) only lth terms and to neglect R_0 and m_0 as compared with R_{rad} and m, respectively. Then we will get the following approximate expression

$$V_0 = \frac{\pi h F_0}{i\omega\rho S_0\beta_l^2 \ln\left(\frac{\xi_l a}{2}\right)} \tag{25}$$

When $\xi_l \to 0$, $V \to 0$ and, consequently, the first term in the right-hand side of Eq. (24) also goes to zero (since the summand is finite); on the other hand, the second term in Eq. (24) will be finite, since then Hankel's function will go to infinity. Substituting (25) into Eq. (24) and replacing Hankel's function by its approximate expression for small values of the argument ($\xi_l r \ll 1$), we get

$$\psi(r, z) = \frac{F_0 \cos kz}{i\omega\rho S_0 \beta_l} \frac{\ln\left(\frac{\xi_l r}{2}\right)}{\ln\left(\frac{\xi_l a}{2}\right)}$$

or, solving the indeterminacy as $\xi_l \to 0$ ($a \neq 0$, $b \neq 0$) /55

$$\psi(r, z) = \frac{F_0 \cos kz}{i\omega\rho S_0 \beta_l}. \tag{26}$$

Thus, when $\xi_l = 0$ only one lth normal wave is excited, and its amplitude does not vary with the distance from the sound source, but remains constant. From the physical point of view this fact is quite obvious: a normal wave at the critical frequency is a standing wave over z, there is no propagation over r and thus it does not depend on r.

REFERENCE

Brekhovskikh, L. M. Volny v sloistykh sredakh [Waves in Layered Media]. USSR Acad. Sci. Press. Moscow 1957.

RADIATION OF AN ELASTIC DISCONTINUOUS WALL IN A MOVING MEDIUM

A. D. Lapin

ABSTRACT: The article considers a sound field which is produced in a homogeneous flow of an ideal fluid by a discontinuous elastic wall, which executes induced vibrations under the effect of random forces. It is assumed that the properties of the wall vary periodically. The qualitative behavior of variations in the field characteristics as a function of variation of wall parameters, the motion of the medium and the properties of the statistical forces is clarified.

The sound field produced in a stationary medium by an elastic, periodically /56* discontinuous wall, vibrating under the action of statistically distributed forces was calculated in [1]. It is of interest to find the sound field which is produced by this wall in a moving medium. In the present paper this problem is examined on the assumption that the medium moves parallel to the wall with constant velocity U. No limitations are placed on the magnitude of discontinuities. It is assumed that the excitation force is a harmonic function of time; the time factor $\exp(-i\omega t)$ will be skipped throughout.

We select a Cartesian coordinate system in such a manner that the plane $z = 0$ will coincide with the wall, the x axis will coincide with the direction of motion of the medium and the z axis will be directed from the wall into the medium. It is assumed for simplicity that the properties of the wall vary only along the x coordinate; the period of these discontinuities is denoted by d. Let the wall be acted upon by a distributed force $f(x, y)$ which is a homogeneous statistical function of the point. We assume that the equation of free vibrations of the wall in the absence of a medium has the form

$$(\rho\omega^2 + L)\zeta = 0,$$

where L is a linear differential operator characterizing the elastic properties of the wall, ρ is the surface density of the wall, and ζ is the lateral displacement. For example, for a membrane $L = T_0 \nabla^2$, where T_0 is the membrane tension. For an inhomogeneous plate executing flexural vibrations, this operator has the form /57

$$L = \left\{(1-\sigma)\frac{\partial^2 D}{\partial x^2}\frac{\partial^2}{\partial y^2} - \nabla^2(D\nabla^2)\right\},$$

*Numbers in the margin indicate pagination in the foreign text.

where σ is Poisson's ratio and D is the cylindrical stiffness. The stiffness is expressed as

$$D = \frac{Eh^3}{12(1-\sigma^2)},$$

where h is the thickness of the plate and E is Young's modulus. We denote the sound pressure in the medium by p(x, y, z). Then the equation of forced vibrations of the wall due to force f(x, y), with the reaction of the medium taken into account, is

$$-(\rho\omega^2 + L)\,\zeta + p\,(x,\ y,\ 0) = f\,(x,\ y). \tag{1}$$

The equality of normal velocity components at the interface between the wall and the moving medium will be written as

$$\left(\frac{\partial p}{\partial z}\right)_{z=0} = \rho_0 c_0^2 \left\{k_0 + i\beta\,\frac{\partial}{\partial x}\right\}^2 \zeta, \tag{2}$$

where ρ_0 and c_0 are, respectively, the density of the medium and the speed of sound in it, $\beta = U/c_0$ is the Mach number, and $k_0 = \omega/c_0$.

We shall seek the solution by the Fourier method. According to [2], we shall expand function f(x, y) into harmonics by the Fourier-Stieljes integral

$$f(x, y) = \int_{-\infty}^{\infty}\int \exp\left[i\,(mx + ny)\right] dg\,(m, n), \tag{3}$$

where g(m, n) is a random function with uncorrelated increments. This means that this function satisfies the expression

$$\overline{dg\,(m, n)\,dg^*\,(m', n')} = \begin{cases} 0 & \text{when } m \neq m' \text{ or } n \neq n' \\ G\,(m, n)\,dm\,dn & \text{when } m = m',\ n = n', \end{cases}$$

where the asterisk denotes a conjugate complex quantity and the bar denotes statistical averaging. Function G(m, n) is related to the correlation function of the force

$$R\,(x - x',\ y - y') = \overline{f\,(x, y)\,f^*\,(x', y')}$$

by the expression

$$G\,(m, n) = \frac{1}{(2\pi)^2}\int_{-\infty}^{\infty}\int R\,(\tau_x,\ \tau_y)\exp\left[-i\,(m\tau_x + n\tau_y)\right] d\tau_x\,d\tau_y. \tag{4}$$

Let us now find fields produced separately by each of the harmonics of expansion (3). The sought field will then be obtained by adding these fields. /58

First we find the solution for the inducing force

$$f_{mn}(x, y) = a(m, n) \exp[i(mx + ny)].$$

Since the properties of the wall vary periodically along the x axis, the displacement ζ_{mm} which is due to force f_{mm} can be represented in the form

$$\zeta_{mn}(x, y) = a \exp[i(mx + ny)] F(x),$$

where F(x) is a periodic function with the same period. This function will be sought in the form of the Fourier series

$$F(x) = \sum_{q=-\infty}^{\infty} B_q \exp(i\Omega_q x),$$

where $\Omega_q = \frac{2\pi}{d} q$. The sound field p_{mn} satisfies the wave equation in the moving medium

$$\nabla^2 p_{mn} = \left\{\beta \frac{\partial}{\partial x} - ik\right\}^2 p_{mn}$$

and the boundary condition

$$\left(\frac{\partial p_{mn}}{\partial z}\right)_{z=0} = \rho_0 c_0^2 \left\{k_0 + i\beta \frac{\partial}{\partial x}\right\}^2 \zeta_{mn} =$$

$$= \sum_{q=-\infty}^{\infty} a\rho_0 c_0^2 \{k_0 - \beta(m + \Omega_q)\}^2 B_q \exp\{i[(m + \Omega_q)x + ny]\}.$$

This field can be represented in the form

$$p_{mn}(x, y, z) = \sum_{q=-\infty}^{\infty} aA_q \exp\{i[(m + \Omega_q)x + ny + \sqrt{[k_0 - \beta(m + \Omega_q)]^2 - \gamma_q^2}\, z]\},$$

where

$$A_q = -i \frac{\rho_0 c_0^2 [k_0 - \beta(m + \Omega_q)]^2}{\sqrt{[k_0 - \beta(m + \Omega_q)]^2 - \gamma_q^2}} B_q; \quad \gamma_q^2 = [(m + \Omega_q)^2 + n^2].$$

Thus the sound field produced by force f_{mn} consists of plane waves ("spectra"), the direction cosines of which are governed by a condition similar to Bragg's condition.

Quantities B_q will be determined from Eq. (1). We expand the parameters characterizing the inhomogeneous properties of the wall into a Fourier series, substitute these series and the quantities ζ_{mn}, p_{mn} and f_{mn} into Eq. (1), then equate the coefficients of the same exponents in the right and left-hand sides. Then we will get an infinite system of algebraic equations for B_q /59

$$\sum_{l=-\infty}^{\infty} \{L_{ql} + \omega^2 M_l\} B_{(q-l)} + i\rho_0 c_0^2 \frac{[k_0 - \beta(m+\Omega_q)]^2}{\sqrt{[k_0 - \beta(m+\Omega_q)]^2 - \gamma_q^2}} B_q = -\delta_{0q}, \tag{5}$$

where

$$L_{ql} = \frac{1}{d} \int_{-d/2}^{d/2} \exp\{-i[(m+\Omega_q)x + ny]\} L\{\exp\{i[(m+\Omega_{q-l})x + ny]\}\} dx,$$

$$M_l = \frac{1}{d} \int_{-d/2}^{d/2} \rho(x) \exp(-i\Omega_l x)\, dx,$$

$$\delta_{0q} = \begin{cases} 0 \text{ when } q \neq 0 \\ 1 \text{ when } q = 0. \end{cases}$$

For example, for a membrane $L_{ql} = T_0 \gamma_q^2 \delta_{0l}$, while for a plate we have

$$L_{ql} = \{(1-\sigma) n^2 \Omega_l^2 - \gamma_q^2 \gamma_{(q-l)}^2\} N_l,$$

where

$$N_l = \frac{1}{d} \int_{-d/2}^{d/2} D(x) \exp(-i\Omega_l x)\, dx.$$

Solving Eqs. (5), we get B_q, and consequently A_q. Summing the effect of all the f_{mn}, we get

$$\zeta(x, y) = \sum_{q=-\infty}^{\infty} \iint_{-\infty}^{\infty} B_q(m, n) \exp\{i[(m + \Omega_q)x + ny]\}\, dg,$$

$$p(x, y, z) = \sum_{q=-\infty}^{\infty} \iint_{-\infty}^{\infty} A_q(m, n) \exp\{i[(m + \Omega_q)x + ny + \sqrt{[k_0 - \beta(m + \Omega_q)]^2 - \gamma_q^2}\, z]\}\, dg. \quad (6)$$

These formulas give the solution for the problem for an infinite wall.

We shall now find the sound field radiated by a finite wall which vibrates due to an inducing force f(x, y). The correlation radius of this force will be assumed small as compared to the dimensions of the wall. On this assumption /60 it is possible to assume that the displacement of the wall far from its edges does not depend on boundary conditions and is expressed by Eq. (6). We shall calculate the sound field from Green's single-term formula. In the "compressed" coordinate system $(\tilde{x} = \frac{x}{\sqrt{1-\beta^2}}, y, z)$, this formula is written in the form

$$p_M = -\frac{1}{2\pi} \iint_S \frac{\partial p}{\partial z} \frac{e^{ik_0 \tilde{r}}}{\tilde{r}}\, dS,$$

where S is the surface of the wall, $\tilde{r} = [(\tilde{x} - \tilde{x}_M)^2 + (y - y_M)^2 + (z - z_M)^2]^{1/2}$ is the distance from surface element dS to the point of observation M with coordinates $(\tilde{x}_M, y_M, z_M)$, $r = \frac{\tilde{r} + \beta(\tilde{x} - \tilde{x}_M)}{\sqrt{1-\beta^2}}$. According to Eqs. (2) and (6), the quantity $(\partial p/\partial z)_{z=0}$ has the form

$$\left(\frac{\partial p}{\partial z}\right)_{z=0} = \rho_0 \omega^2 \iint_{-\infty}^{\infty} g_1(m, n) \exp[i(mx + ny)]\, dm dn, \quad (7)$$

where

$$g_1(m, n) = \left(1 - \beta \frac{m}{k_0}\right)^2 \sum_{q=-\infty}^{\infty} g(m - \Omega_q, n) B_q(m - \Omega_q, n). \quad (8)$$

We shall assume that the point of observation is situated at a large distance of the wall, in the Fraunhofer region. Then we can write (see [3])

$$\frac{e^{ik_0 \tilde{r}}}{\tilde{r}} \approx \frac{1}{\tilde{r}_0} \exp\left\{i\left[\frac{k_0(\tilde{r}_0 - \beta\tilde{x}_M)}{\sqrt{1-\beta^2}} - \sqrt{1-\beta^2}\, \tilde{m}\tilde{x} - \tilde{n}y\right]\right\}, \quad (9)$$

where

$$\tilde{m} = \frac{k_0(\cos\tilde{\theta}\cos\tilde{\varphi} - \beta)}{(1-\beta^2)}, \quad \tilde{n} = \frac{k_0 \cos\tilde{\theta}\sin\tilde{\varphi}}{\sqrt{1-\beta^2}}$$

$\tilde{r}_0$ is the distance from the origin to point M, $\tilde{\theta}$ is the angle between the direction to the point of observation and the wall, $\tilde{\varphi}$ is the angle between the projection of this direction onto the wall and axis $\tilde{x}$. Angles $\tilde{\theta}$ and $\tilde{\varphi}$ differ from the corresponding angles θ and φ in the (x, y, z) coordinate system by a magnitude of the order β^2. Substituting Eqs. (7) and (9) into Green's formula and integrating it by the method presented in [4], we get /61

$$p_M = -\frac{2\pi\rho_0\omega^2}{\tilde{r}_0} g_1(\tilde{m}, \tilde{n}) \exp\left\{i\left[\frac{k_0(\tilde{r}_0 - \beta\tilde{x}_M)}{\sqrt{1-\beta^2}}\right]\right\}.$$

We now calculate the root-mean-square sound pressure in the moving medium. This quantity is given by

$$\overline{p_M p_M^*} = \frac{4\pi^2\rho_0^2\omega^4}{\tilde{r}_0^2} \overline{g_1(\tilde{m}, \tilde{n}) g_1^*(\tilde{m}, \tilde{n})}.$$

Using Eq. (8) and the expression

$$\overline{g(m, n) g^*(m, n)} = \frac{1}{(2\pi)^4} \iint_S \iint_S \overline{f(x, y) f^*(x', y')} \times$$
$$\times \exp\{i[m(x' - x) + n(y' - y)]\}\, dx\, dy\, dx'\, dy' = \frac{S}{(2\pi)^2} G(m, n),$$

we get

$$\overline{p_M p_M^*} = \frac{\rho_0^2\omega^4}{r_0^2}\left(1 - \beta\frac{\tilde{m}}{k_0}\right)^4 S \sum_{q=-\infty}^{\infty} |B_q(\tilde{m} - \Omega_q, \tilde{n})|^2 G(\tilde{m} - \Omega_q, \tilde{n}). \qquad (10)$$

Substituting into this expression coefficients B_q which are obtained by solving system of equations (5), and the spectral density of intensity G calculated from Eq. (4), we will find the root-mean-square of the sound pressure.

In the general case it is convenient to seek the solution of system of equations (5) by the method of successive approximations. To make the use of this method possible, it is sufficient that the system of equations be regular [5]. It can be shown that in the case at hand the condition of regularity is satisfied if the functions characterizing the inhomogeneous properties of the wall are sufficiently smooth. In the zero approximation of the method of successive approximations, we have

$$B_q = -\frac{\delta_{0q}}{\left\{L_\infty + \omega^2 M_0 + i\frac{\rho_0 c_0^2 (k_0 - \beta m)^2}{\sqrt{(k_0 - \beta m)^2 - \gamma_0^2}}\right\}}.$$

Substituting these cooefficients into Eq. (10), we will get a solution of the problem for a homogeneous wall, which is identical with the solution found by another method in [6]. In the first approximation we get /62

$$B_q = -\frac{\{\delta_{0q} + (1-\delta_{0q})[L_{qq} + \omega^2 M_q] B_0\}}{\left\{L_{q0} + \omega^2 M_0 + i\frac{\rho_0 c_0^2 [k_0 - \beta(m+\Omega_q)]^2}{\sqrt{[k_0 - \beta(m+\Omega_q)]^2 - \gamma_q^2}}\right\}}$$

This approximation takes into account the effect of small inhomogeneities of the wall on its radiation. For large inhomogeneities use should be made of higher-order approximations.

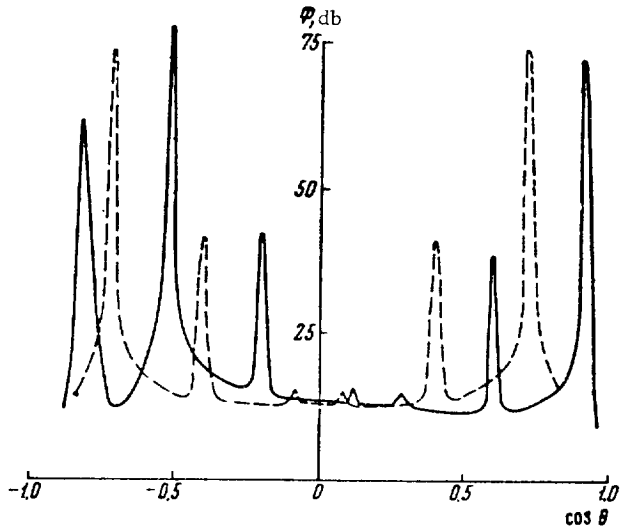

Figure 1. Characteristic Curve of Radiation for $k_0\tau_0 = 1$.

As was pointed out above, the spectral density of intensity can be calculated from Eq. (4) by specifying the correlation function of the force. For an isotropic force, the correlation function depends only on $\tau = \sqrt{\tau_x^2 + \tau_y^2}$. In this case Eq. (4) simplifies to the form

$$G(m,n) = \frac{1}{2\pi}\int_0^\infty \tau R(\tau) J_0(\sqrt{m^2+n^2}\,\tau)\, d\tau,$$

where J_0 is a zero-order Bessel function. For example, for correlation functions specified in the form

$$R(\tau) = \sigma^2 \exp(-\tau^2/\tau_0^2) \text{ and } R(\tau) = \sigma^2 \exp\left(-\frac{|\tau|}{\tau_0}\right),$$

where $\sigma^2 = \overline{f(x, y)\, f^*(x, y)}$ and τ_0 is the characteristic scale of the force, we have /63

$$G(m, n) = \frac{(\sigma\tau_0)^2}{4\pi} \exp\left\{-\frac{1}{4}(m^2 + n^2)\tau_0^2\right\} \tag{11}$$

and

$$G(m, n) = \frac{1}{2\pi} \frac{(\sigma\tau_0)^2}{[1 + (m^2 + n^2)\tau_0^2]^{3/2}}.$$

As an illustration, we calculate the radiation from a steel plate with thickness

$$h(x) = h_0 + h_1 \cos\left(\frac{2\pi}{d} x\right),$$

in air. It is given that

$h_1/h_0 = 0.25$, $k_0 h_0 = 0.4$, $k_0 d = 20$, $\rho_0 = \rho/h = 7.8$ grams/cm^3;
$E = 2.1 \cdot 10^{12}$ dynes/cm^2; $\sigma = 0.29$, $\rho_0 = 0.0013$ grams/cm^3; $c_0 = 330$ m/sec.

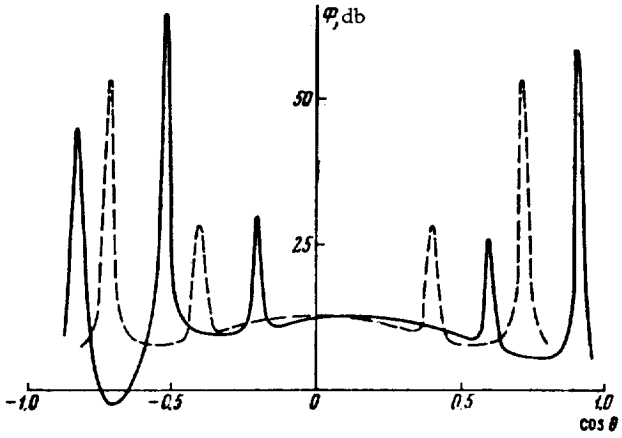

Figure 2. Characteristic Curve for $k_0\tau_0 = 5$.

We specify the spectral density of the intensity of the force in the form of Eq. (11). The solid lines in Figs. 1 and 2 show the graphs of the quantity

$$\Phi(\theta) = 10 \lg \left\{4\pi \cdot 10^8 \frac{(x_M^2 + z_M^2)}{(k_0\tau_0\sigma)^2 S} \overline{(p_M p_M^*)}_{\rho=0}\right\}$$

as a function of $\cos\theta$, calculated by the above method for $\beta = 0.2$ at $k_0\tau_0 = 1$ and $k_0\tau_0 = 5$, respectively. For comparison, the same figures show by dashed lines the corresponding graphs obtained with $\beta = 0$. It can be seen from these graphs /64 that the motion of the medium has a pronounced effect on the characteristic curve of the radiation of an inhomogeneous plate.

REFERENCES

1. Lapin, A.D. Izlucheniye zvuka koleblyushcheysya neodnorodnoy stenkoy [Sound Radiation by an Inhomogeneous Vibrating Wall]. Akusticheskiy zhurnal. Vol. 13, No. 1, 70-75, 1967.
2. Yaglom, A.M. Vvedeniye v teoriyu stantsionarnykh sluchaynykh funktsiy [Introduction to the Theory of Stationary Random Functions]. Usp. Mat. Nauk, Vol. 7, 5 (51), 3-168, 1952.
3. Blokhintsev, D.I. Akustika neodnorodnoy dvizhushcheysya sredy [Acoustics of an Inhomogeneous Moving Medium]. OGZ GTI [United State Publishing Houses, State Publishing House of Technical and Theoretical Literature]. Moscow-Leningrad. 1946.
4. Isakovich, M.A. Izlucheniye uprugoy stenki, koleblyushcheysya pod deystviyem statisticheski raspredelennykh sil [Radiation of an Elastic Wall Set into Oscillations by Statistically Distributed Forces]. In the collection Issledovaniya po eksperimental'noy i teoreticheskoy fizike [Studies in Experimental and Theoretical Physics]. Published in memory of G.S. Landsberg. USSR Acad. Sci. Press. Moscow. pp. 117-120, 1959.
5. Kantrovich, L.V. and V.I. Krylov. Priblizhennyye metody vysshego analiza [Approximate Methods of Higher Analysis]. GTTI. Moscow. 1949.
6. Lyamshev, L.M. Izlucheniye zvuka uprugimy obolochkami, vozbuzhdayemymi turbulentnym aerodinamicheskim potokom [Sound Radiation by Elastic Shells Excited by a Turbulent Aerodynamic Flow]. Akusticheskiy zhurnal. Vol. 7, No. 1, 59-66, 1961.

PULSATIONS OF COLLIDING AXISYMMETRICAL JETS OF GASEOUS OXIDIZER AND PROPELLANT

V. I. Kondrat'yev

ABSTRACT: The present article describes the pulsations of flames produced upon collisions between axisymmetrical jets of propane-butane and oxygen, and the sound formation attendant to it. Pictures obtained with a high-speed movie camera show the mode of the flame pulsations. Flame pulsation frequencies at different oxidizer and propellant speeds are also presented.

A special kind of a "singing" flame, which is produced on the collision of /65* plane jets of gaseous oxygen and propane-butane was described in [1]. Using the same setup as in [1], experiments were performed with colliding axisymmetrical jets. The latter were obtained from nozzles with a circular cross section from 1.0 to 4.0 mm in diameter, with the diameter of the oxygen nozzle being larger than that of the propane nozzle. The mode of flame pulsation was recorded by a high-speed SKS-1M moving-picture camera. The characteristics of the noise formed on the flame pulsations were recorded by an 1/4" B&K microphone and by an S4-7 analyzer.

A head-on collision between axisymmetrical jets of gaseous propane-butane and oxygen produces a flame the mode and behavior of whose pulsations varies depending on the relationship between the gas jet speeds, the diameters /66

№	f	v_1	v_2	S	d_1	d_2
1	110	10.23	3.82	15	1.8	1.1
2	115	6.30	4.80	24	2.6	0.85
3	133	8.30	4.80	11	2.6	0.85
4	143	7.86	5.98	12	1.8	1.0
5	373	10.23	5.10	12	1.8	1.1

of the outlet and the distance between the nozzles. The flame may be stable, not radiating sound (and in this case the flame front is clearly delineated) and unstable, pulsating randomly, radiating "white noise" or a periodic noise ("singing" flame). The periodic flame pulsations which are observed for overall oxidizer and propellant speeds from 2 to 30 m/sec and distances of from 5 to 30 mm between the nozzle can be divided into three kinds:

*Numbers in the margin indicate pagination in the foreign text.

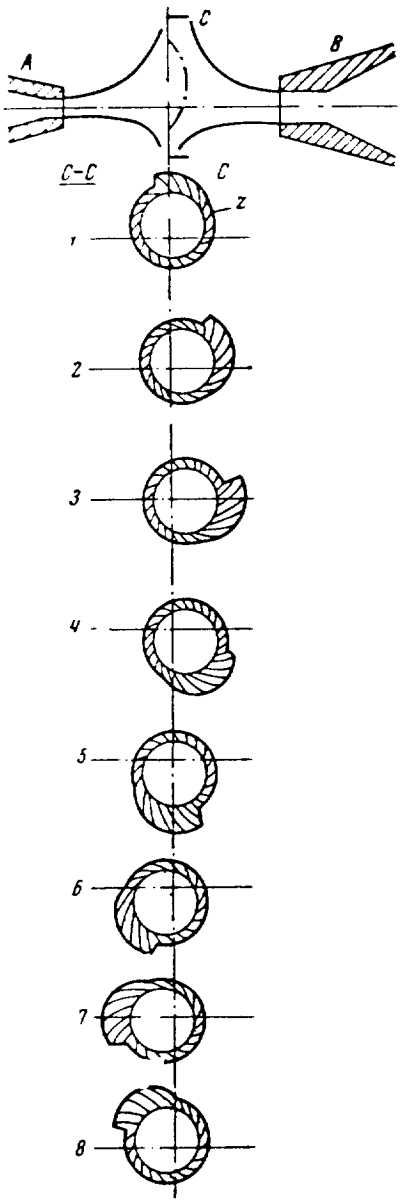

Schematic Diagram of Flame Pulsations on Rotation of the Jets. 1 through 8 is a Time Sequence of Frames.

1) flame pulsations similar to those which arise on symmetrical collisions of plane jets [1];

2) elliptically-polarized flame pulsations, i.e., flame pulsations of the first kind in a plane rotating about its axis of symmetry;

3) rotation of the flame about its axis of symmetry.

The second kind of pulsations, which is observed quite infrequently, was noted at speeds of 8.3 and 4.8 m/sec of the oxidizer and propellant, respectively, and at a distance of 11 mm between the nozzles. The fundamental frequency of the sound which was radiated was the same as the pulsation frequency of the flame, i.e., 390 cps; here the frequency of rotation of the plane in which the pulsations took place was 39 cps. The figure /67 depicts schematically flame pulsations of the third kind which are apparently due to the rotation of the jets. The hump distorting the outer boundary of the flame front is produced by the fact that the end of propellant jet B is deflected more at the point of collision than the end of oxygen jet A. The frequency Z of the rotation of the hump and the flame as a whole is the same as the fundamental frequency of the radiated sound. An idea about the relationship between the flame rotation frequency and the jet speeds for different distances between the nozzles can be obtained from the appended table.

In the table f is the flame rotation frequency in cps, V_1 and V_2 are the oxidizer and propellant velocities, averaged over the cross section, in m/sec, S is the distance between nozzles in mm, and d_1 and d_2 are the diameters of the oxygen and propane nozzles, respectively.

REFERENCE

1. Kondrat'yev, V.I. Zvukoobrazovaniye pri stolknovenii gazovykh struy [Sound Formation on Collision of Gas Jets]. Akusticheskiy zhurnal, Vol. X, 1. 1964.

FREQUENCY CHARACTERISTICS OF BAR-TYPE GAS-JET ACOUSTIC GENERATORS

Yu. Ya. Borisov and N. M. Gykina

ABSTRACT: The present article presents results of an experimental study of the relationship between the internal structure of the jet and the frequency of sound vibrations produced by the generator and the geometric dimensions of some of its principal elements, i.e., the bar and jet diameter, resonator dimensions, etc.

As a result of work performed in developing acoustic nozzles for atomizing liquid fuel [1, 2] a great deal of interest is expressed lately in gas-jet generators, in particular in bar-type radiators, which are most economical and stable in operation [3, 4]. Bar-type radiators, similar to Hartmann's generator, have inherent resonance frequencies at which the acoustic power, and consequently also the efficiency are maximum [5]. /68*

The design of gas-jet radiators involves difficulties not only in estimating the power, but also the frequency for the specified parameters of the device. This is in part due to the almost total lack of theoretical work on this problem (of certain interest in this respect is the recent article by Mørch [6], although it is concerned with a simpler model—generation of sound by a supersonic jet colliding with a flat reflecting disk). Another cause is the large number of factors affecting the frequency of radiation, i.e., diameters d_n of the nozzle, d_r of the resonator, d_b of the bar, the resonator depth h, the nozzle-to-resonator distance l, as well as the compressed air pressure P (see the schematic of a bar-type radiator in Fig. 1).

In the process of developing new gas-jet radiators of acoustic energy we have experimentally clarified some relationships between the generation frequency and the tuning parameters and the structural dimensions of the whistle.

It is known that in the sonic (conical) nozzle, the length of the first cell of the jet of air discharged to the atmosphere is determined by [7] /69

$$\Delta_0 = 1{,}12 d_n \sqrt{P - 0{,}9}$$

(here Δ_0 and d_n are expressed in mm, and P is in kg/cm^2). Due to the inavailability of data on distortion of the jet upon introduction of a center bar and

*Numbers in the margin indicate pagination in the foreign text.

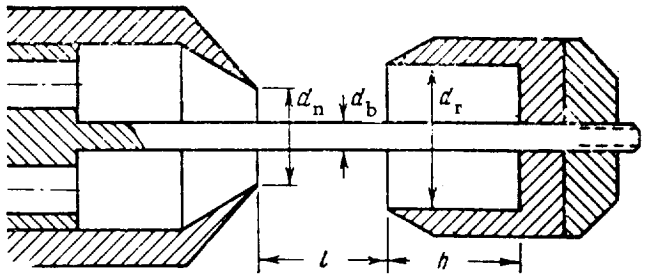

Figure 1. Schematic Diagram of a Bar-Type Radiator.

a resonant cavity into it, we have performed studies to determine the effect of these components on the distribution of static pressure in the jet. The measurements were made by means of a pressure measuring tube 1 mm in diameter. Figure 2 shows the length of the first cell of the jet (for a nozzle pressure of 3 atm gage) as a function of the nozzle and bar diameters. Similar measurements were also made at other air pressures for the same range of nozzle and bar diameters (d_n = 3-13 mm, d_b = 3-8 mm). It can be seen from this figure that, as the bar diameter is made larger, i.e., as the effective opening of the nozzle becomes smaller, the length of the cell decreases. The empirical formula which was derived on the basis of our measurements has the form

$$\Delta_0 = (1.1d_n - 0.08d_b^2 - 0.15d_b)\sqrt{P - 0.9}\ .$$

Since the operating frequency of Hartmann's generator is inversely proportional to the nozzle diameter, while the energy of the jet and consequently the radiation power is determined by the jet's cross section, then an increase in frequency in ordinary radiators involves an appreciable reduction in the acoustic power. From this point of view bar-type radiators are of great interest, since reducing the cell length by introducing a central bar permits increasing the frequency without appreciably changing the jet's cross section. This makes it possible to attempt developing higher power high-frequency radiators by increasing the energy of the jet in the annular nozzle.

The coaxial placing of a resonant cylindrical cavity in a jet produces high-power acoustic vibrations in the system; the frequency of these vibrations is determined by the length of the cell, as well as by the parameter's of the resonator. However, Hartmann has noted that elastic vibrations may appear in the jet even when the resonator is replaced by a reflecting disk. This fact, as well as examination of Töpler [schlieren] photographs of the shock wave moving in the jet when the latter impinges on a wall served as a basis for Mørch's suggestion that generation proceeds by a resonance mechanism. /70

According to this hypothesis, the appearance of sound is due to oscillation of the shock wave, the former being produced by disturbances reflected from the stiff surface. Here the natural frequency of the shock wave-resonator system is determined by the time it takes for the disturbance to travel from the shock wave to the wall and back.

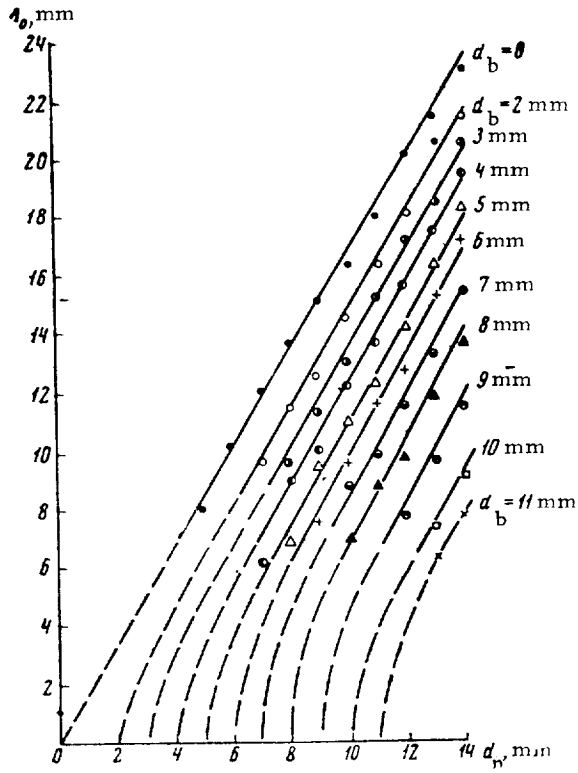

Figure 2. The Length of the First Cell as a Function of the Nozzle and Bar Diameters.

The above hypothesis has been qualitatively verified by us by visual observation of the shock wave motion when the jet impinged on the reflecting disk in bar-type and bar-less systems. In addition, such a generation mechanism satisfactorily explains the appearance of lower frequency in the radiation than would follow from the relaxation theory. In fact, if we regard the distance between the shock wave and the reflecting wall as a quarter-wave tube with one stiff and one compliant wall, which is capable of varying its dimensions by moving away the shock wave from the bottom of the resonator when the counter-pressure in it increases, then such a scheme of the resonating system, taking into account radiation from the open end, may make it possible to theoretically determine the natural frequencies of the radiation. /71

We have performed an experimental study of the distortion of jet by placing a reflecting disk and resonator into it. The characteristic curves of static-pressure distribution along the jet as a function of the distance from the reflector are presented in Fig. 3b through f for the case of d_n = 13 mm, d_b = 6 mm, disk diameter D= 19 mm and P= 3 atm gage. Figure 3a shows, for comparison, the pressure distribution of the annular jet without the reflector. The data thus obtained show that placing a disk in a jet appreciably changes the character of the latter; here the cell located near the reflector is deformed, i.e., its length

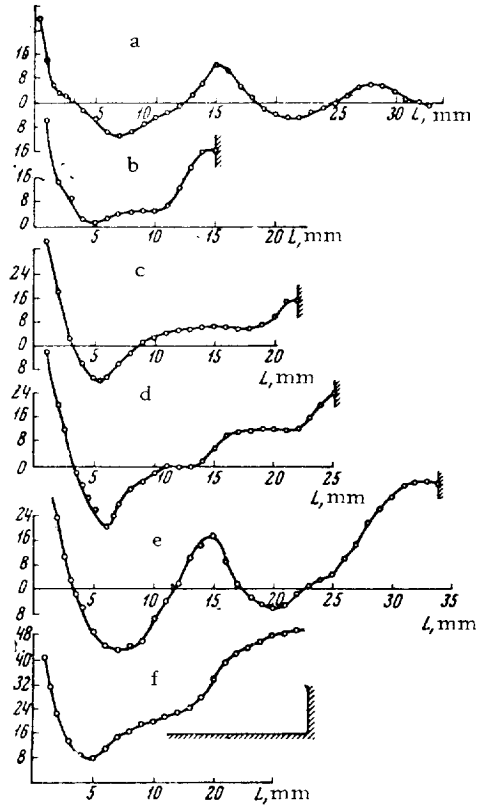

Figure 3. Pressure Distribution along a Jet (a Pressure P = 3 Atm Gage Is Laid off on the Ordinate).

may be increased appreciably. When the disk is moved to the end of the second cell (Fig. 3e) the jet is reconstructed and the first cell is found to be almost undistorted (compare the distributions of Figs. 3a and 3e).

The frequency of vibrations as a function of the distance from the reflector for the case of generation by placing a disk in the jet is shown in Fig. 4. Generation of sound is observed up to A = l + h = 24.8 mm, with the frequency decreasing monotonically with an increase in A. As the reflector is moved past this point, the generation ceases and the signal received by the microphone is only the (intrinsic) noise of the jet. Comparison of the frequency curve with the pressure distributions of Fig. 3 shows that continuous variation of frequency is observed as long as the first cell undergoes forced elongation in the presence of the reflecting wall. When the second cell is formed in the jet (between the nozzle and the reflector), generation ceases. As will be shown below, in systems with a resonator it is possible to have generation even when the shock wave oscillates in the second cell. /72

Replacement of the reflecting disk by a resonating cavity also somewhat changes the pressure distribution in the jet. The absolute pressures at the bottom of the resonator increase (see Fig. 3f), producing an increase in the back pressure; here the shock wave moves closer to the nozzle. This increases the time needed by the disturbances for traveling to the bottom of the resonator and back and correspondingly decreases the vibratory frequency of the pressure wave- resonator system. Hence increasing h, the resonator depth, starting as early as h = 0, reduces the radiation frequency.

The frequency characteristics of gas-jet bar-type radiators were studied on a unit in which the resonator could be moved by remote control relative to the nozzle and in which the resonator depth could be varied. A set of replaceable nozzles, bars and resonators was used for changing the parameters of the radiator within wide limits. The work was performed in the majority of cases at air pressures of 3 atm gage. The frequency was determined by means of wide-band, ball-type piezoelectric pickup, the signal from which was fed to an AS-3 spectrum analyzer. The range within which the different parameters of the gas-jet radiator under study were varied is shown in the table. /74

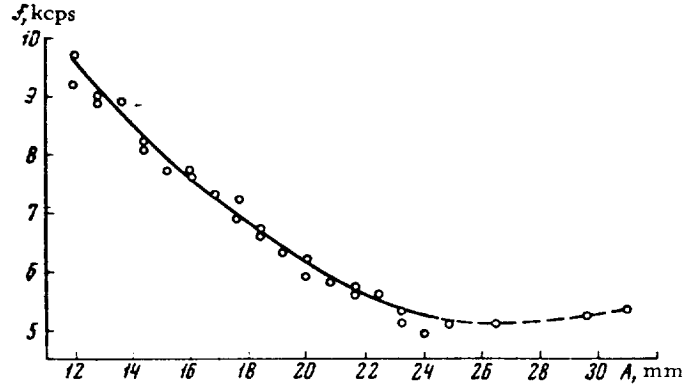

Figure 4. The Frequency as a Function of the Distance From the Reflector.

To illustrate the effect of parameters l and h on the radiation frequency and on the possibility of generation in the second cell of the jet, Fig. 5 presents graphs for a radiator with d_n = 12 mm, d_r = 17 mm and d_b = 8 mm. As follows from the figure, generation on oscillation of the shock wave in the first cell of the jet is observed for h = 3-13 mm. For h in excess of 13 mm generation starts already in the second cell, since for Δ_0 = 10 mm (see Fig. 2) and h exceeding 13 mm, the value A = l + h exceeds 18 mm, i.e., twice the cell length (the /75

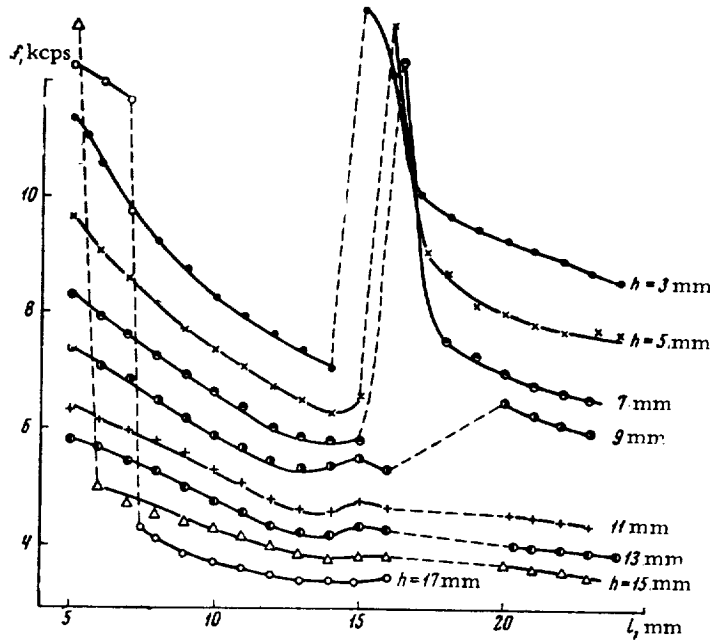

Figure 5. The Acoustic Frequency as a Function of the Nozzle-Resonator Distance for Different Resonator Depths.

TABLE

d_n, mm	d_b, mm	d_r, mm				Limits of Variation	
						l, mm	h, mm
13	7	13	15	17	19	5—14	1—15
13	8	—	—	—	19	5—14.8	0—15
13	6	—	—	—	19	5—14.8	1—15
13	5	—	—	—	19	5—14.8	0—15
13	4	—	—	—	19	5—14.8	0—15
12	7	13	15	17	19	3—22	8—15
12	8	—	—	17	—	5—24	4—1.
10	7	13	15	17	19	4—13	1—1[illegible]
9	7	13	15	17	19	4—12	1—14

second cell is by 10-15% shorter than the first). For l exceeding 14 mm ($A \geq$ 17 mm, $h \leq 13$ mm), generation ceases; the jet is reexcited when $l > 19$ mm, i.e., when the shock wave oscillates in the second cell of the jet. Within the limits of the possible distortion of the cell the frequency variations are sufficiently smooth. Similar frequency curves were obtained by us also for other values of d_n, d_b and d_r with only this difference that for systems with a large cell length ($d_n - d_b$ is large) and in range of variation of l and h under study the measurements were performed always in the first generation region (first cell). It is natural that with an increase in Δ_0 the boundaries of smooth variation of the frequency become wider. /75

The effect of the bar diameter on the acoustic frequency can be illustrated by graphs (Fig. 6) for a radiator with d_n = 13 mm, d_r = 19 mm, P = 3 atm gage and h = 10 mm. It should be noted that for small l the size of the diameter affects the frequency more than for large l.

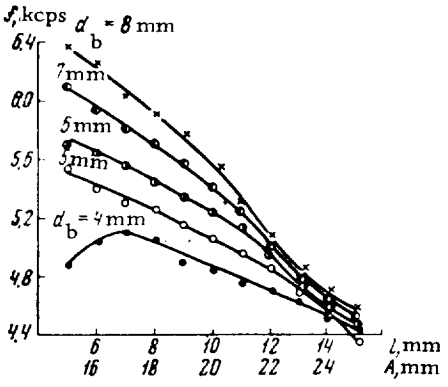

Figure 6. Effect of Bar Diameter on the Acoustical Frequency.

Figure 7 shows the radiation frequency as the nozzle-to-resonator distance for d_n = 12 mm and d_b = 7 mm, with h = 19 and 12 mm. The frequency curves for different d_r are identical, which is apparently due to identical values of parameter A. The frequency reduction with increasing the resonator diameter is attributable to the increase in the volume of air stagnated in the resonator and to the attendant change in the back pressure. /76

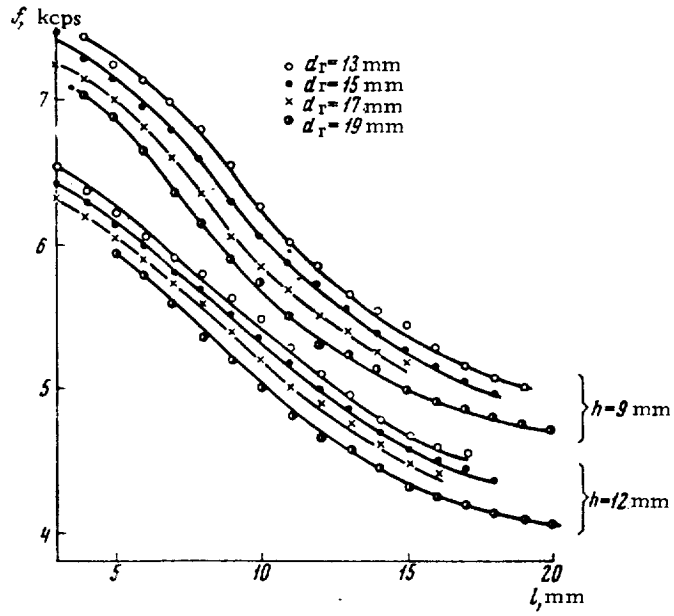

Figure 7. Acoustic Frequency as a Function of the Nozzle-to-Resonator Distance.

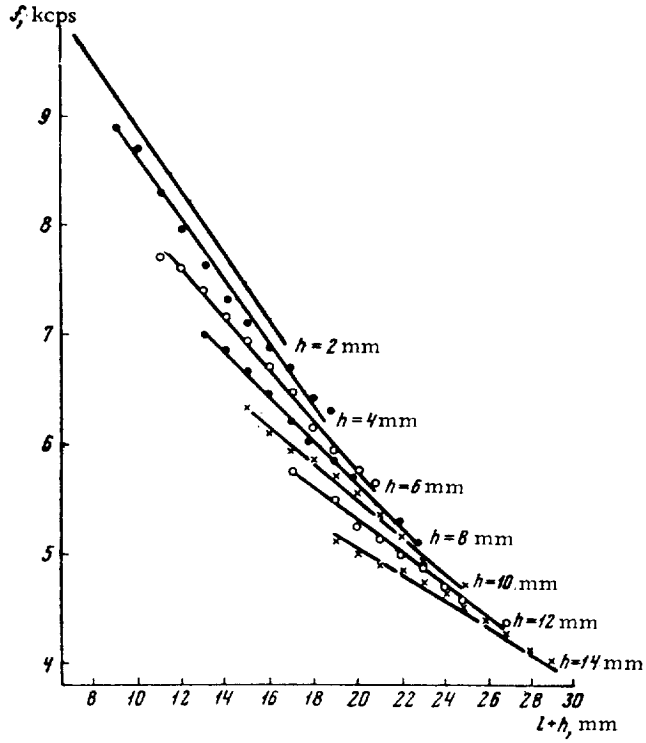

Figure 8. The Acoustic Frequency as a Function of the Sum of Distances (A = l + h).

Figure 8 shows the frequency as a function of parameter A; here, unlike a similar curve presented in [5], this curve shows the effect of the value of h. This curve is for a resonator with d_n = 13 mm, d_b = 7 mm and d_r = 17 mm.

The most detailed studies which we have performed with a radiator with d_n = 13 mm, made it possible to obtain for the given nozzle diameter a formula relating the effect of different parameters of the radiator (within the limits shown in the table) on the radiation frequency. The formula is valid for a radiator operating in the first cell of the jet (taking into account its distortion, which was pointed out above) with a maximum error of ±10%

$$f = \frac{c}{4[h + (0.4 - 0.015h)(d_r - d_b) + 0.4l]},$$

where l, d_r, d_b and h are in mm, f in cps, and c is the speed of sound at 20° C in mm/sec.

Similar expressions can be obtained also for other nozzle diameters.

REFERENCES

1. Lamekin, N. S. Metod rascheta zazora generatora forsunki zhidkogo topliva [A Method of Calculating the Gap of the Generator of a Liquid-Fuel Burner]. VUZov, ser. machinostroyen., No. 10, 114-123, 1961.
2. Fortman, W. K. Acoustic Generator and Shock Wave Radiator. [USA Pat. cl. 116-137, No. 3064619, 1962].
3. Landais, M. Le. Research on the Stem—Jet Acoustic Whistle. Ultrasonic News, Vol. 4, No. 4, 7-9, 1960.
4. Litsios, J. Industrial Application of Gas—Jet Sonic Generators. IEEE. Trans. Ultrasonic Eng. Vol. 10, No. 2, 91-95, 1963.
5. Borisov, Yu. Ya., V. N. Ginin and N. M. Gynkina. Razrabotka i issledovaniye sterzhnevogo gazostruynogo izluchatelya GSI-4 [Development and Investigation of the GSI-4 Bar-Type Gas-Jet Radiator]. Akusticheskiy zhurnal, 11, No. 2, 140-147. 1965.
6. Mørch, K. A. A Theory for the Mode of Operation of the Hartmann Air—Jet Generator. J. Fluid Mech., Vol. 20, No. 1, 141-159, 1964.
7. Gartmann, J. The Acoustic Air—Jet Generator. Ingeniørvidenskabelige skrifter, 1939, No. 4.

THE SUPERSONIC AIR JET AS A SOURCE OF SOUND

V. M. Mamin and A. V. Rimskiy-Korsakov

ABSTRACT: This article is devoted to the timely problem of experimental study of the noise of a supersonic air jet.

The discharge of air jets into open space is accompanied by radiation of /77* high-intensity sound. This phenomenon is characteristic of subsonic as well as supersonic jets, in the last case this becomes particularly interesting. The cause of the jet noise is the instability of the tangential velocity discontinuity i.e., instability of the boundary between the jet and the surrounding medium, which is demonstrated in amplification of small perturbances formed at the base of the jet (as these propagate along the jet). This results in the formation of a boundary layer which develops gradually into a turbulent region which finally absorbs it.

The noise in a supersonic jet is produced in its subsonic part, as well as in its supersonic flow body. The noise in the subsonic parts does not differ in principle from the noise of the subsonic jet which was described in satisfactory detail by Lighthill [1].

The noise produced by the main supersonic body of the flow is more complex. It may be formed by two mechanisms. These are the feedback mechanism suggested by Powell [2] for explaining the radiation of a discrete tone by the jet and a mechanism based on the known fact that if a disturbance travels at the interface of two media with a speed greater than the speed of sound in one of them, then an acoustic wave is radiated into this medium.

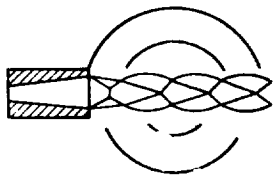

Figure 1. Schematic of an Overexpanded Supersonic Jet and Acoustic Waves.

The noise of supersonic jets has been studied by many authors. However, they describe results obtained with converging nozzles. The relatively low velocities which are obtained with these nozzles do not suffice for discovering some acoustic phenomena which are related to a developed supersonic main body of the flow. The selection of a converging nozzle meant that the only kind of discharge which would be obtained /78 would be an incompletely expanded jet. In addition, these authors have studied only a relatively small pressure range in which radiation of a discrete tone was observed. In performing the experiments described below we have attempted, as far as possible, to eliminate these shortcomings.

*Numbers in the margin indicate pagination in the foreign text.

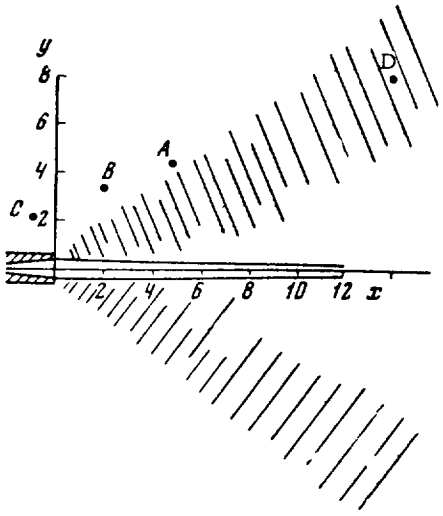

Figure 2. Schematic of the Jet Produced under Design Condition and of the Acoustic Waves.

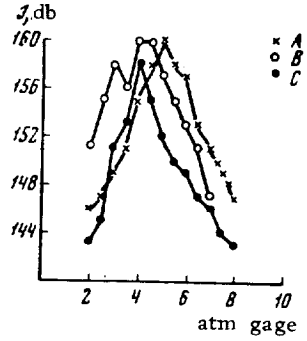

Figure 3. Intensity of the Discrete Sound as a Function of the Initial Pressure (0 db = 2.10^{-4} bars).

The measurements were made on an impulse-type setup. Air was supplied from a bank of air bottles through a control valve into a antechamber and then to the nozzle. Pressures of up to 15 atm gage can be obtained in this chamber. In our experiments we have used two geometrically similar nozzles: one with throat diameter of 4.5 and outlet diameter of 6.3 mm; all the dimensions of the second nozzle were half of the first.

Our studies have verified the fact that phenomena observed in jets discharged from the large and small nozzles are completely similar (the similarity factor was $K = L_1/L_2$, where L_1 and L_2 are the characteristic dimensions of the large and small nozzles). For this reason all the results presented below were reduced to the large nozzle.

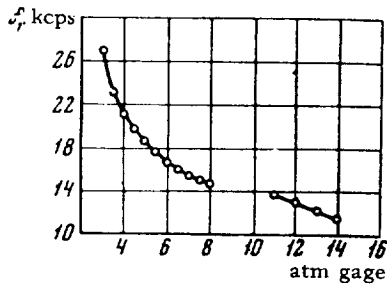

Figure 4. The Tone Frequency as a Function of the Antechamber Pressure.

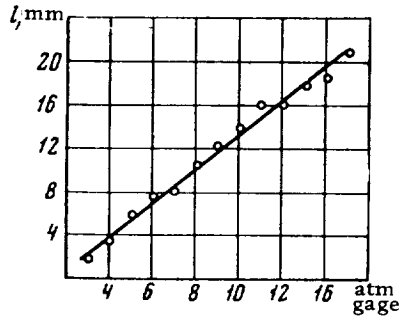

Figure 5. The Length of the Jet's Cell as a Function of the Antechamber Pressure.

The velocity of discharge from the nozzle was 530 m/sec, and the Mach number was 2.17. Design operating conditions prevailed when the pressure in the antechamber was approximately 9 atm gage.

We have obtained photographs of the jet and of the acoustic waves and the spectra of the jet's noise; we have measured the length l of the first cell (mm) and the absolute peak sound level I (db) for different pressures P (atm gage) in the antechamber and for different positions of the microphone

$A\ (x = 4.5$ cm; $y = 4.2$ cm),
$B\ (x = 2.1$ cm; $y = 3.3$ cm),
$C\ (x = -0.7$ cm; $y = 2.1$ cm),
$D\ (x = 14$ cm; $y = 8$ cm).

For P = 2 atm gage, a supersonic main body of the flow with a cellular structure starts forming (Fig. 1). When P = 3 atm gage, a narrow peak, corresponding to the radiation of a discrete tone, appears in the noise spectrum. Its intensity increases rapidly and at P = 4-5 atm gage it exceeds the noise level by 25-30 db. As the pressure is increased further, the peak decreases and near /80
the design operating conditions (approximately P = 8 atm gage) it disappears. For P = 9-10 atm gage the jet takes on its design shape and loses its cellular structure (Fig. 2). At P = 11 atm gage shock waves appear again and together with them a small peak appears in the jet's noise spectrum. This peak increases slowly as the pressure is raised and reaches 5 db at P = 15 atm gage. In addition to the fundamental tone, the second, third and fourth harmonics are [also] observed in the noise spectrum.

The radiation of the discrete tone is accompanied by concentrical spherical waves with a center in the region of the sixth cell. This radiation does not have a clearly pronounced directivity. The sound levels measured with the microphone in locations A, B and C have a maximum of approximately the same height for those P for which maximum radiation of the discrete tone is observed (Fig. 3).

Figure 4 shows the graph of the tone frequency f vs pressure P in the antechamber. It can be seen from the figure that both parts of the graph can be connected and this almost does not affect the general shape of the curve,

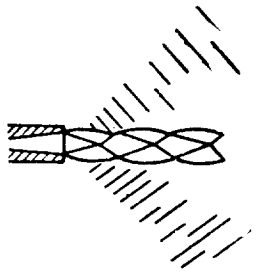

Figure 6. Schematic of an Incompletely Expanded Jet and of the Acoustic Waves.

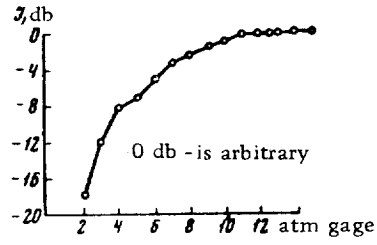

Figure 7. Intensity of Sound in the Region of a Directed "Beam" as a Function of Pressure.

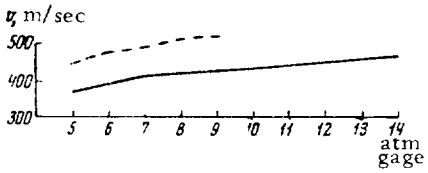

Figure 8. Comparison of the Speed of a Disturbance with the Velocity of the Jet as a Function of the Antechamber Pressure (the Dashed Line Denotes the Calculated Speed, the Solid Line Designates the Speed Found from the Photograph, $v = c/\arccos \varphi$).

i.e., the behavior of f(P) does not change suddenly when passing through operation under design conditions. The curve of the jet's cell length as a function of P (Fig. 5) behaves similarly. Reducing the dimensions of the nozzle reduces by the same factor the length of the cell and together with it the wavelength of the radiated tone. All this shows that a close relation exists between the internal structure of the jet and the frequency of the discrete tone.

We now consider the radiation of the second type mentioned at the start of this article. In order for such radiation to exist it is necessary to have a developed supersonic body of the flow, since otherwise the perturbance cannot be amplified to the extent that the radiation would become perceptible. Hence it is difficult to expect that it would be found at small P. Since the main body of the jet has a finite length, it should be expected that the radiation will appear on a photograph in the form of an expanding beam. Radiation of this kind was found at $P \geqslant 6$ atm gage. It emerged from the surface of the jet in the region of the first cell and had the shape of a beam with an opening angle of approximately 25° (Fig. 6). The sound field intensity inside this beam increases with an increase in P to about 13 atm gage and then remains constant (Fig. 7, microphone position D).

According to T. Kh. Sedel'nikov and V. M. Mamin, acoustic waves of this type should be radiated at an angle to the jet's axis which is

$$\varphi = \arccos \frac{c}{v} \qquad (1)$$

(c is the speed of sound in the surrounding medium and v is the speed of propagation of the disturbance, which is close to the speed of the jet proper near its boundary), which can be determined from the photograph. In order to compare /81
the theoretical and experimental results we have calculated the velocity of the disturbance from Eq. (1) and the velocity of the jet in the region of the first cell for the case of isentropic flow. Figure 8 shows these quantities as a function of P. The shape of both curves is qualitatively the same. Calculations show that the ratio of the rate of propagation of the disturbance to the velocity of the jet for the same pressures is approximately 0.82. This is in agreement with experimental results obtained by Davies and Oldfield [3] for the rate of propagation of eddies in a boundary and agrees with the estimated rate of propagation of disturbances of different form along the boundary of a jet made by Sedel'nikov in an article published in the present collection.

The spectrum of this radiation is similar to the noise spectra of the turbulent part of the jet with a superimposed discrete tone, when the latter occurs. This should have been expected, since the jet here acts as an amplifier of disturbances and converts them into directed radiation, while the noise of the turbulent part of the jet and the discrete tone serve as the disturbance sources.

All the aforementioned verifies the assumption by Sedel'nikov and Mamin that radiation of this type exists. A jet being discharged from a supersonic nozzle is thus a source of acoustic radiation of three types:

a) radiation of the turbulent part of the jet, which takes place for any /82
antechamber pressures; b) radiation of a discrete tone, which is characteristic of moderate antechamber pressure and incompletely expanded jet, and 3) radiation produced by rapidly propagating boundary disturbances, characteristic of the design operating conditions and incompletely expanded jet, for quite high antechamber pressures.

REFERENCES

1. Lighthill, M.J. Proc. Roy. Soc., Vol. 211, 1107 (1952); Vol. 222, 1148 (1954).
2. Powell, A. Proc. Phys. Soc., Vol. 66, 408B (1953); Vol. 67, 412B (1954).
3. Davies, M.J. and D.E.S. Oldfield. Acustica, Vol. 12, 257 (1962).

THE FREQUENCY SPECTRUM OF THE NOISE OF A SUPERSONIC JET

T. Kh. Sedel'nikov

ABSTRACT: This paper presents a theoretical explanation of certain features of the noise spectrum of supersonic jets. It shows that using linearized equations of the acoustics of a moving medium, it is possible to calculate the frequency of the maximum of the frequency spectrum of the noise of a hot supersonic jet.

Statement of the Problem

/83*

There exist a number of experimental facts which cannot be coherently explained by the existing sound-formation theories. Primary among these is the frequency spectrum of the noise of a jet, which peaks out at Strouhal numbers of 0.2-0.4 [1].

According to Lighthill's theory [2], the noise of a jet has its origin in the quadrupole radiation of sound by the jet's turbulence, which is regarded as given. This leaves open the question of the frequency spectrum of the noise radiated by it.

The turbulence in the jet is produced by a velocity discontinuity at the interface between the jet and the surrounding gas, which represents as if a "delta-shaped" turbulence. Photographs of hot and cold supersonic jets show that, up to appreciable distance to the nozzle's outlet section this tangential velocity discontinuity is quite thin, while the oscillation of the boundary of this layer is quite small.

We make the following simplifying assumptions: 1) the jet is strictly cylindrical, the angle of its "divergence" is disregarded; 2) the tangential velocity discontinuity at the boundary of the jet is infinitesimally thin; 3) the jet discharge conforms to its design shape, the presence of "barrels" (cells) in the jet is disregarded; 4) the amplitude of the oscillations of the jet's boundary is small, so that the linear approximation is valid; 5) the viscosity of the gas of the jet and of the surrounding gas is disregarded.

The Dispersion Equation

/84

The assumptions made above make it possible to regard the gas flow as laminar and to regard the disturbances of this flow as infinitesimal. They are acoustic in character and obey the wave equations. We introduce the notation: ρ - density of the undisturbed medium, c - speed of sound in the latter, v -

*Numbers in the margin indicate pagination in the foreign text.

macroscopic velocity of the medium, φ - acoustic potential, ω- circular frequency, Δ - Laplacian operator, a - radius of the jet.

The subscript of a quantity will denote the region of the medium to which it pertains. We use a stationary system of cylindrical coordinates with the z axis along the jet, with radius vector r and azimuth γ.

The wave equations have the form [3]

$$\Delta\varphi_i = \frac{1}{c_i^2}\left(\frac{\partial}{\partial t}+v_i\frac{\partial}{\partial z}\right)^2\varphi_i . \tag{1}$$

Quantities pertaining to the surrounding gas are denoted by "0" as the subscript, the subscript of quantities pertaining to the gas of the jet being by "1."

Only receding waves should exist at infinity, while the acoustic potential should be finite everywhere. On the boundary of the jet we have equality of pressures

$$\rho_0\left(\frac{\partial}{\partial t}+v_0\frac{\partial}{\partial z}\right)\varphi_0\Big|_{r=a}=\rho_1\left(\frac{\partial}{\partial t}+v_1\frac{\partial}{\partial z}\right)\varphi_1\Big|_{r=a} \tag{2}$$

and compatibility [equality] of the displacements of the jet's boundary

$$\left(\frac{\partial}{\partial t}+v_1\frac{\partial}{\partial z}\right)\frac{\partial\varphi_0}{\partial r}\Big|_{r=a}=\left(\frac{\partial}{\partial t}+v_0\frac{\partial}{\partial z}\right)\frac{\partial\varphi_1}{\partial r}\Big|_{r=a}. \tag{3}$$

We shall seek the solution of Eq. (1) satisfying the condition at infinity and the requirement that the potential be finite in the form

$$\left.\begin{matrix}\varphi_0(r,\gamma,z,t)\\ \varphi_1(r,\gamma,z,t)\end{matrix}\right\}=\cos n\gamma\cdot e^{i(kz-\omega t)}\times\begin{cases}AH_n^{(1)}(\varkappa_0 r),\\ BJ_n(\varkappa_1 r),\end{cases} \tag{4}$$

where A, B and k are constants, $H_n^{(1)}(x)$ is an nth order Hankel function of the first kind, and J_n is an nth order Bessel function

$$\varkappa_i^2=\left(\frac{\omega-kv_i}{c_i}\right)^2-k^2. \tag{5}$$

Using Eqs. (2) and (3) we can eliminate A and B and get an expression relating k and ω

$$\frac{1}{(\omega - kv_0)^2}\frac{\varkappa_0 H_n^{(1)'}(\varkappa_0 a)}{\rho_0 H_n^{(1)}(\varkappa_0 a)} = \frac{1}{(\omega - kv_1)^2}\frac{\varkappa_1 J_n'(\varkappa_1 a)}{\rho_1 J_n(\varkappa_1 a)} \tag{6}$$

which is the so-called dispersion equation. Henceforth we shall for simplicity drop the superscript of Hankel's function and set $v_0 = 0$. For long-wave disturbances ($\varkappa a \to 0$) we find /85

$$\frac{kv}{\omega} = \begin{cases} 1 \pm i\sqrt{\frac{\rho_0}{\rho_1}}, & n \neq 0 \\ 1, & n = 0. \end{cases} \tag{7}$$

It follows from the above expression together with Eq. (7) that long-wave disturbances propagate along the boundary of the jet with the jet's velocity

$$\varphi_0, \varphi_1 \sim \exp\left[i\omega\left(\frac{z}{v} - t\right)\right] \times \begin{cases} \mathscr{C} + Fz, & n = 0 \\ \exp\left[\pm\frac{\omega}{v}\sqrt{\frac{\rho_0}{\rho_1}}z\right], & n \neq 0 \end{cases} \tag{8}$$

with the n = 0 mode increasing (decreasing) linearly, while all the modes n > 0 increase (decrease) exponentially.

Estimating the shape of the frequency spectrum of the jet on low frequencies, we find

$$I = 20\log\frac{|p|}{p_0} = \text{const} + 10\pi\log_{10}e\frac{z}{2a}\text{St}, \tag{9}$$

where

$$\text{St} = \frac{2af}{v_1}\frac{c_1}{c_0} \tag{10}$$

and it was assumed that

$$\rho_0 c_0^2 \cong \rho_1 c_1^2, \tag{11}$$

which is valid for the same ratio of specific heats for the gas of the jet and that of the surrounding medium.

In the opposite case of short-wave disturbances ($|\varkappa a| \to \infty$) we assume that the roots of Eq. (6) are complex. Then it will take on the form

$$\frac{\rho_0}{\varkappa_0} + \frac{\rho_1}{\varkappa_1}(1 - \xi)^2 = 0, \quad \xi = \frac{kv}{\omega}. \tag{12}$$

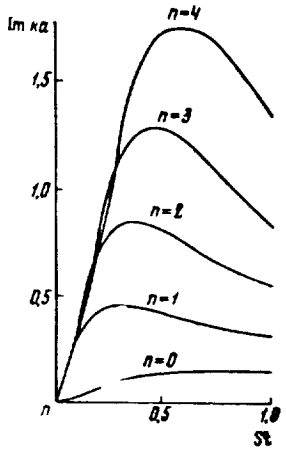

Figure 1.
Imaginary Part of the Projection of the Wave Number on the Axis of the Jet.

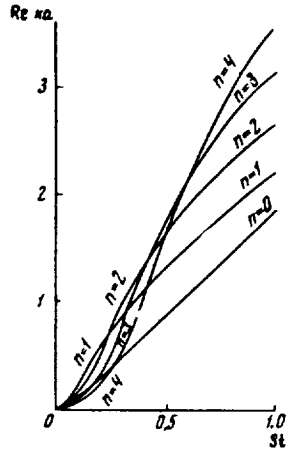

Figure 2.
Real Part of the Projection of the Wave Number on the Axis of the Jet.

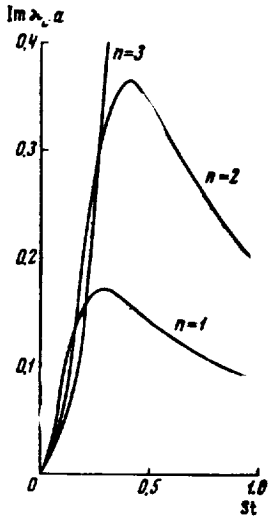

Figure 3.
Imaginary Part of the Projection of the Wave Number on a Plane Perpendicular to the Axis of the Jet.

Following Landau [4], it can be shown that this equation with conditions (11) and

$$v_1^{2/3} > c_1^{2/3} + c_0^{2/3} \tag{13}$$

has only real roots. This contradiction leads to the conclusion that on condition (11) for sufficiently high velocities and frequencies, Eq. (6) has only real roots.

Numerical Solution of the Dispersion Equation /86

Equation (6) was solved numerically on the Minsk-2 computer by a method close to the Newton-Rafson method [5]. For illustration we present the roots of Eq. (6) for a hot supersonic jet with $v_0 = 0$, $v_1/c_1 = 2.5$ and $\rho_0/\rho_1 = 9$ (Figs. 1, 2 and 3) as a function of the Strouhal number (10).

Physical Analysis of Results /87

It follows from analyzing the results of the numerical solution that the rate of increase of the disturbance along the jet for a purely radial mode of vibrations ($n = 0$) is always lower than for axially unsymmetrical modes. For some Strouhal numbers the rate of increase of the disturbance reaches a maximum.

We now express the acoustic pressure away from the jet in terms of ξ, the amplitude of vibrations of the jet's boundary

$$\frac{|p|}{\xi} = \omega^2 \cdot \left| \frac{H_n^{(1)}(\varkappa_0 a)}{\varkappa_0 H_n^{(1)}(\varkappa_0 a)} \right| \cdot \frac{a^2}{r^2} \exp\left[- \operatorname{Im} \varkappa_0 (r - a) \right]. \tag{14}$$

The graph shows $\operatorname{Im} \varkappa_0$ as a function of the Strouhal number of the mode. It is seen that the main contribution to the far sound field is made by the first mode, which has the smallest $\operatorname{Im} \varkappa_0$. It has its maximum for a Strouhal number of 0.2-0.3, which is in satisfactory agreement with experimental results [1].

In the near sound field a contribution is made also by higher modes, which correspond to a spectrum with higher frequencies.

REFERENCES

1. Yudin, Ye. Ya, editor. Bor'ba s shumom [Sound Abatement]. Stroygiz. 1964.
2. Lighthill, M.J. Proc. Roy. Soc., Vol. A.211,546 (1952); Vol. A.222, 1 (1954).
3. Andreyev, N.N. and I.G. Rusakov. Akustika dvizhushcheysya sredy [Acoustics of a Moving Medium]. GTTI, 1934.
4. Landau, L. Doklady AN SSSR, Vol. 44 (1944).
5. Lance, G.N. Numerical Methods for High-Speed Computers. [Translated from English], 1962.

THE DISCRETE COMPONENT OF THE FREQUENCY SPECTRUM OF THE NOISE OF A FREE SUPERSONIC JET

T. Kh. Sedel'nikov

ABSTRACT: This article presents a theoretical explanation of the discrete component of the frequency spectrum of the noise of a jet. The instability of pulsations of plane and axisymmetrical jets is analyzed to show the feasibility of predicting the formation of a discrete component in a jet's noise spectrum.

Basic Relationships Governing the Radiation of a Discrete Component of the Noise Spectrum of a Jet

/88

A feature peculiar to the radiation of sound by cold supersonic jets is the presence of a discrete component in the frequency spectrum of the noise of these jets. Experiments show that this component is directly related to the cellular structure of the supersonic jet, i.e., to the presence of oblique shock waves [pressure discontinuities] in it. The available theoretical concepts of the mechanism of formation of this component is primarily due to Powell [1]. The disturbances which move along the jet pass through the shock wave and thus result in radiation of waves into the surrounding medium. Propagating in all directions, these waves are diffracted at the edge of the nozzle, which creates the disturbance in the jet, etc.

Interesting experimental work on the acoustics of transonic jets was done by Hammitt [2], Davies [3], Merle [4] and others. The quantitative behavior which is observed can be reduced to the following basic facts:

1. The discrete component of the frequency spectrum of a jet's noise is directly related to the presence of cells in the jet and when the mode of operation approaches the design mode it disappears.

2. The discrete component is more pronounced in small-diameter cold jets and is absent in hot supersonic jets.

3. The frequency of the discrete component decreases with an increase in velocity and is well described by the formula [1]

$$f_n = \frac{1}{L}\frac{vc_0}{v+c_0}n, \qquad (1)$$

*Numbers in the margin indicate pagination in the foreign text.

where L is the length of the cell, v is the velocity at which the disturbance travels along the jet, c_0 is the speed of sound in the surrounding air and n is the number of the harmonic. At transonic speeds several small discontinuities are observed in the frequency of the discrete component with hysteresis as a function of the velocity. /89

4. The discrete component is radiated near the boundaries of the 3-4th or 5-7th cells (according to different authors).

5. The radiation is practically isotropic, however it was noted that the first harmonic concentrates along the direction of motion of the jet and along the opposite direction, while the second harmonic lies at almost a right angle to the axis of the jet.

6. The radiation is relatively stable for nonround jets, while instability regions are observed in circular jets at Mach numbers of 1.2-1.5. The plane jet undergoes flexural vibrations, while the mode of vibration in the round jet near the instability region changes from radial (beaded) to axially unsymmetrical.

We now examine photographs of the sound field of a cold supersonic jet emerging from a Lava nozzle under different modes of operation (Figs. 1 through 6).* We note the following types of acoustic waves:

A. All the photographs show practically plane waves, which propagate at an angle of 30-45° to the axis of the jet.

B. At the modes at which the cells in the jet are clearly expressed, it is possible to see practically circular waves, receding from the boundaries of cells.

C. At very low pressures one sees waves emerging at the very discharge section of the nozzle. These are due to the appearance of an additional discrete tone in the Laval nozzle at supersonic speeds.

The first type of acoustic waves is attributable to a disturbance which travels along the boundaries of the jet, increasing in the process; this phenomenon was examined theoretically in [5]. The second type of waves arises when the disturbances pass through the pressure discontinuities in the jet. Below an attempt is made to clarify theoretically some of the quantitative relationships observed.

The Dispersion Equation of a Plane Jet

We shall attempt to explain the predominantly flexural character of the pulsations of the plane jet. We introduce a system of orthogonal coordinates with the z axis aligned with the direction of the jet; the latter will occupy a space

*These photographs were obtained by Mamin and Podol'skiy.

$-\Delta/2 < x < \Delta/2$. Following [5] we write the wave equations for the acoustic potential φ_0 outside the jet and φ_1 in the jet:

$$\Delta\varphi_0 = \frac{1}{c_0^2}\left(\frac{\partial}{\partial t} + v_0\frac{\partial}{\partial z}\right)^2\varphi_0, \tag{2}$$

$$\Delta\varphi_1 = \frac{1}{c_1^2}\left(\frac{\partial}{\partial t} + v_1\frac{\partial}{\partial z}\right)^2\varphi_1, \tag{3}$$ /90

with the boundary conditions at the jet's boundaries

$$\rho_0\left(\frac{\partial}{\partial t} + v_0\frac{\partial}{\partial z}\right)\varphi_0\Big|_{x=\pm\frac{\Delta}{2}} = \rho_1\left(\frac{\partial}{\partial t} + v_1\frac{\partial}{\partial z}\right)\varphi_1\Big|_{x=\pm\frac{\Delta}{2}}, \tag{4}$$

$$\left(\frac{\partial}{\partial t} + v_1\frac{\partial}{\partial z}\right)\frac{\partial\varphi_0}{\partial x}\Big|_{x=\pm\frac{\Delta}{2}} = \left(\frac{\partial}{\partial t} + v_0\frac{\partial}{\partial z}\right)\frac{\partial\varphi_1}{\partial x}\Big|_{x=\pm\frac{\Delta}{2}}. \tag{5}$$

Here v_1 and v_0 are the velocities of the jet and of the surrounding air, c_1 and c_0 are the corresponding speeds of sound and ρ_1, ρ_0 are the corresponding densities.

We break up the disturbances of the jet's boundary into symmetrical and asymmetrical. For the first the acoustic velocity at $x = 0$ is zero, while for the second the acoustic pressure at $x = 0$ is zero

$$v = \frac{\partial\varphi}{\partial x}\Big|_{x=0} = 0, \text{ (sym)} \tag{6}$$

$$p|_{x=0} = \dot{\varphi}|_{x=0} = 0. \text{ (asym)} \tag{7}$$

Conditions (6) or (7) make it possible to henceforth examine only one of the half spaces $x < 0$ or $x > 0$. We seek the solution of Eqs. (2) and (3) in the form

$$\varphi_0(x, y, z, t) = A\cdot\exp\left[i\left(Ly + kz - \omega t + \varkappa_0 x\right)\right], \tag{8}$$

$$\varphi_1(x, y, z, t) = B\cdot\exp\left[i\left(Ly + kz - \omega t\right)\right]\times\begin{cases}\cos\varkappa_1 x, \text{ (sym)}\\ \sin\varkappa_1 x, \text{ (asym)}\end{cases} \tag{9}$$

where 1/L is the period of the disturbance along the y axis, A, B and k are constants, ω is the circular frequency, while $\varkappa_0$ and $\varkappa_1$ are given by the expressions

$$\varkappa_i^2 = \left(\frac{\omega - kv_i}{c_i}\right)^2 - k^2 - L^2. \tag{10}$$

Equation (8) for Re $\varkappa_0 > 0$ corresponds to the case of receding waves. Eliminating A and B by means of Eqs. (4) and (5), we get the dispersion equation of a plane jet

$$i\frac{\varkappa_0}{\rho_0(\omega - kv_0)^2} + \frac{\varkappa_1}{\rho_1(\omega - kv_1)^2}\tan\frac{\varkappa_1\Delta}{2} = 0, \text{ (sym)} \tag{11}$$

$$i\frac{\varkappa_0}{\rho_0(\omega - kv_0)^2} - \frac{\varkappa_1}{\rho_1(\omega - kv_1)^2}\cot\frac{\varkappa_1\Delta}{2} = 0. \text{ (asym)} \tag{12}$$

In the case of low frequencies for the branch $k \to 0$ we have /91

$$\frac{\rho_1}{\rho_0}\left(\frac{\omega - kv_1}{\omega - kv_0}\right)^2 + \tanh\frac{L\Delta}{2} = 0, \text{ (sym)} \tag{13}$$

$$\frac{\rho_1}{\rho_0}\left(\frac{\omega - kv_1}{\omega - kv_0}\right)^2 + \coth\frac{L\Delta}{2} = 0, \text{ (asym)} \tag{14}$$

and at high frequencies and with Im $k \neq 0$, we have

$$\frac{\varkappa_0}{\rho_0(\omega - kv_0)^2} + \frac{\varkappa_1}{\rho_1(\omega - kv_1)^2} = 0. \text{ (both cases)} \tag{15}$$

From Eqs. (13) and (14) we find for $v_0 \ll v_1$

$$\frac{kv_1}{\omega} \cong 1 \pm i\sqrt{\frac{\rho_0}{\rho_1}\Gamma}, \tag{16}$$

Impulse photographs of the sound field of a cold supersonic jet at pressures of 1, 3, 6, 8, 11 and 14 atm gage in the antechamber (Figs. 1 through 6).

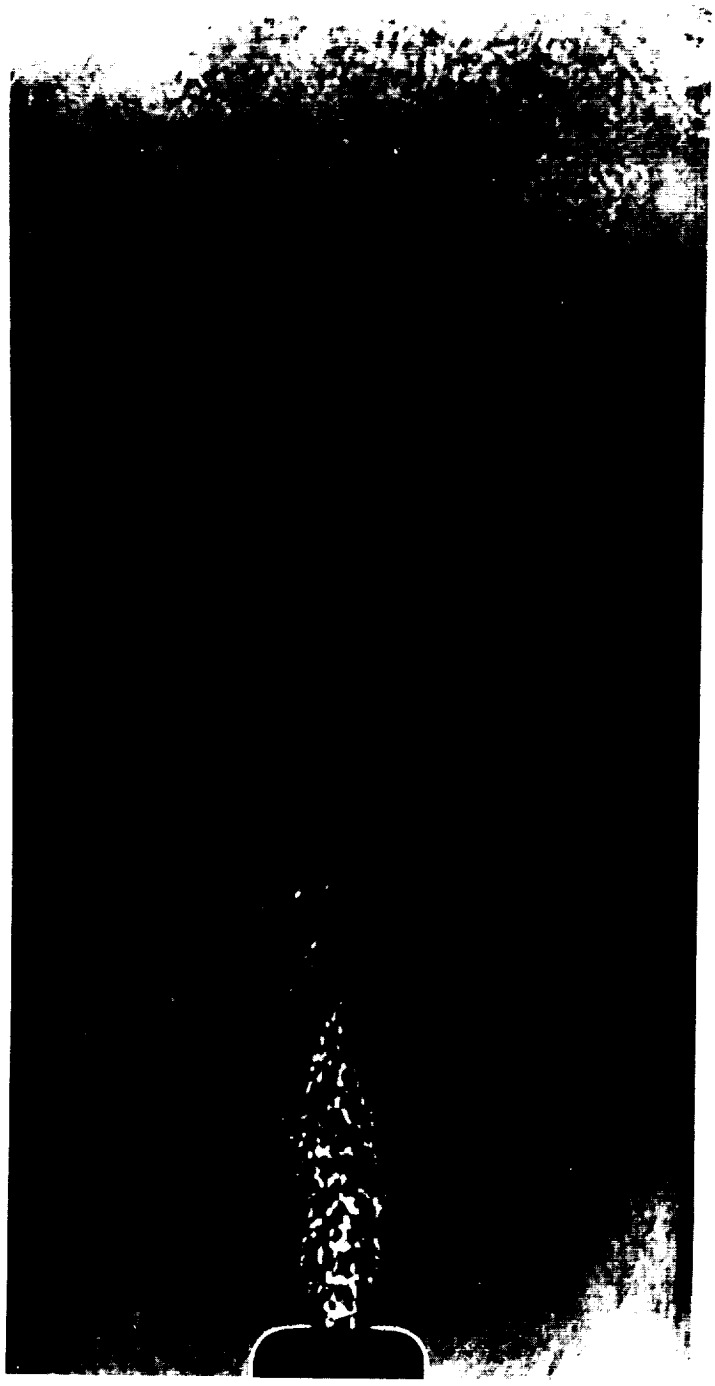

/90 a

Figure 1.

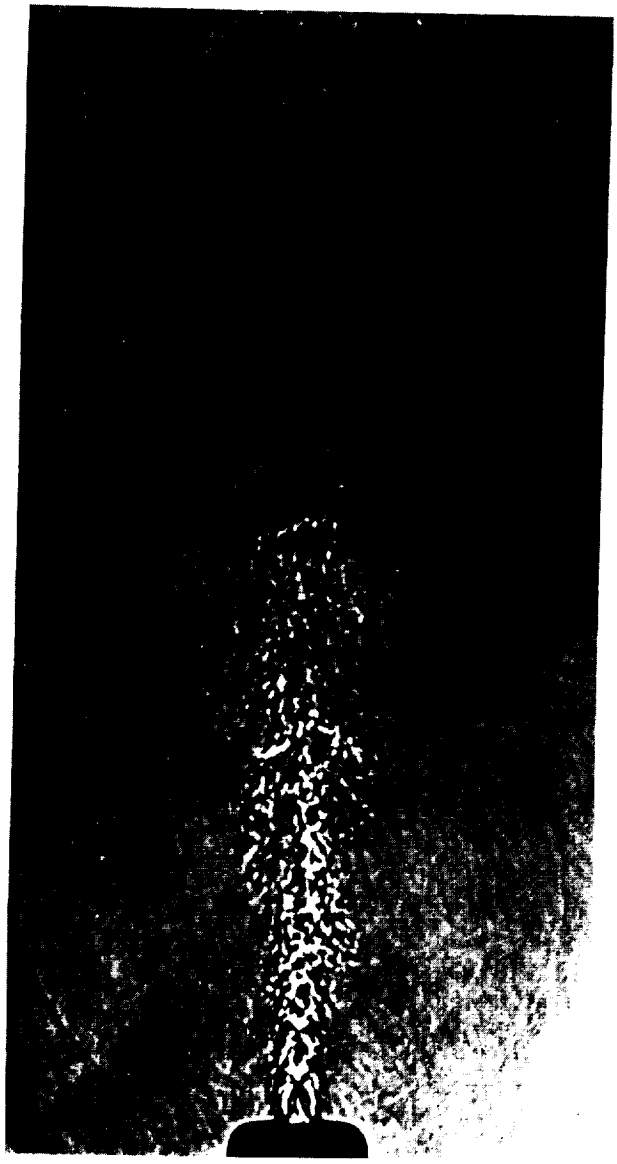

/90 b

Figure 2.

/90c

Figure 3.

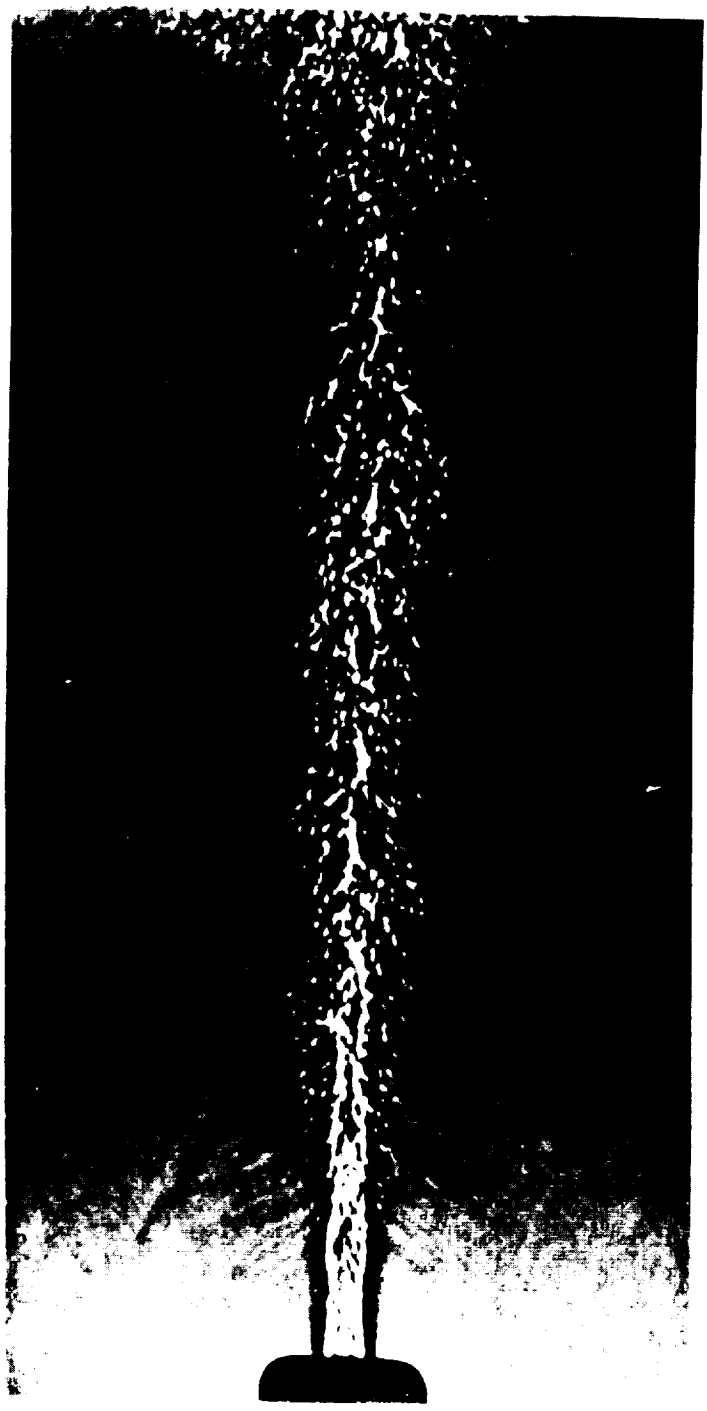

/90d

Figure 4.

/90e

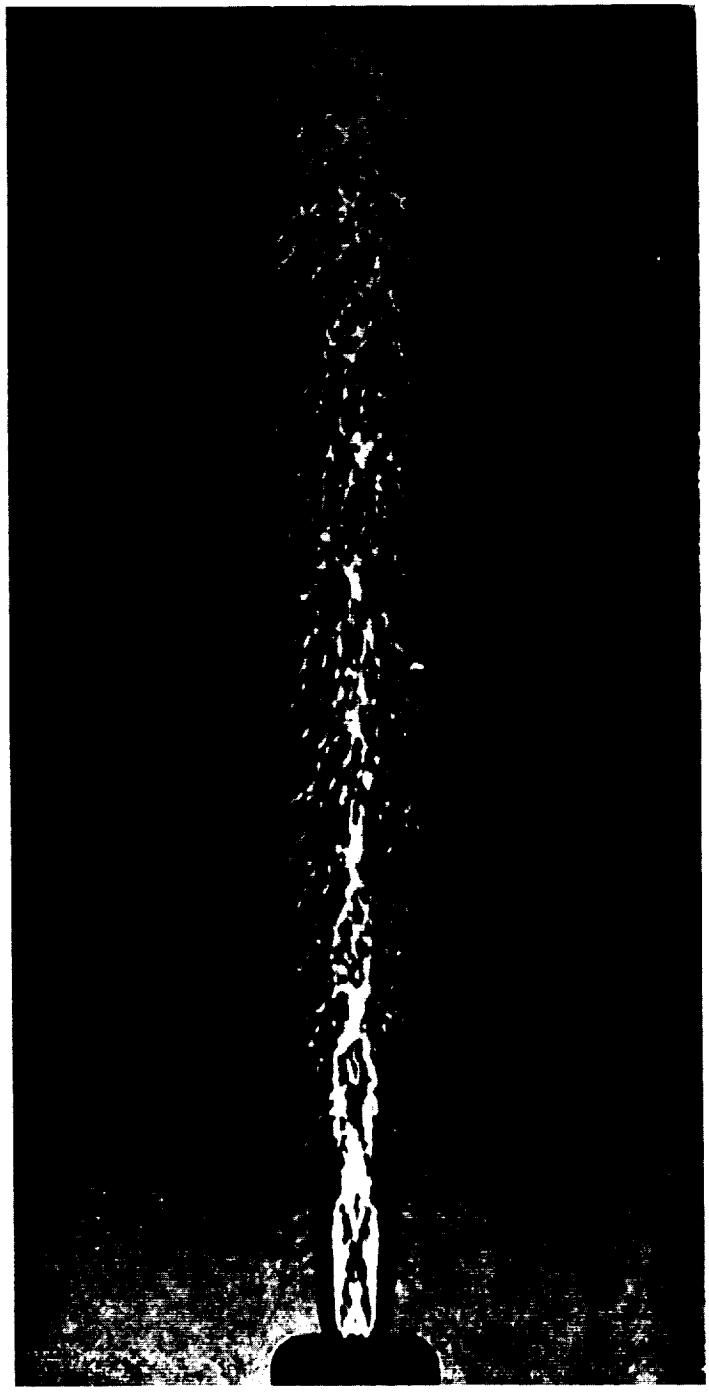

Figure 5.

/90f

Figure 6.

where

$$\Gamma = \begin{cases} \tanh \frac{L\Delta}{2}, \text{(sym)} \\ \coth \frac{L\Delta}{2}. \text{(asym)} \end{cases} \tag{17}$$

It can be seen that for all the $L\Delta$ the imaginary part of the increment (Im k) for symmetrical disturbances is smaller than for asymmetrical disturbances. It can be concluded from this that the principal mode of disturbances is the flexural mode (paragraph 6).

/91

The Dispersion Equation of a Circular Jet

We shall analyze the circular supersonic jet by the dispersion equation from [5]

$$\frac{\varkappa_0}{\rho_0(\omega - kv_0)^2} \frac{H_n^{(1)'}(\varkappa_0 a)}{H_n^{(1)}(\varkappa_0 a)} = \frac{\varkappa_1}{\rho_1(\omega - kv_1)^2} \frac{J_n'(\varkappa_1 a)}{J_n(\varkappa_1 a)}. \tag{18}$$

Here $H_n^{(1)}(x)$ is an n-order, first kind Hankel's function, $J_n(x)$ is an n-order Bessel function, a is the radius of the jet and n is the number of the mode. This equation for cold air jets was solved numerically on the Minsk-2 electronic computer by the Newton-Rafson method [6] as a function of the Mach number (parameter) and the Strouhal number (independent variable). The remaining quantities used in the calculations were expressed in terms of the Mach number using ordinary gasdynamic formulas; it was assumed that the gas surrounding the jet is at rest. The graphs of Figs. 7, 8, 9, and 10 show the imaginary and real parts of the roots of Eq. (18) corresponding to increasing disturbances.

It is possible to calculate the Strouhal number corresponding to the frequency of the discrete component if we assume that the rate at which the disturbance propagates along the jet is expressed as

$$v = \frac{v_1}{\operatorname{Re}\left(\frac{kv_1}{\omega}\right)}. \tag{19}$$

The Strouhal numbers thus obtained are tabulated below

/ 93

M	1.2	1.6	2.0	2.4
St_D	0.48	0.20	0.12	0.085

It can be seen that (by virtue of viscosity, etc.) the mode with n = 0 (bead-like pulsations) should predominate at M < 1.2, while modes with n > 0, i.e., azimuthal-unsymmetrical modes (paragraph 6) should predominate at M > 1.6.

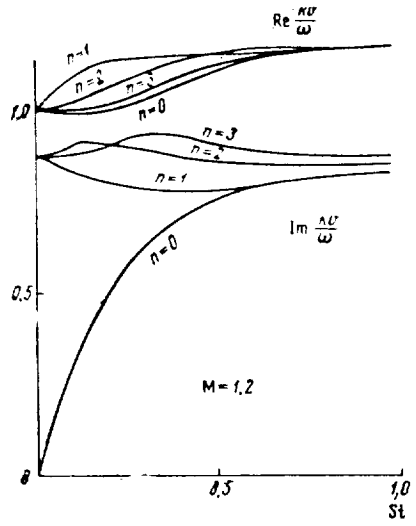

Figure 7. The Imaginary and Real Parts of kv/ω as a Function of the Strouhal Number for M = 1.2 in the Jet.

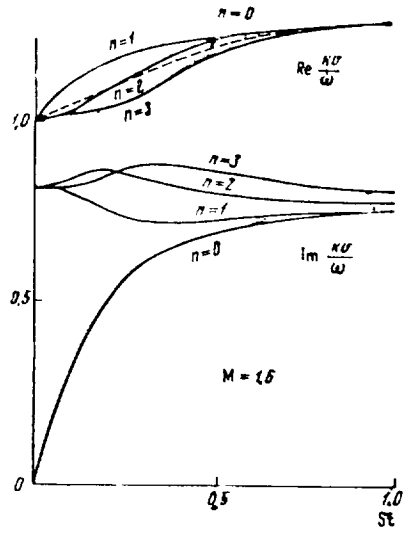

Figure 8. The Imaginary and Real Parts of kv/ω as a Function of the Strouhal Number for M = 1.6 in the Jet.

/92

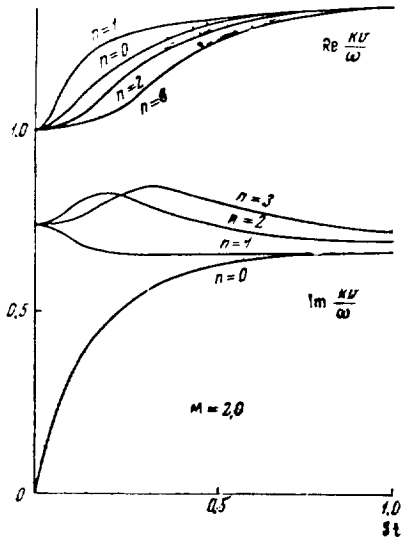

Figure 9. The Imaginary and Real Parts of kv/ω as a Function of the Strouhal Number for M = 2.0 in the Jet.

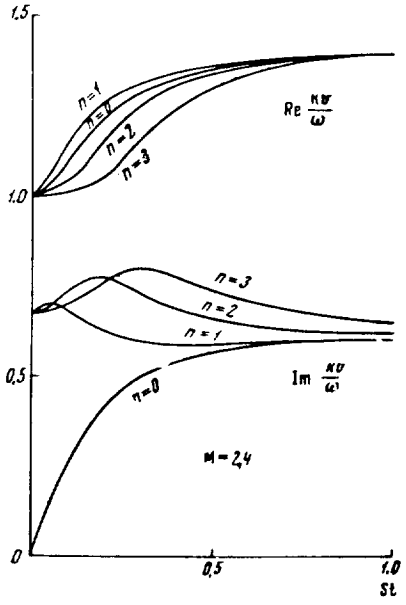

Figure 10. The Imaginary and Real Parts of kv/ω as a Function of the Strouhal Number for M = 2.4 in the Jet.

Estimate of the Radiation of Waves by Disturbances Passing Through Oblique Pressure Discontinuities [Shock Waves]

The passing of an acoustic-type disturbance through an oblique shock wave was examined in great detail by Kontorovich [7]. In the case of a jet the problem is more complex since, firstly, after passing the shock wave the disturbance has to pass through a rarefaction wave and secondly, only a part of the disturbance, which moves inside the jet is attenuated.

We shall estimate the part of the disturbance energy which is radiated as the disturbance passes through the shock and then through the rarefaction wave using the expression

$$n \simeq \frac{E_-(r<a) - E_+(r<a)}{E_-(r<a)} \cdot \frac{E(r>a)}{E}. \qquad (20)$$

Here E is the total acoustic energy of the down-stream disturbance, E $(r < a)$ and E_+ $(r > a)$ are parts of this energy which are contained in the jet and outside it, the subscripts minus and plus pertaining to the disturbance before and after passing the boundaries of the cell (Fig. 11a). It was assumed in writing Eq. (20) that, due to the reduction in the force of the disturbance inside the jet on passing through the shock wave, the force of the disturbance outside the jet is no longer that of equilibrium and a part of the acoustic energy is radiated. In other words, it can be imagined that the energy flux through the surface of the jet has a step in it (Fig. 11b). / 94

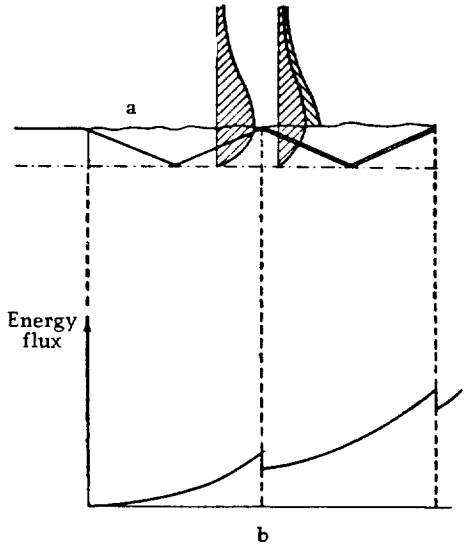

Figure 11. Acoustic Energy Density of the Acoustic Field of a Jet (a). Acoustic Energy Flux Through the Jet's Boundary (b).

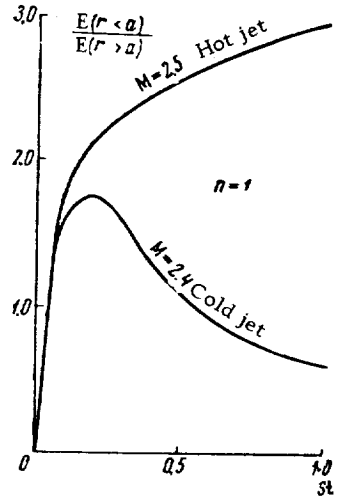

Figure 12. The Ratio of the Acoustic Energy of the Jet to the Acoustic Energy Outside the Jet as a Function of the Strouhal Number.

Estimating the acoustic energy on the basis of known formulas, we find

$$\frac{E(r<a)}{E(r>a)}=\frac{\rho_0 c_0^2}{\rho_1 c_1^2}\cdot\Lambda, \tag{21}$$

where

$$\Lambda=\frac{1-\frac{n^2}{\varkappa_1^2 a^2}+\left[\frac{J_n'(\varkappa_1 a)}{J_n(\varkappa_1 a)}\right]^2}{1-\frac{n^2}{\varkappa_0^2 a^2}+\left[\frac{H_n^{(1)'}(\varkappa_0 a)}{H_n^{(1)}(\varkappa_0 a)}\right]^2}. \tag{22}$$

The graph of Fig. 12 shows (St) for a cold air jet with M = 2.4 and for a hot jet with M = 2.5, ρ_0/ρ_1 = and $\rho_0 c_0^2 = \rho_1 c_1^2$ for the most provable mode of radiation, i.e., n = 1. It can be seen that the expression /94

$$\frac{E(r>a)}{E}=\left\{1+\frac{E(r<a)}{E(r>a)}\right\}^{-1} \tag{23}$$

yields a much higher value for the cold than for the hot jet.

The first factor of Eq. (20) is determined solely by the processes inside the jet and does not depend on the ambient air temperature. It appears that by analyzing it it will be possible to determine the manner in which the intensity of the discrete component of the frequency spectrum of the noise depends on the mode of discharge.

REFERENCES

1. Powell, A. Proc. Phys. Soc., Vol. B66, 1039, 1953. Aero Quart., Vol. IV, p. 11, 103-122, 1961.
2. Hammitt, A.J. J. Aerospace Sci., Vol. 28, 673, 1961.
3. Davies, M.J. and D.E.S. Oldfield. Acustica, Vol. 12, 257, 1962.
4. Merle, M. Comptes Rendus, Vol. 248, 1953, 1959.
5. Sedel'nikov, T.Kh. The Frequency Spectrum of the Noise of a Supersonic Jet. Present Collection.
6. Lance, G.H. Numerical Methods for High-Speed Computers. [Translated from English], 1962.
7. Kontorovich, V.M. Akusticheskiy zhurnal, Vol. V, Issue 3, 314, 1959.

THE DISPERSION EQUATION OF A PLANE EJECTOR

L. I. Nazarova and T. Kh. Sedel'nikov

ABSTRACT: This article presents a theoretical study of the stability of the boundaries of a plane supersonic jet in a plane ejector. It also gives a theoretical explanation of some features of the noise spectrum of a jet discharged from a nozzle in the presence of an ejector.

Experimental Data on the Noise of Ejectors

/95*

Work performed by a number of authors shows that noise formation in ejectors has its specific features. The most characteristic feature is the complex frequency spectrum of the noise, consisting of relatively sharp peaks on the smooth part of the spectrum [1]. A second feature is the dependence of the intensity of these discrete components on the distance between the outlet section of the nozzle and the outlet section of the ejector, i.e., on the length of the jet which is located in the ejector. The third feature of noise formation in an ejector consists in the presence of two types of discrete frequencies in the noise, one of which decreases its frequency with an increase in the ratio of the ejector radius to the jet radius, while the other does not change its frequency, but nonmonotonically changes its intensity. This second group disappears when the jet loses its cellular [beadlike] structure. No explanations are available for the above features of noise formation in ejectors.

The Dispersion Equation of a Plane Ejector

We shall now derive the dispersion equation for a plane ejector. This will be done similarly to the derivation of Eq. (11) of [2]. Only here the radiation conditions are replaced by the impedance conditions at the ejector's wall (Fig. 1). For a wide frequency range the ejector can be regarded as acoustically stiff

$$\left.\frac{\partial \varphi_0}{\partial x}\right|_{x=\pm b} = 0. \qquad (1)$$

The condition that the potential on the axis of the jet is finite, which is needed for cylindrical jets, is here useless. Following the derivation of Eqs. (11) and (12) in [2], we break up the disturbances of the boundary into symmetrical and asymmetrical. In symmetrical fluctuations the acoustic velocity in the middle plane of the jet is zero

/96

* Numbers in the margin indicate pagination in the foreign text.

$$\left.\frac{\partial \varphi_1}{\partial x}\right|_{x=0} = 0, \text{ (sym)} \tag{2}$$

while in asymmetrical fluctuations the pressure in this plane is zero

$$\left.\frac{\partial \varphi_1}{\partial t}\right|_{x=0} = 0. \text{ (asym)} \tag{3}$$

We shall seek the solutions of wave equations

$$\Delta \varphi_i = \frac{1}{c_i^2}\left(\frac{\partial}{\partial t} + v\frac{\partial}{\partial z}\right)^2 \varphi_i \tag{4}$$

in the form

$$\varphi_i(x, y, z, t) = \exp(iLy)\cdot\exp[i(kz - \omega t)]\cdot\Phi_i(x). \tag{5}$$

For Φ_i we get

$$\Phi_i''(x) + \varkappa_i^2 \Phi_i(x) = 0, \tag{6}$$

where

$$\varkappa_i^2 = \left(\frac{\omega - kv_i}{c_i}\right)^2 - k^2 - L^2. \tag{7}$$

Here L is the periodicity of the disturbance along the y axis.

For Φ_0 we can immediately write the expression

$$\Phi_0(x) = A\cos\varkappa_0(b - x), \tag{8}$$

which satisfies Eq. (1).

For Φ_1 we get two expressions

$$\Phi_1(x) = B \times \begin{cases} \cos\varkappa_1 x & \text{(sym)} \\ \sin\varkappa_1 x & \text{(asym)} \end{cases} \tag{9}$$

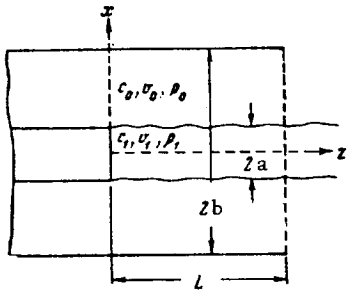

Figure 1.
Schematic for Calculations for a Plane Ejector.

Using conditions at the boundary of the jet /97

$$\rho_0\left(\frac{\partial}{\partial t}+v_0\frac{\partial}{\partial z}\right)\varphi_0\Big|_{x=a}=\rho_1\left(\frac{\partial}{\partial t}+v_1\frac{\partial}{\partial z}\right)\varphi_1\Big|_{x=a}, \tag{10}$$

$$\left(\frac{\partial}{\partial t}+v_1\frac{\partial}{\partial z}\right)\frac{\partial\varphi_0}{\partial x}\Big|_{x=a}=\left(\frac{\partial}{\partial t}+v_0\frac{\partial}{\partial z}\right)\frac{\partial\varphi_1}{\partial x}\Big|_{x=a}, \tag{11}$$

we can eliminate constants A and B and obtain the dispersion equations

$$\varkappa_0\tan\varkappa_0 l=-\frac{\rho_0}{\rho_1}\left(\frac{\omega-kv_0}{\omega-kv_1}\right)^2\varkappa_1\tan\varkappa_1 a, \text{ (sym)} \tag{12}$$

$$\varkappa_0\tan\varkappa_0 l=\frac{\rho_0}{\rho_1}\left(\frac{\omega-kv_0}{\omega-kv_1}\right)^2\varkappa_1\cot\varkappa_1 a, \text{ (asym)} \tag{13}$$

where $l = b - a$.

We introduce the notation

$$\xi=\frac{kv_1}{\omega},\ \delta=\frac{v_0}{v_1},\ \beta=\left(\frac{c_1}{v_1}\right)^2=\frac{1}{M_1^2},\ \gamma=\left(\frac{c_0}{c_1}\right)^2 \tag{14}$$

and write Eqs. (12) and (13) in the form

$$(1-\xi)^2=-\frac{\rho_0}{\rho_1}(1-\delta\cdot\xi)^2\frac{X\tan X}{Y\tan Y}, \tag{15}$$

$$(1-\xi)^2=\frac{\rho_0}{\rho_1}(1-\delta\cdot\xi)^2\frac{X}{\tan X}\frac{1}{Y\tan Y}, \tag{16}$$

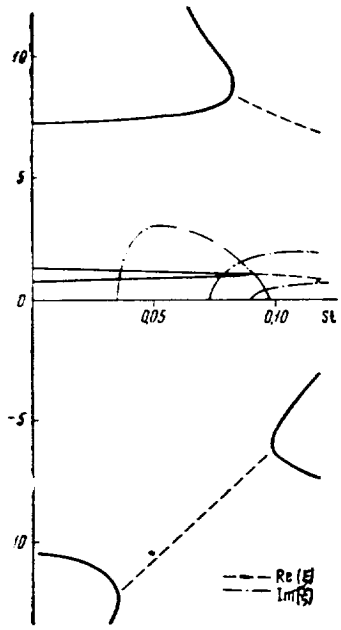

Figure 2. The Real and Imaginary Parts as a Function of the Strouhal Number for a Symmetrical Disturbance.

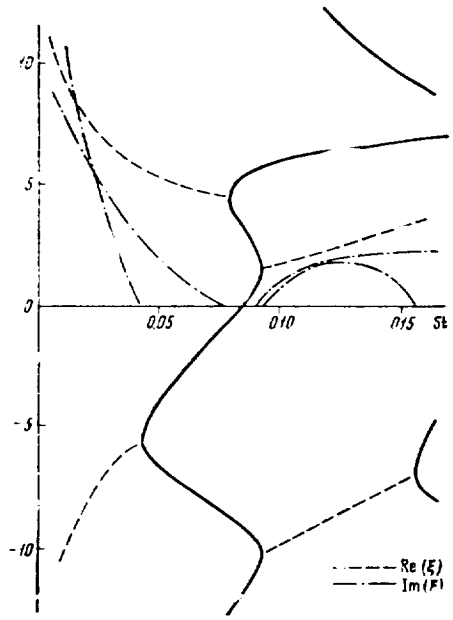

Figure 3. The Real and Imaginary Parts as a Function of the Strouhal Number for an Asymmetrical Disturbance.

where

$$X = \frac{\omega a}{c_1}\sqrt{(1-\xi)^2 - \beta\xi^2}, \quad (L=0),$$
$$Y = \frac{\omega l}{c_0}\sqrt{(1-\delta\cdot\xi)^2 - \beta\gamma\xi^2}. \quad (L=0) \tag{17}$$

We first examine Eq. (15), restricting ourselves to the case of hot supersonic jets. If we seek roots with a moderate absolute magnitude, i.e.,

$$|\xi| \sim 1, \tag{18}$$

then in the limit of low frequencies we will have

$$Y \sim \frac{\omega l}{c_0} = t, \quad X \sim \frac{\omega a}{c_1} \ll Y.$$

Equation (15) will take on the form

$$(1-\xi)^2 \cong -\frac{\rho_0 c_0^2}{\rho_1 c_1^2}\frac{a}{l}\frac{t}{\tan t}\left[(1-\xi)^2-\beta\xi^2\right]. \tag{19}$$

whence we get

$$\xi \cong \left[1 \pm \beta^{1/2}\left(1+\frac{l}{a}\frac{\gamma_1}{\gamma_0}\frac{\tan t}{t}\right)^{-1/2}\right]^{-1}. \tag{20}$$

It can be seen that for some t real roots will become complex roots. /98

It is convenient to continue the examination of Eq. (15) by setting X, Y, $1-\xi$ and $(1-\delta\xi)$ equal to zero one after the other. The real roots can be found by setting ξ = const and solving the equation thus obtained for St. The complex roots can be found from the iteration formula

$$\xi_{n+1} = 1 \pm i\sqrt{\frac{\rho_0}{\rho_1}}\left[(1-\delta\cdot\xi)^2\frac{X\tan X}{Y\tan Y}\right]^{1/2}_{\xi=\xi_n}. \tag{21}$$

A formula analogous to Eq. (20) can also be found from Eq. (16)

$$\xi \cong 1 \pm \sqrt{\frac{\rho_0 l}{\rho_1 a}\frac{1}{t\tan t}}, \tag{22}$$

but the limits of its applicability are somewhat narrower.

As an illustration we have examined a hot supersonic jet with parameters $M_1 = 2.5$, $\delta = 0.02$, $\rho_0/\rho_1 = 9$, a/b = 1/3 and L = 0.

We reduce the graphs (Figs. 2 and 3) of roots ξ of Eqs. (12) and (13) for low Strouhal numbers /99

$$St = \frac{2af}{v_1}\frac{c_1}{c_0}. \tag{23}$$

Since these roots are complex conjugates [of one another] only one each of the two conjugate roots were reduced.

Let us now examine the physical meaning of the results so far, by considering a finite plane ejector. Acoustic self-excitation in such an ejector may occur as follows. The disturbances which arise at the outlet section of the nozzle propagate along the jet and increase [in intensity]. Passing through the inlet section of the ejector this disturbance produces a reverse wave inside the

ejector due to the radical change in the boundary conditions. The reverse wave is then redecomposed [rearranged] at the outlet section of the nozzle, thus producing a disturbance.

In order for such a mechanism to exist, the phase and amplitude conditions must be satisfied. Due to the inevitable losses on rearrangement, due to viscosity, etc., it is required that the increase in the disturbance when moving down the jet exceed the reduction in the disturbance on moving upstream of the jet. This condition is called the amplitude condition

$$\Delta \operatorname{Im} \xi = |\operatorname{Im} \xi|_{\operatorname{Re} \xi > 0} - |\operatorname{Im} \xi|_{\operatorname{Re} \xi < 0} > 0. \tag{24}$$

It can be seen from examination of the graphs that for given parameters of the jet and ejector stable self-excitation of the ejector is possible for Strouhal numbers

$$\begin{array}{rl} & \mathrm{St} > 0.087 \quad \text{(sym. case)} \\ 0.077 > & \mathrm{St} > 0.03 \quad \text{(asym. case)} \\ & \mathrm{St} > 0.12 \end{array}$$

In the first case the maximum of $\Delta \operatorname{Im} \xi$ is reached for $\mathrm{St} > 0.98$, and in the second case it corresponds to $\mathrm{St} = 0.44$ and $\mathrm{St} > 0.156$.

We now turn to the phase conditions. If the phase losses 2δ on reflection of the disturbance from the ejector inlet and nozzle outlet sections are known, then τ, the time of one cycle, can be written in the form

$$\tau\left(1 - \frac{2\delta}{2\pi}\right) = \frac{L}{V_{\rightarrow}} + \frac{L}{V_{\leftarrow}}, \tag{25}$$

where $V_{\rightarrow}$ and $V_{\leftarrow}$ are the phase velocities of the disturbances traveling down and upstream of the jet. Using Eq. (19) of [3], we can write the phase condition in the form

$$\frac{L}{2a} \frac{1}{\left(1 - \frac{2\delta}{2\pi}\right)} = \frac{c_1}{c_0} [\,|\operatorname{Re} \xi_{\leftarrow}| + |\operatorname{Re} \xi_{\rightarrow}|\,] \cdot \mathrm{St}. \tag{26}$$

Stable self-excitation of an ejector is thus possible not at all lengths L, /100
but only for discrete L.

Returning to the amplitude condition, we write the amplification factor of the cycle as

$$k_{\text{cyc}} = k_{\text{ref.}} \cdot e^{\mu}, \tag{27}$$

where k_{ref} is the product of the absolute values of the disturbance reflection factors from the respective nozzle and ejector sections, while μ is expressed by

$$\mu = L\frac{\omega}{v}\left[\left|\operatorname{Im}\xi_{\rightarrow}\right| - \left|\operatorname{Im}\xi_{\rightarrow}\right|\right]. \tag{28}$$

Using Eq. (26), we find

$$\frac{\mu}{1-\frac{2\delta}{2\pi}} = 2\pi\frac{\left|\operatorname{Im}\xi_{\rightarrow}\right| - \left|\operatorname{Im}\xi_{\leftarrow}\right|}{\left|\operatorname{Re}\xi_{\rightarrow}\right| + \left|\operatorname{Re}\xi_{\leftarrow}\right|}.$$

Thus, the considerations presented above make it possible to find regions of Strouhal numbers which are most probable from the point of view of self-induced vibrations, as well as to understand the discrete character of the frequency spectrum of ejector noise.

It should be added that above we have considered a jet at its design discharge mode, i.e., in the absence of the fine structure. In the case of "cells" or "barrels" disturbances may be reflected also from the ends of these and this produces additional self-excitation frequencies. All the expressions obtained above remain valid, except that then L will denote the length of the "barrel" or "cell."

REFERENCES

1. Midlton, D. and E.J. Richards. Discrete Frequency Noise from Ejector Nozzle.
2. Sedel'nikov, T.Kh. The Frequency Spectrum of the Noise of a Supersonic Jet. Article in present collection.
3. Sedel'nikov, T.Kh. The Discrete Component of the Frequency Spectrum of the Noise of a Supersonic Jet. Article in present collection.

THE DISPERSION EQUATIONS FOR MULTILAYER JETS AND FOR SEVERAL JETS

T. Kh. Sedel'nikov

ABSTRACT: Of great interest at present is the determination of the frequency spectrum of the noise of an annular jet, several jets, etc. The present article derives dispersion equations for determining the stability of the boundaries of multilayer jets and of several jets.

The Dispersion Equation of an Annular Jet

/101*

Let us consider a twin-layer cylindrical infinite supersonic jet. As in [1], we shall disregard the angle of divergence of the jet, its cellular structure, viscosity of the gas in the jet, and we shall regard the amplitude of vibrations of the jet's boundary as infinitesimal. The selected coordinate system is seen clearly in Fig. 1. The variables pertaining to the gas surrounding the jet are denoted by the subscript "0," subscript "1" is assigned to the gas of the inner jet, while subscript "2" designates the gas of the outer [annular] jet. We use the following notation: ρ - density of the undisturbed gas, c - speed of sound in it, v - velocity of the undisturbed gas, ω - circular frequency, Δ - Laplacian operator, φ - acoustic potential, t - time.

We now write the wave equations and the boundary conditions [1]

$$\Delta\varphi_i = \frac{1}{c_i^2}\left(\frac{\partial}{\partial t} + v_i\frac{\partial}{\partial z}\right)^2\varphi_i, \tag{1}$$

$$\rho_i\left(\frac{\partial}{\partial t} + v_i\frac{\partial}{\partial z}\right)\varphi_i\Big|_S = \rho_j\left(\frac{\partial}{\partial t} + v_j\frac{\partial}{\partial z}\right)\varphi_j\Big|_S, \tag{2}$$

/102

$$\left(\frac{\partial}{\partial t} + v_j\frac{\partial}{\partial z}\right)\frac{\partial\varphi_i}{\partial n}\Big|_S = \left(\frac{\partial}{\partial t} + v_i\frac{\partial}{\partial z}\right)\frac{\partial\varphi_j}{\partial n}\Big|_S, \tag{3}$$

where S are the bounding surfaces, while n are the normals to them, i, j = 0, 1, 2.

We shall seek the solution of Eqs. (1) in the form

*Numbers in the margin indicate pagination in the foreign text.

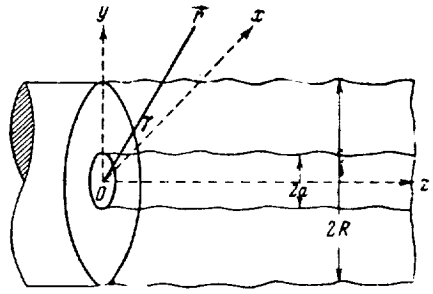

Figure 1. Schematic and Designations for a Twin-Layer Jet.

$$\left.\begin{matrix}\varphi_0(r,\gamma,z,t)\\ \varphi_1(r,\gamma,z,t)\\ \varphi_2(r,\gamma,z,t)\end{matrix}\right\} = \cos n\gamma\cdot\exp[i(kz-\omega t)]\times\begin{cases}AH_n^{(1)}(\varkappa_0 r),\\ DI_n(\varkappa_1 r),\\ BI_n(\varkappa_2 r)+CN_n(\varkappa_2 r),\end{cases} \tag{4}$$

where the so-called radiation condition is already satisfied, while $\varkappa_i$ is given by the expression

$$\varkappa_i^2 = \left(\frac{\omega - kv_i}{c_i}\right)^2 - k^2; \tag{5}$$

and A, B, C, D and k are constants.

Eliminating A, B, C and D by means of conditions (2) and (3) for r = a and r = R, we get the so-called dispersion equation relating k and ω

$$\begin{aligned}&M_n'(\varkappa_2 a_1, \varkappa_2 R) - M_n'(\varkappa_1 a_1, \varkappa_2 R)\frac{\rho_2\varkappa_1}{\rho_1\varkappa_2}\left(\frac{\omega-kv_2}{\omega-kv_1}\right)^2\frac{J_n'(\varkappa_1 a)}{J_n(\varkappa_1 a)} +\\ &+ M_n(\varkappa_1 a_1, \varkappa_2 R)\frac{\rho_2\varkappa_1}{\rho_1\varkappa_2}\left(\frac{\omega-kv_2}{\omega-kv_1}\right)^2\frac{J_n'(\varkappa_1 a)}{J_n(\varkappa_1 a)}\frac{\rho_2\varkappa_0}{\rho_0\varkappa_2}\left(\frac{\omega-kv_2}{\omega-kv_0}\right)^2\frac{H_n'(\varkappa_0 R)}{H_n(\varkappa_0 R)} -\\ &- M_n'(\varkappa_2 a_1, \varkappa_2 R)\frac{\rho_2\varkappa_0}{\rho_0\varkappa_2}\left(\frac{\omega-kv_2}{\omega-kv_0}\right)^2\frac{H_n'(\varkappa_0 R)}{H_n(\varkappa_0 R)} = 0,\end{aligned} \tag{6}$$

where the notation is

$$M_n(x, y) = J_n(x)H_n^{(1)}(y) - J_n(y)H_n^{(1)}(x) \tag{7}$$

and the primes to the left or right of M denote differentiation with respect to the first or second argument [respectively]. When a = R or a = 0, Eq. (6) becomes the dispersion equation for a simple jet.

In the limiting case of long-wave disturbances Eq. (6) simplifies to

$$\begin{aligned}&1 + \frac{\rho_2^2}{\rho_0\rho_1}\left(\frac{\omega-kv_2}{\omega-kv_0}\right)^2\left(\frac{\omega-kv_2}{\omega-kv_1}\right)^2 + \frac{R^{2n}+a^{2n}}{R^{2n}-a^{2n}}\left[\frac{\rho_2}{\rho_0}\left(\frac{\omega-kv_2}{\omega-kv_0}\right)^2 +\right.\\ &\left.+\frac{\rho_2}{\rho_1}\left(\frac{\omega-kv_2}{\omega-kv_1}\right)^2\right] = 0.\end{aligned} \tag{8}$$

Of particular interest is the case of an annular jet with $v_0 = v_1$, $\rho_0 = \rho_1$ and $c_0 = c_1$. In this case Eq. (8) has the solution /103

$$\frac{k}{\omega} = \frac{v_0 + \frac{\rho_2}{\rho_0} T v_2 \pm i \sqrt{\frac{\rho_2}{\rho_0} T (v_0 - v_2)}}{v_0^2 + \frac{\rho_2}{\rho_0} T v_2^2}, \tag{9}$$

where

$$T_1 = \left(\frac{R^n + a^n}{R^n - a^n}\right)^2, \qquad T_2 = \frac{1}{T_1}, \qquad n \neq 0. \tag{10}$$

For n = 0 Eq. (6) for long-wave disturbances has the form

$$\left(1 - \frac{kv_2}{\omega}\right)^2 \cong 1 \tag{11}$$

where $kv_2/\omega = 1$. In the opposite case of short-wave disturbances for complex k we get the expression

$$\left[1 + \frac{\rho_2 \varkappa_0}{\rho_0 \varkappa_2}\left(\frac{\omega - kv_2}{\omega - kv_0}\right)^2\right]\left[1 - \frac{\rho_2 \varkappa_1}{\rho_1 \varkappa_2}\left(\frac{\omega - kv_2}{\omega - kv_1}\right)^2\right] = 0, \tag{12}$$

which corresponds to separate propagation of disturbances along each of the boundaries.

It is possible to obtain dispersion equations also for multilayer jets. We present here the dispersion equation for a triple-layer jet $0 < a \leq b \leq R < \infty$

$$\frac{\varkappa_2}{\rho_2(\omega - kv_2)^2} \frac{\varkappa_2 M_n'(\varkappa_2 b, a_2 a) - \lambda' M_n(a_2 b, a_2 a)}{a_2 M_n'(a_2 b, a_2 a) - \lambda M_n(a_2 b, a_2 a)} =$$
$$= \frac{\varkappa_3}{\rho_3(\omega - kv_3)^2} \frac{\varkappa_3' M_n'(a_3 b, a_3 R) - \mu' M_n(\varkappa_3 b, \varkappa_3 R)}{\varkappa_3 M_n'(\varkappa_3 b, \varkappa_3 R) - \mu M_n(\varkappa_3 b, \varkappa_3 R)}. \tag{13}$$

Here subscript "3" denotes the outer annular jet $b \leq r \leq R$ and the notation used is

$$\mu = \frac{\varkappa_0 \rho_3}{\varkappa_3 \rho_0}\left(\frac{\omega - kv_3}{\omega - kv_0}\right)^2 \frac{H_n'(\varkappa_0 R)}{H_n(\varkappa_0 R)},$$
$$\lambda = \frac{\varkappa_1 \rho_2}{\varkappa_2 \rho_1}\left(\frac{\omega - kv_2}{\omega - kv_1}\right)^2 \frac{J_n'(\varkappa_1 a)}{J_n(\varkappa_1 a)}. \tag{14}$$

Dispersion Equations for Several Jets

We shall now obtain the dispersion equation for an infinite cylindrical jet, situated near a flat, acoustically stiff wall which is parallel to the jet's axis, or for two identical parallel jets. Disregarding the interaction between the gas flows in the jets, we shall assume that the jets are in the shape of circular cylinders. Without writing out in detail the wave equations for the acoustic potentials, we immediately write the acoustic potential outside of the jet /104

$$\varphi_1(r, \gamma, z, t) = \exp[i(kz - \omega t)] \times \times \sum_n A_n [H_n^{(1)}(\varkappa_1 r_1) \exp(in\gamma_1) \pm H_n^{(1)}(\varkappa_0 r_2) \exp(in\gamma_2)]. \quad (15)$$

It is easy to see in Fig. 2, that the plus (minus) sign corresponds to the case of symmetrical (asymmetrical) modes of vibrations, with the stiff screen corresponding to the first case. The acoustic potential inside the left jet can be taken in the form

$$\varphi_1(r, \gamma, z, t) = \exp[i(kz - \omega t)] \sum_m C_m J_m(\varkappa_1 r_1) \exp(im\gamma_1). \quad (16)$$

Using the "addition theorem" for Hankel's functions, it is possible to write Eq. (15) in the coordinate system related to the left jet

$$\varphi_1(r_1, \gamma_1, z, t) = \exp[i(kz - \omega t)] \sum_n \sum_l [\exp(in\gamma_1)] A_l \beta_{nl}(r_1), \quad (17)$$

where

$$\beta_{nl}(r) = \delta_{nl} H_n^{(1)}(\varkappa_1 r) \pm J_n(\varkappa_0 r) H_{l-n}^{(1)}(\varkappa_0 \Delta), \quad (18)$$

while δ_{nl} is Kronecker's delta ($\delta_{nl} = 0$ if $n \neq l$ and $\delta_{nl} = 1$ if $n = l$). Eliminating constants C_m by means of boundary conditions at $r = a$, it is possible to obtain a system of homogeneous equations for constants A_l

$$\sum_l A_l \left[\beta'_{nl}(a) - \frac{\varkappa_1 \rho_0}{\varkappa_0 \rho_1} \left(\frac{\omega - kv_0}{\omega - kv_1}\right)^2 \frac{J'_n(\varkappa_1 a)}{J_n(\varkappa_1 a)} \beta_{nl}(a)\right] = 0. \quad (19)$$

Equating its determinant to zero, we shall find the sought dispersion equation

$$|\delta_{nl} \pm \Gamma_n H_{l+n}^{(1)}(\varkappa_0 \Delta)| = 0, \quad (20)$$

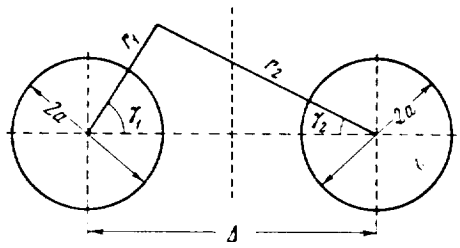

Figure 2. Systems of Cylindrical Coordinates for Two Jets.

/ 104

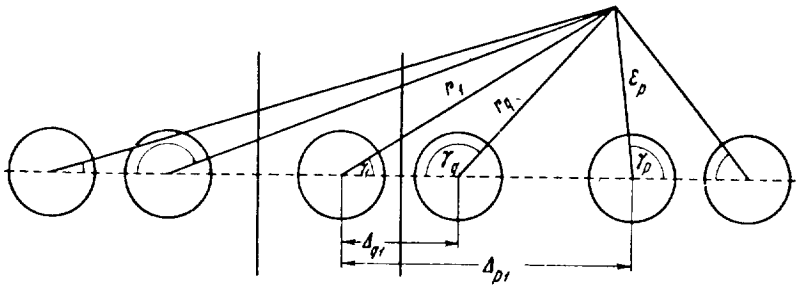

/105

Figure 3. System of Cylindrical Coordinates for a Jet Between Walls.

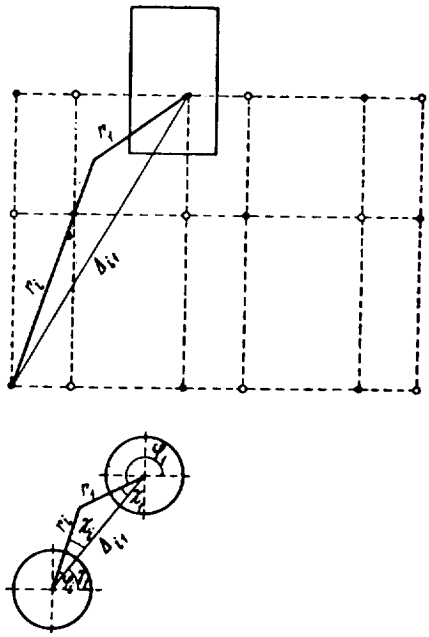

Figure 4. System of Cylindrical Coordinates for a Jet in a Rectangular Duct.

where

$$\Gamma_n = \frac{J_n'(\varkappa_0 a) - \Lambda_n J_n(\varkappa_0 a)}{H_n^{(1)'}(\varkappa_0 a) - \Lambda_n H_n^{(1)})(\varkappa_0 a)}, \tag{21}$$

$$\Lambda_n = \frac{\varkappa_1 \rho_0}{\varkappa_0 \rho_1}\left(\frac{\omega - k v_0}{\omega - k v_1}\right)^2 \frac{J_n'(\varkappa_1 a)}{J_n(\varkappa_1 a)}. \tag{22}$$ /106

Similar dispersion equations can be obtained for a jet between two acoustically stiff walls parallel to one another and to the axis of the jet (Fig. 3). Equation (20) remains valid, but quantity $H_{l+n}^{(1)}(\varkappa_0 \Delta$ is replaced by the expression

$$M_{ln} = (-)^n \left[\sum_{p \neq 1} H_{l-n}^{(1)}(\varkappa_0 \Delta_{p1}) + \sum_q H_{l+n}^{(1)}(\varkappa_0 \Delta_{q1})\right], \tag{23}$$

where summation in the first sum is over all the jets with "positively directed rotation of disturbances" and in the second sum it is over all the jets with "negatively directed disturbances."

A jet in a rectangular duct or a jet situated symmetrically in a duct in the form of a regular hexagon or triangle is considered identically, except that Eq. (23) is then replaced by the expression

$$M_{ln} = \sum_{p \neq 1} \{\exp[i(l+n)\gamma_i]\} H_{l-n}^{(1)}(\varkappa_0 \Delta_{p1}) + \\ + \sum_q (-)^n \{\exp[-i(l+n)\gamma_q]\} H_{l+n}^{(1)}(\varkappa_0 \Delta_{q1}). \tag{24}$$

The notation is clear from Fig. 4.

REFERENCES

1. Sedel'nikov, T.Kh. The Frequency Spectrum of the Noise of a Supersonic Jet. Present collection.
2. Watson, G.N. Theory of Bessel Functions. Cambridge, 1923.

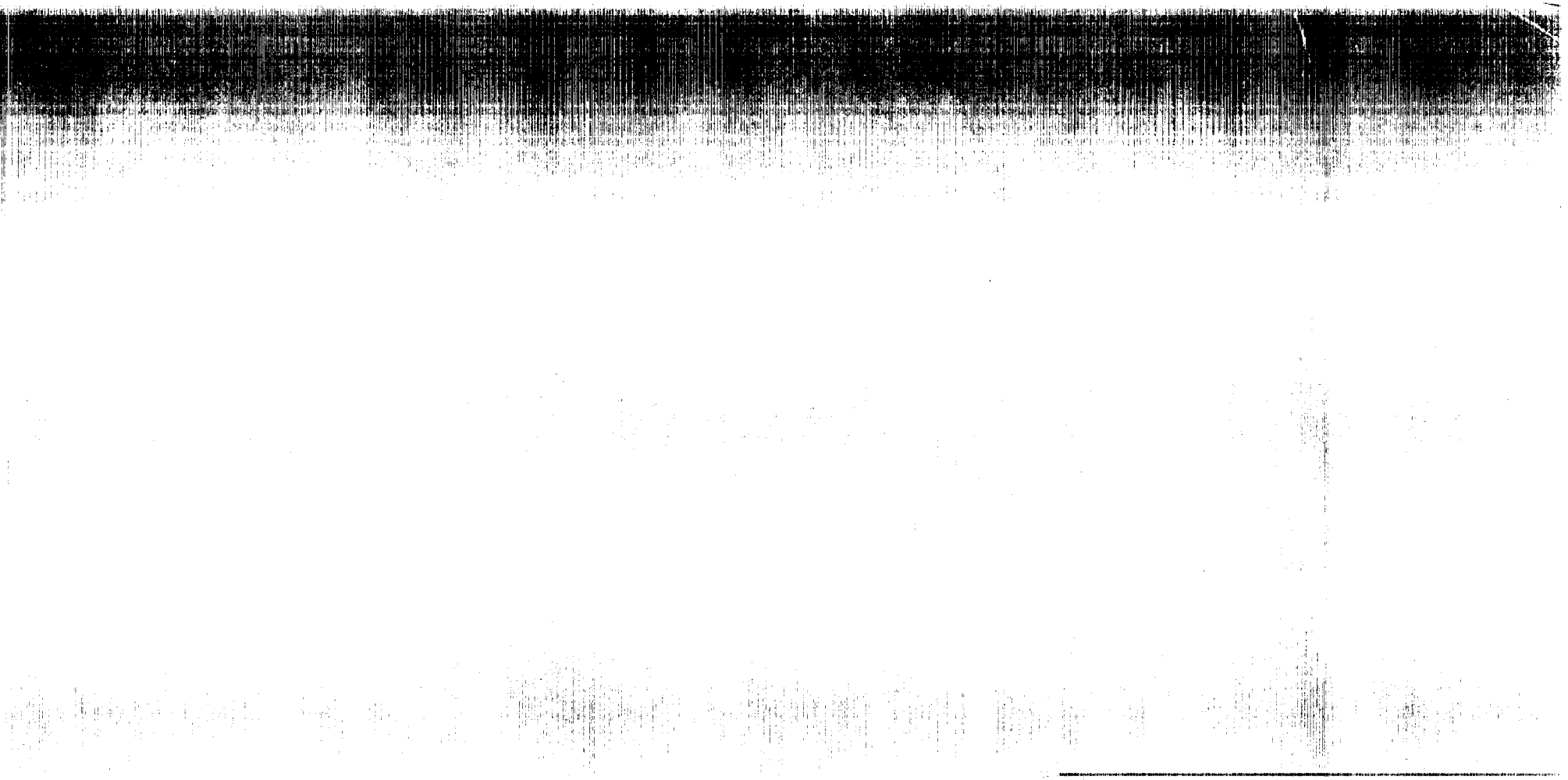

NATIONAL AERONAUTICS AND SPACE ADMINISTRATION
WASHINGTON, D.C. 20546

OFFICIAL BUSINESS

FIRST CLASS MAIL

POSTAGE AND FEES PAID
NATIONAL AERONAUTICS AND
SPACE ADMINISTRATION

POSTMASTER: If Undeliverable (Section 158
Postal Manual) Do Not Return

"The aeronautical and space activities of the United States shall be conducted so as to contribute . . . to the expansion of human knowledge of phenomena in the atmosphere and space. The Administration shall provide for the widest practicable and appropriate dissemination of information concerning its activities and the results thereof."

— NATIONAL AERONAUTICS AND SPACE ACT OF 1958

NASA SCIENTIFIC AND TECHNICAL PUBLICATIONS

TECHNICAL REPORTS: Scientific and technical information considered important, complete, and a lasting contribution to existing knowledge.

TECHNICAL NOTES: Information less broad in scope but nevertheless of importance as a contribution to existing knowledge.

TECHNICAL MEMORANDUMS: Information receiving limited distribution because of preliminary data, security classification, or other reasons.

CONTRACTOR REPORTS: Scientific and technical information generated under a NASA contract or grant and considered an important contribution to existing knowledge.

TECHNICAL TRANSLATIONS: Information published in a foreign language considered to merit NASA distribution in English.

SPECIAL PUBLICATIONS: Information derived from or of value to NASA activities. Publications include conference proceedings, monographs, data compilations, handbooks, sourcebooks, and special bibliographies.

TECHNOLOGY UTILIZATION PUBLICATIONS: Information on technology used by NASA that may be of particular interest in commercial and other non-aerospace applications. Publications include Tech Briefs, Technology Utilization Reports and Notes, and Technology Surveys.

Details on the availability of these publications may be obtained from:

SCIENTIFIC AND TECHNICAL INFORMATION DIVISION

NATIONAL AERONAUTICS AND SPACE ADMINISTRATION

Washington, D.C. 20546